

# DESIGNING AND OPTIMIZING GRATINGS FOR SOFT XRAY DIFFRACTION EFFICIENCY

A Thesis Submitted to the  
College of Graduate Studies and Research  
in Partial Fulfillment of the Requirements  
for the degree of Master of Science  
in the Department of Physics and Engineering Physics  
University of Saskatchewan  
Saskatoon

By  
Mark Boots

©Mark Boots, October 2011. All rights reserved.

## PERMISSION TO USE

In presenting this thesis in partial fulfilment of the requirements for a Postgraduate degree from the University of Saskatchewan, I agree that the Libraries of this University may make it freely available for inspection. I further agree that permission for copying of this thesis in any manner, in whole or in part, for scholarly purposes may be granted by the professor or professors who supervised my thesis work or, in their absence, by the Head of the Department or the Dean of the College in which my thesis work was done. It is understood that any copying or publication or use of this thesis or parts thereof for financial gain shall not be allowed without my written permission. It is also understood that due recognition shall be given to me and to the University of Saskatchewan in any scholarly use which may be made of any material in my thesis.

Requests for permission to copy or to make other use of material in this thesis in whole or part should be addressed to:

Head of the Department of Physics and Engineering Physics  
Rm 123 Physics Building  
116 Science Place  
University of Saskatchewan  
Saskatoon, Saskatchewan  
Canada  
S7N 5E2

# ABSTRACT

This is the abstract of my thesis.

# ACKNOWLEDGEMENTS

Acknowledgements go here. Typically you would at least thank your supervisor.

This is the thesis dedication (optional)

# CONTENTS

<b>Permission to Use</b>	<b>i</b>
<b>Abstract</b>	<b>ii</b>
<b>Acknowledgements</b>	<b>iii</b>
<b>Contents</b>	<b>v</b>
<b>List of Tables</b>	<b>vii</b>
<b>List of Figures</b>	<b>viii</b>
<b>List of Abbreviations</b>	<b>xiii</b>
<b>1 Introduction</b>	<b>1</b>
<b>2 Motivation: Why grating efficiency matters</b>	<b>2</b>
2.1 Soft X-ray Spectroscopy Techniques . . . . .	4
2.1.1 Absorption spectroscopy . . . . .	5
2.1.2 Emission spectroscopy . . . . .	6
2.1.3 Importance of Soft X-ray Spectroscopy (SXS) . . . . .	7
2.2 Spectroscopy Instrumentation . . . . .	8
2.2.1 Beamline optics: Monochromators and Spectrometers . . . . .	11
2.2.2 Goals for Soft X-ray Instruments . . . . .	14
2.2.3 Challenges of Soft X-ray Applications . . . . .	16
2.3 REIXS spectrometer project . . . . .	17
2.4 Summary: Why Grating Efficiency Matters . . . . .	18
<b>3 Theory: How to calculate grating efficiency</b>	<b>20</b>
3.1 Introduction of grating theory . . . . .	20
3.1.1 Simplifying Assumptions . . . . .	23
3.1.2 Electromagnetic field and polarization . . . . .	24
3.1.3 Maxwell's equations for sinusoidal time-varying fields . . . . .	25
3.1.4 Periodicity of gratings and fields (aka, pseudo-periodic functions and the Fourier basis) . . . . .	27
3.1.5 Deriving the Grating Equation . . . . .	28
3.2 Defining Grating Efficiency . . . . .	33
3.3 Solving for efficiency . . . . .	37
3.3.1 Numerical Challenges . . . . .	37
3.3.2 Applying boundary conditions within the groove region . . . . .	37
3.3.3 Handling stacks of gratings . . . . .	37
3.4 XRays and materials: how do they interact? . . . . .	37
<b>4 Implementation of Theory: What people and I did to implement the theory using computers</b>	<b>40</b>
4.1 Methods . . . . .	40
4.1.1 Rigorous Coupled Wave method: GSolver . . . . .	40
4.1.2 Differential method: Gradif by Michel Neviere . . . . .	40
4.2 Improving the usability and efficiency of calculation methods . . . . .	40
4.2.1 Visual interface to the Gradif code . . . . .	41
4.2.2 Detecting convergence failures . . . . .	45

4.2.3	Open Source, Open Access, and Future Work . . . . .	45
4.3	General trends and factors affecting efficiency . . . . .	47
4.3.1	Effect of Grating Profile: Groove Shape . . . . .	47
4.3.2	Effect of Groove Density . . . . .	56
4.3.3	Effect of Coating Thickness . . . . .	56
4.3.4	Comparison of coating materials . . . . .	59
4.3.5	Effect of photon energy / wavelength . . . . .	61
4.3.6	Effect of incidence angle . . . . .	62
4.3.7	TODO Applications to beamline and instrument design . . . . .	63
4.4	Validation: comparison of theory to experimental results . . . . .	66
<b>5</b>	<b>Design: How David and I applied these tools to make the REIXS optical design</b>	<b>71</b>
5.1	Application to spectrometer design . . . . .	71
5.1.1	Design Goals: (simultaneously) . . . . .	71
5.1.2	Comparative examples . . . . .	71
5.2	Design Process . . . . .	71
5.2.1	Justification of Design choices: . . . . .	71
5.3	High-resolution (3rd order) design . . . . .	74
5.3.1	Options for reaching extreme resolution: . . . . .	74
5.4	Coating choices: . . . . .	74
5.5	Optimization . . . . .	76
5.6	Summary of Final Design . . . . .	76
<b>6</b>	<b>Characterization: How we measured the actual grating performance, and accounted for differences</b>	<b>80</b>
6.1	AFM measurements of manufactured grating profile . . . . .	80
6.2	Diffraction measurements of actual grating efficiency . . . . .	80
6.2.1	Beamline 6.3.2 Diffraction . . . . .	80
6.3	Real-world grating effects . . . . .	80
6.3.1	Stray Radiant Energy . . . . .	80
6.3.2	Blaze angle errors shift the efficiency peak . . . . .	85
6.3.3	Coating oxidation changes the reflectivity spectrum . . . . .	85
6.4	Grating results . . . . .	85
6.4.1	LEG . . . . .	85
6.4.2	IMP . . . . .	85
6.4.3	MEG . . . . .	85
6.4.4	HEG . . . . .	86
6.4.5	HRMEG and HRHEG . . . . .	86
<b>7</b>	<b>Real-World results: Why there aren't any yet</b>	<b>95</b>
<b>8</b>	<b>Future work: What should have been in Chapter 6</b>	<b>96</b>
	<b>References</b>	<b>97</b>
<b>A</b>	<b>Sample Appendix</b>	<b>97</b>
<b>B</b>	<b>Another Sample Appendix</b>	<b>98</b>

# LIST OF TABLES

4.1	Critical incidence angles for “total external reflection” at 410 eV for the grating coatings shown in Figure 4.15. . . . .	63
-----	--	----



# LIST OF FIGURES

2.1	A rather sensitive, compact, visible light spectrometer (Ocean Optics USB4000-UV-VIS). [TODO cite figure] It uses a blazed reflection grating optimized for 300nm light, and connects to a personal computer using USB. . . . .	3
2.2	In this schematic of a grating monochromator, light from the source is focussed by mirrors and dispersed by the grating. An exit slit picks out the desired wavelength or energy range, and blocks the remaining light. Depending on the design, the output wavelength can be adjusted by changing the angle of the grating, the angle of the mirrors, and/or the position of the exit slit. (The resolution – the energy bandwidth of the outgoing light – depends on the dispersion of the grating, the geometry, and the size of the exit slit. An ideal monochromator would produce truly monochromatic light, but this would require an infinitely small slit.) . . . . .	9
2.3	In this schematic of a grating spectrometer, mirrors are used to focus light from the source (or entrance slit) onto the detector, passing over a plane grating en-route to disperse the light by wavelength. (This is a <i>Czerny-Turner</i> arrangement, typical of compact visible-light designs like the one in Figure 2.1.) Since the grating diffracts different wavelengths at different angles, the intensity distribution across the detector surface creates to a spectrum related to the wavelength (or photon energy). . . . .	10
2.4	The spectrometer in this schematic uses a curved grating to both disperse light by wavelength, and focus it onto the detector. (This is typical of soft x-ray designs where the poor reflectivity of additional mirrors is usually avoided.) The intensity distribution along the surface of the detector can be converted into a spectrum with respect to wavelength or energy. Since the detector only captures a limited range of outgoing angles, it can be moved to pick out the desired wavelength window for each measurement. . . . .	10
2.5	The Petersen Plane Grating Monochromator, as implemented on the HE-PGM-3 beamline at BESSY. In (TODO REF), Petersen et. al. provide a good overview of monochromator focussing techniques, prior to the widespread adoption of VLS designs. . . . .	12
2.6	The SXF endstation spectrometer on Beamline 8.0.1 of the Advanced Light Source – a typical “workhorse” spectrometer. It uses spherical gratings in a Rowland Circle design; four gratings let users choose between higher resolution or higher efficiency at different energy ranges. The resolving power of this machine is compared with other leading spectrometers in Figure 5.1. Source: (TODO REF Jia paper) . . . . .	13
2.7	A detector image and corresponding spectrum produced by the SXF spectrometer in Figure 2.6. (This particular scan is of the nitrogen emission lines in nitrogen-doped zinc oxide.) The curvature of the spherical gratings provides focussing in the dispersion direction ( $x$ -axis), but unfortunately produces a curved image in the perpendicular direction ( $y$ -axis). This curvature is corrected by aligning rows along the red curve when the image is summed to produce the spectrum on the right. . . . .	14
2.8	The detector has an effective spatial resolution $dx$ which is the minimum distance required to resolve two adjacent incident rays. Except for the $n = 0$ order, the grating produces an angular dispersion $d\theta_{2,n}/d\lambda$ , which is the angular separation between infinitesimally-adjacent wavelengths. To increase the spacing between adjacent wavelengths on the detector, we can either increase the grating-detector distance $r'$ , or increase the angular dispersion. . . . .	15
2.9	A variety of soft x-ray spectroscopy techniques, and the number of gratings required in the beam path to accomplish each one. Of these techniques, those in <i>italic text</i> are possible on the REIXS beamline using the emission spectrometer endstation. For all these techniques – and particularly those using two gratings – more efficient gratings would increase the speed of experiments, improve the quality of data, and increase the minimum concentration of samples that can be feasibly studied. . . . .	19
3.1	A one-dimensional grating with in-plane incidence. . . . .	20

3.2	The Rayleigh expansion describes the electric field (TE polarization) or magnetic field (TM polarization) in homogenous media, above and below the grating. The terms in the expansion include a finite number of propagating plane waves – the diffraction orders – and an infinite number of decaying, or “evanescent” plane waves. From the geometry of the diffracted and transmitted wave vectors, we can derive the grating equation, but we need to solve the $A_n$ and $B_n$ coefficients to determine the efficiency of each order. . . . .	31
3.3	The total electromagnetic flux through this highlighted area ( $Q_2$ ) is used to define the grating efficiency of a diffraction order $n$ , as the ratio of the flux of the diffracted wave $\bar{S}_n^{(2)}$ compared to the incident wave $\bar{S}^{(2)}$ . . . . .	35
3.4	Arbitrarily-complicated structures can be handled by dividing the grating into layers, where each layer is either homogenous (constant refractive index), or modulated (with a refractive index that changes periodically as a function of $x$ at any given height $y$ ). . . . .	38
3.5	Modulated layers in a complicated stack of gratings. In between every layer, we can insert an imaginary, infinitely-thin homogenous layer where the Rayleigh expansion applies. The $A'_n$ and $B'_n$ expansion coefficients connect the boundary conditions between layers. Within each layer, the Rayleigh expansion does not apply – inside the grooves, the field cannot be represented as a simple sum of plane waves – and numerical methods are required to approximate it. . . . .	39
4.1	The RCW method approximates every real grating as a stack of rectangular gratings, where the boundary conditions are easy to solve and the problem can be reduced to algebraic methods. . . . .	40
4.2	This web application provides a graphical user interface for calculating grating efficiencies. Forms prompt users for the grating parameters... . . . . .	42
4.3	This web application provides a graphical user interface for calculating grating efficiencies. The results are plotted, and users can download a text-based table for further analysis. . . . .	44
4.4	This ‘Options’ page configures the numerical precision of the calculations, the diffraction orders of interest, and the polarization of the incident light. It also sets some other house-keeping options for where users want to store their data. . . . .	46
4.5	5 common groove profiles and their geometry parameters. The rectangular profile (a) and triangular profile (b) are idealized versions of those produced by mechanical ruling. The trapezoidal profile (c) is usually produced accidentally while trying to rule a rectangular profile with an imperfect ruling tip. The sinusoidal profile (d) is the natural shape produced by holographic ruling; the result can be ion-etched to approximate a triangular profile (e). . . . .	48
4.6	Henry Rowland’s ruling engine, mechanically engraving a grating under the operation of his instrument maker Theodore Schneider. Photographed at Johns Hopkins University, Baltimore. <b>Image credit:</b> EMILIO SEGRE VISUAL ARCHIVES/AMERICAN INSTITUTE OF PHYSICS/SCIENCE PHOTO LIBRARY (TODO ref <a href="http://www.sciencephoto.com/media/150151/enlarge">http://www.sciencephoto.com/media/150151/enlarge</a> ) . . . . .	49
4.7	The MIT ‘B’ ruling engine, now owned and operated by Richardson Gratings (a division of the Newport Corporation). It can rule gratings up to 420 mm wide, with grooves up to 320 mm long. The maximum groove density is 1500 lines/mm. Equipped with a servo system for advancing the grating carriage and interferometric feedback using frequency-stabilized lasers, it is the most accurate ruling engine in the world. To control for thermal expansion of the engine, the room temperature is controlled to 0.005°C; the system even compensates for changes in room air pressure since a change of just 2.5 mm of mercury will affect the refractive index of air (and therefore the interferometer wavelength) by one part per million. The entire engine is suspended from springs to dampen vibrations between 3Hz to 60Hz, which could otherwise be transmitted to the diamond tip. <b>Image credit:</b> DIFFRACTION GRATING HANDBOOK (TODO REF). . . . .	50

4.8	Master gratings can be replicated using a resin which hardens while in contact with the master (or subsequently, a submaster replicated from the first master). First, a parting agent (2) is applied to the surface of the master; it must be thin and uniform otherwise it will affect the profile. A metallic (aluminum or gold) coating about 1 $\mu$ m thick is then applied above the parting agent; this coating will eventually end up as the top surface of the replicated grating, and is called the <i>transfer coating</i> (3). Finally, the replica blank (5) is cemented from above using a resin ( $\sim$ 10 $\mu$ m thick) that hardens under UV exposure or over time (4). Once the resin is cured, the gratings are separated at the parting agent layer, leaving the hardened resin in the shape of the grooves, with the metal coating adhered to the top. This will produce a mirror image of the master grating; to create a perfect replica, this first replica needs to be replicated again. <b>Image credit:</b> DIFFRACTION GRATING HANDBOOK (TODO REF). . . . .	51
4.9	The Sheridan technique for recording pseudo-blazed holographic gratings uses a single light beam reflected back on itself to make a regular interference pattern of standing waves. The master substrate consists of a <i>transparent</i> photoresist material which is hardened or weakened by exposure to the light. By placing the substrate at an angle $\theta$ to the light path, the light and dark fringes are stretched out parallel to the grating surface; additionally, the angled incidence creates a lopsided sinusoidal intensity pattern that mimics blazed gratings. <b>Image credit:</b> DIFFRACTION GRATING HANDBOOK (TODO REF). . . . .	52
4.10	In the blazed condition, the desired order diffraction angle – in this case, 1st order – is aligned with the direction of specular reflection off the groove surfaces. . . . .	54
4.11	0th order, 1st order, and 2nd order efficiency of three different groove profiles, all optimized for use at 400eV. The blazed grating is superior in both 1st and 2nd order. All gratings: 1200 lines/mm, Platinum coating. Blazed: 1.46° angle, 60° anti-blaze angle. Sinusoidal: 13.7nm groove depth. Laminar (rectangular): 9.6nm groove depth, 50% duty cycle. . . . .	55
4.12	Increasing the groove density always decreases the diffraction efficiency – at least for all the useful orders ( $n \neq 0$ ). In these plots, we’ve tried to control for inter-related factors: For the blazed grating in (a), the blaze angle has been adjusted with the groove density (using Equation 4.8) to maintain the on-blaze condition. In (b), the sinusoidal grating depth was optimized at 1200 lines/mm, and then the depth-to-period ratio was maintained across changes to the groove density. . . . .	57
4.13	In the soft x-ray regime under grazing incidence, metal-coated dielectric gratings are indistinguishable from pure metal gratings... as long as the coating is thicker than $\sim$ 20nm (although the exact thickness depends on the material, photon energy, and incidence angle). These calculations show Pt coatings of varying thickness over an SiO <sub>2</sub> substrate, as well as an infinitely thick pure Pt grating. (Blazed grating, 1200 lines/mm, 1.46° blaze angle, 88° incidence. . . .	58
4.14	The reflectivity of a pure mirror at grazing incidence (88°), as a function of photon energy. Lighter elements like carbon and nickel have the highest peak reflectivity, but have strong absorption features. Heavier metals, particularly those within the platinum group, have reasonable reflectivity over the entire soft x-ray region of interest. Up to 200eV, Gold has a higher reflectivity than Pt and Ir. . . . .	59
4.15	A comparison of the mirror reflectivity, 0th order, and 1st order efficiency for different coating materials, as a function of photon energy. (Gratings: Sinusoidal profile, 88° incidence angle, 1200 lines/mm, 13.7nm groove depth) Note that the 1st order efficiency has energy-dependent features that aren’t visible in the simple reflectivity. . . . .	60
4.16	The effect of incidence angle on diffraction efficiency for various grating profiles. While the 0th order efficiency/reflectivity always increases as the incident light becomes more grazing, there is an optimal incidence angle below 90° for higher-order light. The critical angle for total external reflection in Platinum is 83.3°; clearly both the 0th-order and 1st-order efficiency drop off significantly below this angle. (Gratings: 1200 lines/mm, platinum coating, 400 eV; blaze angles and profiles as indicated.) . . . . .	64

4.17	While the blaze angle can always be used to tune a grating for a required incidence angle, there is still a particular <i>optimal</i> incidence angle that – when combined with a corresponding optimized blaze angle – would produce the highest achievable efficiency. This optimal angle doesn't seem to depend on the material, but only on the groove density and energy. (Gratings: all 1200 lines/mm; coatings, blaze angles, and energies as indicated.) . . . . .	65
4.18	Comparison of grating efficiency calculations to diffractometer measurements. Blazed grating, 1440 lines/mm, 2.2° blaze angle, 12.8° anti-blaze angle. Incidence: 160° constant included angle to the 1st inside order. . . . .	67
4.19	Comparison of grating efficiency calculations to diffractometer measurements. Rectangular grating, 600 lines/mm, 22.2 nm depth, 0.833 $\mu$ m valley width. Incidence: 167° constant included angle to the 1st inside order. . . . .	68
4.20	Comparison of grating efficiency calculations to diffractometer measurements. Trapezoidal grating, 300 lines/mm, 57° side angles, 49.3 nm depth, 2.46 $\mu$ m valley width. Incidence: 167° constant included angle to the 1st inside order. . . . .	69
4.21	Comparison of grating efficiency calculations to diffractometer measurements. Trapezoidal grating, 390 lines/mm, 57° side angles, 54 nm depth, 1.39 $\mu$ m valley width. Incidence: 160° constant included angle to the 1st inside order. . . . .	70
5.1	Resolving power performance comparison of existing spectrometer designs, calculated with all detectors having a 20 $\mu$ m pixel size. The legend specifies the spectrometer and grating choice (size and/or line density). [Source: David Muir M.Sc. thesis.] . . . . .	72
5.2	Approximation of the process used to design the optics of the REIXS spectrometer. [Source: David Muir M.Sc. thesis.] . . . . .	73
5.3	Common errors in the manufacture of ruled and holographic gratings. Holographic exposure creates a sinusoidal profile; subsequent ion-etching (b) can only approximate a triangular profile. Ruled gratings can suffer from blaze angle errors (c), or errors due to the shape and/or depth of the diamond tip (e). If the ruling engine introduces periodic errors in the groove position, this additional structure (d) creates additional diffraction peaks (ghosts). . . . .	73
5.4	todo todo todo . . . . .	75
5.5	Theoretical diffraction efficiency for the Low Energy Grating and Impurity Grating, as designed	77
5.6	Theoretical diffraction efficiency for the Medium Energy and High Energy Gratings, as designed	78
5.7	Theoretical diffraction efficiency for the High Resolution Gratings, optimized to be used in 3rd order. . . . .	79
6.1	The Low Energy Grating has a smooth regular profile, shown in this example image measured using an Atomic Force Microprobe (AFM). . . . .	81
6.2	The diffractometer on Beamline 6.3.2 at the Advanced Light Source allows for independently setting the angle of the gratings in the beam, and setting the angle of a pinhole photodiode detector. Upstream, filters in the beamline are used to remove contamination from the higher-order light of the monochromator. . . . .	82
6.3	The simplest diffractometer experiment scans the detector angle while illuminating the grating with a constant photon energy. The diffraction orders are visible as peaks along the outgoing angle axis (here, measured up from the grating surface at 0 °). The 0th order (reflection) peak is easily visible at twice the incident angle. (Grating: HRHEG) . . . . .	83
6.4	When the groove density of a grating is accurately known, the detector angle can be scanned in synchronization to keep it on the diffraction peak as the incident photon energy is scanned. This allows faster, continuous efficiency measurements as a function of photon energy. (Grating: LEG) . . . . .	84
6.5	Roughness of the grating surface scatters stray light outside the diffraction orders . . . . .	85
6.6	Unprotected Nickel quickly forms a surface oxide of NiO, which strongly reduces the reflectivity at the Oxygen edge (525eV) . . . . .	86
6.7	AFM measurements of the Low Energy Grating (LEG) profile, averaged along the grooves (TODO $\mu$ m x TODO $\mu$ m). The best-fit blaze angle is at the centre of the grating. . . . .	87
6.8	Theoretical and measured efficiency of the Low Energy Grating (LEG). . . . .	88

6.9	AFM measurements of the Impurity Grating (IMP) profile, averaged along the grooves (TODO um x TODO um). The best-fit blaze angle is at the centre of the grating. . . . .	89
6.10	Theoretical and measured efficiency of the Impurity Grating (IMP). . . . .	89
6.11	AFM measurements of the Medium Energy Grating (MEG) profile, averaged along the grooves (TODO um x TODO um). The best-fit blaze angle is at the centre of the grating. . . . .	90
6.12	Theoretical and measured efficiency of the Medium Energy Grating (LEG). . . . .	90
6.13	AFM measurements of the High Energy Grating (HEG) profile, averaged along the grooves (TODO um x TODO um). Severe ruling errors were apparent. The profile wasn't sufficiently triangular to attempt to fit a blaze angle. . . . .	91
6.14	Theoretical and measured efficiency of the High Energy Grating (LEG). . . . .	92
6.15	AFM measurements of the HighRes Medium Energy Grating (HRMEG) profile, averaged along the grooves (TODO um x TODO um). The best-fit blaze angle is at the centre of the grating. . . . .	93
6.16	AFM measurements of the HighRes High Energy Grating (HRHEG) profile, averaged along the grooves (TODO um x TODO um). The best-fit blaze angle is at the centre of the grating. . . . .	94

# LIST OF ABBREVIATIONS

LOF	List of Figures
LOT	List of Tables

# CHAPTER 1

## INTRODUCTION

blah blah blah

remember to include in introduction:

- - define diffraction grating (transmission, reflection)
- - orders... energy dispersiveness of non  $n=0$  orders
- - what is: diffraction efficiency

## CHAPTER 2

### MOTIVATION: WHY GRATING EFFICIENCY MATTERS

In 1821, when Joseph von Fraunhofer first resolved the sodium doublet lines using a diffraction grating he fashioned out of metal wire stretched between the grooves of two screws, he probably would not have anticipated the full scientific impact of his invention. Immediately, these observations helped reinforce Fresnel’s new wave theory of light (TODO REF “Short account of the Results of New Experiments on the Laws of Light, and their Theory”, Gilbert’s *Annalen der Physik*, band 74, p. 337-378. *Edinburgh Journal of Science*, VII., VIII., 1827, 1828). More importantly, the diffraction grating quickly became the foundation of spectroscopy, superseding the prism as a wavelength-dispersive element with higher resolution, and applicable to radiation from the infrared to x-rays. Eventually it would enable a huge range of experiments and new discoveries in all fields of science:

- In astronomy, Fraunhofer himself was the first to conduct spectroscopic measurements on light from the sun, moon, planets, and stars. Shifts in the position of well-known absorption lines proved, using the Doppler Effect, that the universe was expanding. Today, the composition and temperature of galactic objects is routinely measured using grating-based spectroscopic techniques.<sup>1</sup>
- In physics, visible spectroscopy of the hydrogen emission lines (Balmer Series) provided the data for Niels Bohr’s explanation of electron levels in the atom. Peter’s discovery of the Zeeman Effect – the splitting of emission lines in a magnetic field – was accomplished using a 20-foot Rowland Circle spectrometer; his results back up the modern version of quantum theory and the magnetic and spin quantum numbers.
- In chemistry, many elements (such as caesium and rubidium, identified by Kirchhoff and Bunsen in 1860) were first discovered in trace amounts using spectral analysis.
- Biologists and biochemists regularly use spectrophotometers to assay the concentration of a tagged reagent in a solution, making gratings a routine (and almost forgotten) tool in life sciences, pharmaceutical, and genetic research.

One common lamentation of the early spectroscopists was the faintness of the light leaving the grating; indeed, we can imagine them in darkened rooms, peering through telescope objectives, straining to make out

---

<sup>1</sup>In fact, the company that manufactured the gratings for this project also ruled the gratings used in the Hubble Space Telescope.



the faintest lines by eye (Figure TODO):

*Some lines can be distinguished in the spectrum of Procyon; but they are seen with difficulty, and so indistinctly that their positions cannot be determined with certainty. I think I saw a line at the position D in the orange.*

(TODO REF: Fraunhofer: Prismatic and Diffraction Spectra)

Photographic film – and later, modern imaging devices like CCDs – have probably succeeded in removing at least the physical pain associated with spectroscopy. However, increases in grating efficiency are just as important and useful today as they would have been in 1830. At visible wavelengths, more efficient gratings have already enabled a range of desktop spectrometers with very high sensitivity, such as the convenient USB-powered computer peripheral in Figure 2.1. Other wavelength ranges are more challenging; grating efficiency is especially critical to the variety of soft x-ray spectroscopy experiments now taking place at synchrotrons around the world, where the low reflectivity of optical materials makes it difficult to build highly efficient devices.



**Figure 2.1:** A rather sensitive, compact, visible light spectrometer (Ocean Optics USB4000-UV-VIS). [TODO cite figure] It uses a blazed reflection grating optimized for 300nm light, and connects to a personal computer using USB.

Simply put, the *diffraction grating efficiency* is the fraction of useful light out of a grating, relative to the amount of incoming light. (Chapter 3 offers a more formal definition.) While spectroscopy experiments vary in hardware, instrumentation, and purpose, we can make a pair of very general observations on why the grating efficiency is so important. From the point of view of an experimenter, it affects the amount of light available to their sample or detector, and therefore:

1. It affects the *speed* at which experiments can be done, by determining the exposure time required to record data of sufficient quality. In general, improvements in grating efficiency could reduce the amount of time for a given measurement – or equivalently, increase the number of measurements that could be taken in a certain time period. (For example, it takes anywhere from 3 minutes to several hours to measure a soft x-ray emission spectra on the 8.0.1 beamline at the Advanced Light Source, depending on the concentration of the sample and the desired resolution. One could argue that a factor of 2 optimization in the grating efficiency could almost double the number of users or the scientific throughput of the beamline.)

2. It affects the *feasibility* of doing an experiment in the first place. In situations where the experimental light source is extremely weak (for example, spectral analysis of faint stars in astronomy, or emission line measurements of trace elements in material science) the grating efficiency must be sufficient to raise the signal level above the background noise level seen by the detector. This is no longer a question of patience; if the signal level is below the background noise, our unhappy experimentalist could accumulate detector readings all day (or indefinitely) to no avail.<sup>2</sup>

The motivation for this project was therefore to understand the factors affecting the efficiency of diffraction gratings, and to apply this knowledge to their optimization. To accomplish this, we sought the ability to model gratings numerically and calculate their efficiency – a useful outcome for all grating spectroscopy applications.

However, we had another specific, selfish goal, which was actually our primary objective. At the onset of this project, we were involved in the optical design of a soft x-ray emission spectrometer, destined for use on the REIXS beamline at the Canadian Light Source. Working with David Muir, whose studies on spectrometer resolution are published in his M.Sc. thesis (TODO REF), we attempted to simultaneously achieve both *world-class resolution* and *record efficiency* for this machine.<sup>3</sup> Therefore, although the calculation techniques presented in this thesis are general, our examination of trends in diffraction efficiency looks most closely at the types of gratings used in the soft x-ray regime.

Given our specific motivation, the following sections explain the ultimate goal of such a machine, and show how gratings are typically employed in soft x-ray spectroscopy.

## 2.1 Soft X-ray Spectroscopy Techniques

Soft x-rays are photons with energies in the range of approximately 100 to 10 000 eV (or wavelengths of about 10 to 0.1 nm). Unlike with hard x-rays, which are highly penetrating, soft x-ray energies correspond to the binding energies of core-level electrons in common, lightweight elements. This property is ironically responsible for both the experimental challenge of working with them – they are quickly absorbed by any matter over very short distances – as well as their inherent usefulness as a probe of the electronic structure in materials.

Soft x-ray experiments use this light – usually created by a tuneable source such as a synchrotron – and focus it onto a sample to be studied. Two techniques provide complementary information: absorption spectroscopy, and emission spectroscopy.

---

<sup>2</sup>In fact, Zeeman mentions in the introduction to his paper that he was inspired by Faraday, who spent the last years of his life trying, “but in vain, to detect any change in the lines of the spectrum of a flame when the flame was acted on by a powerful magnet”. Zeeman decided “it might be yet worth while to try the experiment again with the excellent auxiliaries of the spectroscopy of the present time...”, brought on by Henry Rowland’s new mechanically-ruled reflection gratings.

<sup>3</sup>As it turns out, these two goals are implicitly in conflict; see Section TODO.

### 2.1.1 Absorption spectroscopy

Absorption spectroscopy measures the absorption rate of photons as a function of their wavelength (or energy). Experimentally, this is done by shining a monochromatic beam of light onto the sample and measuring the amount of light absorbed as the energy of the beam is changed.

Figure TODO shows the available absorption processes. When the photon energy increases to become sufficient to promote an electron transition in the material, dramatically more photons will be absorbed; this is known as an *absorption edge* (Figure TODO). Near the edge, as photons are absorbed by exciting electrons from the core level into unoccupied levels, adjacent unoccupied levels will have different probabilities of experiencing a transition, according to the quantum mechanical nature of the bonding in the material. (Note that according to the selection rule for dipole radiation, only electron transitions with a change in orbital angular momentum quantum number  $\Delta l = \pm 1$  are allowed, since momentum must be conserved and photons have an angular momentum [spin] of one unit.) The absorption will increase for energies where the transition probability is higher; therefore, the absorption spectrum is actually a measure of the *density of unoccupied states* for electrons in the material.<sup>4</sup>

One outstanding question concerns how the absorption rate is measured – how do we know how many photons were absorbed? Perfect absorption spectroscopy would shine the beam clear through the sample, and measure the intensity of the beam before and after to determine the fraction of light absorbed. While *transmission measurements* like this are feasible with hard x-rays, the short attenuation length of soft x-rays would require prohibitively thin samples for any beam to be left on the other side. Instead, different measurements are used as a proxy for the total absorption rate:

#### Total Electron Yield

For the excited electron, the most probable decay mechanism is to quickly relax into a lower-energy state, transferring its energy to a more loosely bound electron in the process. This secondary electron, known as an Auger electron, can then be ejected from the sample – assuming it is close enough to the surface. The **total electron yield** (TEY) method determines the absorption rate by measuring the electric current that must flow into the sample to neutralize the ejected electrons and keep the sample uncharged. (Experimentally, this is done by simply connecting a wire to the sample holder, and placing a sensitive ammeter along the path to a solid ground connection.)

TEY measurements are difficult for some samples, either because an insulating sample doesn't allow current to flow in to replenish the ejected electrons ("sample charging"), or because electrons ejected deep in the material are reabsorbed elsewhere. This makes TEY measurements most sensitive to absorption events on or near the surface ( $\sim 2\text{nm}$ ), and restricted to conductive samples.

---

<sup>4</sup>To be accurate, we should say the '*partial* density of unoccupied states', since the vacancy left behind in the original electron state ("core-hole") will affect the energy of the unoccupied states.

## Total Fluorescence Yield

Total Fluorescence Yield (TFY) measurements overcome these problems by using a light-sensitive detector near the sample. Although less probable than the Auger decay process, excited states can also relax by emission of a photon. Instead of ejected electrons, TFY measures the intensity of all photons emitted during the decay, which makes it applicable to both insulating and non-insulating samples. Because photons have a greater escape depth than electrons, this technique is also able to probe deeper within a material than TEY can. Due to the low probability of fluorescence transitions compared to Auger transitions (TODO ratio?), TFY measurements benefit greatly from concentrated samples and a light source which is capable of high intensity.

### 2.1.2 Emission spectroscopy

While absorption measurements provide information about the *unoccupied* states, we can also study what happens *after* the initial photon is absorbed. When a core-level electron is promoted by the absorption of a photon, it leaves behind a “core-hole”, and the whole atom (or molecule, or crystal) is left in an excited state. While there are many ways for the system to collapse back to the ground state, there is a small probability that some valence-band electron will decay to fill the core-hole by the emission of another photon. Since the energy of the emitted photon will match the energy difference between that valence electron and the core level, the intensity distribution of *all emitted light* will correspond to the probability of finding electrons in the valence band at those energies. Therefore, if we could collect the *fluorescence* emitted from the sample and plot its intensity as a function of energy, we would have a measure of the *density of occupied states* for electrons in the material. In this way, emission spectroscopy provides information on the bound electronic states, which is not present in the absorption spectrum.

Experimentally, XES measurements are done by illuminating the sample with a fixed photon energy above the absorption edge. The fluorescence is captured using an energy- (or wavelength-)sensitive detector which is tuned to the energy range just below the absorption edge. Over time, an intensity spectrum is built up from the collected photons (Figure TODO). Since fluorescence transitions are a random process, and highly improbable compared to other decay mechanisms like Auger decay, XES measurements require a sufficient exposure time to build up good statistics. They also benefit greatly from a high-intensity beam source and an efficient detector.

TODO Figure: XES process

### Resonant Inelastic X-ray Scattering (RIXS)

An advanced form of XES is known as RIXS (*Resonant Inelastic X-ray Scattering*). Instead of exciting a sample with a photon energy well above the absorption edge, the energy of the beam is tuned to match transitions previously identified in the absorption spectrum (or stepped incrementally through this range).

This allows the experimenter to preferentially excite into specific electronic states: at *resonance*, the transition probability will be extremely high because the exciting photon energy exactly matches the transition energy and the emitted photon energy.

RIXS is described as a two-step process which combines absorption and emission: from the initial electronic state, an incoming photon is absorbed, creating a “core-hole” and an excited electronic configuration. This intermediate state decays by the emission of another photon into a final state, and this transition doesn’t necessarily need to involve the original electron. The difference in energy of the emitted and incident photons provides an *energy-loss spectrum* describing the nature of excitations within the material.

As a two-step process, RIXS can probe transitions that would be forbidden by the dipole selection rule. For example, a 2p electron could be excited into a 3d state, and another 3d electron with a slightly different energy could collapse to fill the 2p hole, thereby creating the illusion of a ‘d-d’ excitation (TODO REF).

### 2.1.3 Importance of Soft X-ray Spectroscopy (SXS)

The soft x-ray spectroscopies are valuable tools in material science for their ability to gain insight into the electron environment within a material. Since the electronic structure determines the bonding between atoms and thereby a material’s mechanical, chemical, and physical properties, this is a big deal indeed. Additionally, x-ray spectroscopy has a few complementary advantages over other analytical techniques like (TODO what? neutron diffraction, ...?):

- It is **element-specific**: for a material containing a number of elements, it is usually possible to find absorption edges for each element that don’t overlap with the others, making it possible to independently probe the bonding environment of each. For example, in an organic sample containing carbon, nitrogen, and oxygen, one can probe the oxygen using the O 1s absorption at 543 eV, and then separately excite the nitrogen 1s electrons at 410 eV.
- More than being just element-specific, it is also **site-specific**: soft x-ray spectra make it possible to distinguish, for example, single-bonded carbon atoms at one location in a molecule from double-bonded atoms at another.

Additionally, there are a few experimental considerations which make SXS desirable:

- It can be done **non-destructively** on whole samples, without having to crush them into powders, dilute them in solution, etc. It can also allow in-situ measurements of samples created directly within the vacuum chamber – for example, crystal samples created using sputtering or vapour deposition techniques.
- Because of the high brightness and small size of synchrotron beams, it can be done on **very small samples**. Since the penetration depth of soft x-rays is so short, the interaction volume created by the beam will be tiny regardless of the sample thickness, making it a very useful characterization technique for thin film samples.

One obvious experimental disadvantage is that these techniques require access to synchrotron accelerators to produce the soft x-ray beam, which – at the time of this writing – are not yet available in convenient desktop or bench-top models. Additionally, since soft x-ray experiments must be performed under ultra-high vacuum (UHV) conditions (see section 2.2.3), samples must either be UHV-compatible or carefully isolated from the vacuum environment behind thin windows.

Despite this limitation, SXS techniques have created some notable and very interesting discoveries in physics; some highlights are listed here: (TODO: replace Robert’s comments with more formal explanation)

- First paper showing a comprehensive understanding of soft x-ray XAS in transition metal compounds. This is one of the highest cited soft XAS papers. Not only did it provide some state-of-the-art experimental spectra (at the time), but it gave a thorough interpretation of them:

Phys. Rev. B 42, 54595468 (1990) [http://prb.aps.org/abstract/PRB/v42/i9/p5459\\_1](http://prb.aps.org/abstract/PRB/v42/i9/p5459_1)

- First soft X-ray RIXS of transition metals. Not the highest impact paper as it was just on the dd excitations of MnO, but important for XES/RIXS nonetheless:

Phys. Rev. B 54, 44054408 (1996) [http://prb.aps.org/abstract/PRB/v54/i7/p4405\\_1](http://prb.aps.org/abstract/PRB/v54/i7/p4405_1)

- Using RIXS to measure dispersion of magnetic excitations in cuprate superconductors. This study also found a magnetic dispersion branch that had never been found before (by neutron scattering), and found that these types of materials are in inhomogenous spin states, revealing a bit more about the mysterious nature of cuprate superconductors:

Phys. Rev. Lett. 104, 077002 (2010) <http://prl.aps.org/abstract/PRL/v104/i7/e077002>

- This is a really cool recent paper. These guys measured very high resolution RIXS on O<sub>2</sub> gas, observing the vibronic structure (I would think for the first time with RIXS), and also observed spatial quantum beats in their spectra. It was basically a really cool way to observe quantum mechanical interference (kind of like a double-slit experiment, but using excitations into different states instead of transmission through different slits):

Phys. Rev. Lett. 106, 153004 (2011) <http://prl.aps.org/abstract/PRL/v106/i15/e153004>

## 2.2 Spectroscopy Instrumentation

The preceding sections make it clear that to perform soft x-ray spectroscopy experiments, we need three capabilities:

1. Obviously, one needs a source of soft x-rays – typically, the brighter, the better. This became possible with the advent of synchrotron particle accelerator facilities, which emit broad-spectrum x-rays as

relativistic electrons are forced to change their path by bending magnets.<sup>5</sup>

## 2. For absorption and emission spectroscopy:

From this broad spectrum of light, one needs to produce a nearly monochromatic beam of light to shine onto the sample, and must be able to adjust the energy of this beam. This is the role of a *monochromator*, which takes a broad-spectrum light source and extracts a small range of wavelengths from it (Figure 2.2).

## 3. Additionally, for emission spectroscopy:

One must be able to capture the light emitted from the sample and resolve it by wavelength. The end goal is to measure the relative intensity as a function of wavelength (or energy); this is accomplished using a *spectrometer* (Figure 2.4).

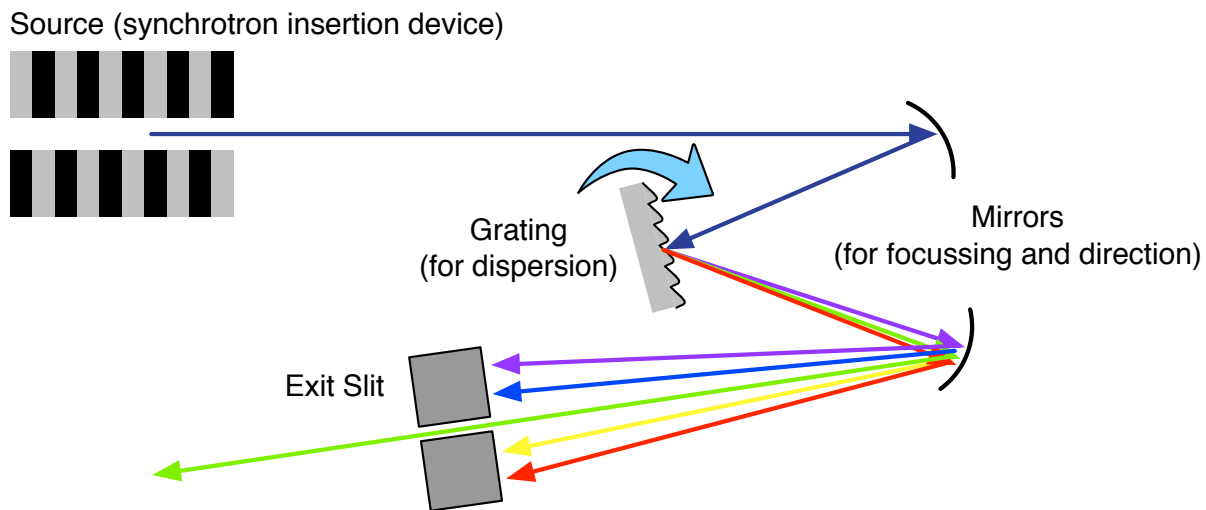


**Figure 2.2:** In this schematic of a grating monochromator, light from the source is focussed by mirrors and dispersed by the grating. An exit slit picks out the desired wavelength or energy range, and blocks the remaining light. Depending on the design, the output wavelength can be adjusted by changing the angle of the grating, the angle of the mirrors, and/or the position of the exit slit. (The resolution – the energy bandwidth of the outgoing light – depends on the dispersion of the grating, the geometry, and the size of the exit slit. An ideal monochromator would produce truly monochromatic light, but this would require an infinitely small slit.)

<sup>5</sup>Much more intense synchrotron light can be generated by “insertion devices” known as *undulators* and *wigglers*, in which an alternating array of magnets in a straight section of the accelerator forces the electron beam to bend many times over a distance of a few meters. Although light from insertion devices still contains a range of wavelengths, its spectrum consists of sharp intensity peaks which can be adjusted to the desired wavelength by changing the strength of the magnetic field. We intentionally avoid going into too much detail on synchrotron physics in this thesis; more information can be found in TODO REF.

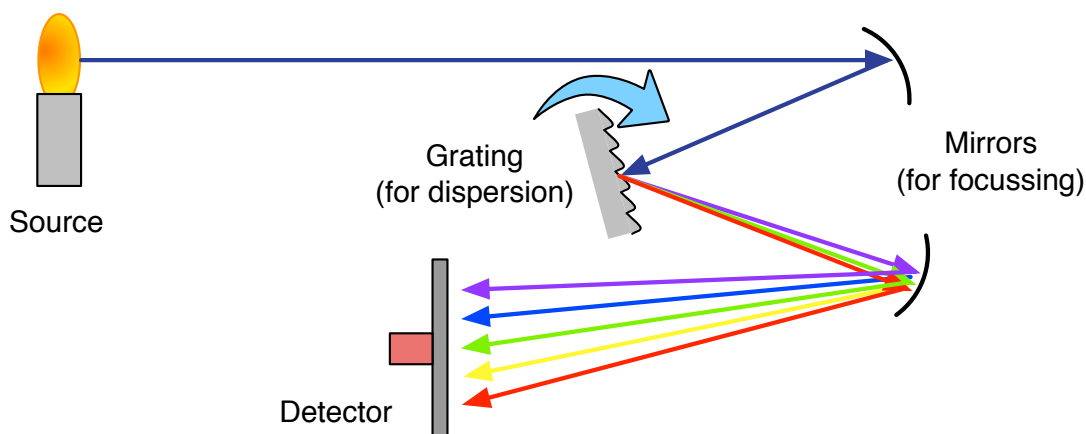


**Figure 2.3:** In this schematic of a grating spectrometer, mirrors are used to focus light from the source (or entrance slit) onto the detector, passing over a plane grating en-route to disperse the light by wavelength. (This is a *Czerny-Turner* arrangement, typical of compact visible-light designs like the one in Figure 2.1.) Since the grating diffracts different wavelengths at different angles, the intensity distribution across the detector surface creates to a spectrum related to the wavelength (or photon energy).

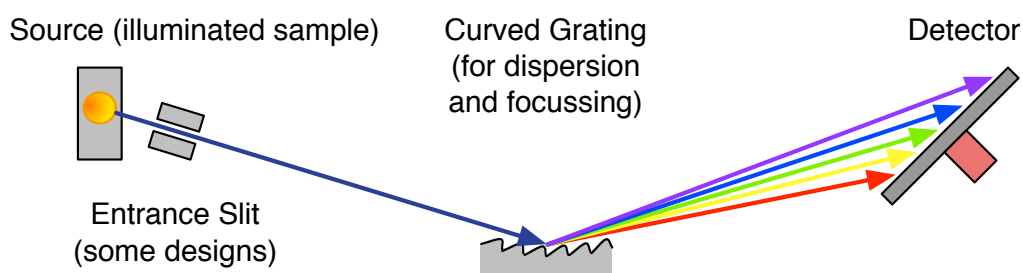


**Figure 2.4:** The spectrometer in this schematic uses a curved grating to both disperse light by wavelength, and focus it onto the detector. (This is typical of soft x-ray designs where the poor reflectivity of additional mirrors is usually avoided.) The intensity distribution along the surface of the detector can be converted into a spectrum with respect to wavelength or energy. Since the detector only captures a limited range of outgoing angles, it can be moved to pick out the desired wavelength window for each measurement.



## 2.2.1 Beamline optics: Monochromators and Spectrometers

### Monochromators

The role of a monochromator (shown schematically in Figure 2.2) is to pick out a narrow range of wavelengths from a chromatic light source, and deliver the monochromatic beam to the experiment. For infrared light out to soft x-rays, diffraction gratings provide the most efficient way of separating the incoming beam based on wavelength.<sup>6</sup> When the incidence angle and mounting angle of the grating are chosen to direct a single ( $n \neq 0$ ) diffraction order toward the exit slit, the wavelength term in the grating equation (equation 3.61)

$$n\lambda/d = \sin \theta_{2,n} - \sin \theta_2$$

creates a dependence on the sine of the outgoing angle  $\theta_{2,n}$ , so that shorter wavelengths leave more normal, and longer wavelengths leave at more grazing angles. Depending on the optical and mechanical design, the output wavelength can be selected by changing the angle of the grating, the angle of the mirrors (and hence the incidence angle onto the grating), and/or the position of the exit slit.

The resolution of the monochromator – ie: the range of wavelengths present in the output light – depends on the angular dispersion of the grating, the geometry, and the size of the exit slit; an ideal device would obviously produce a perfectly monochromatic beam, but this would require an infinitely-small exit slit. (In practice, the size of the exit slit is used to adjust the resolution, in an unavoidable trade-off against the amount of flux produced.) Resolution is measured as the energy bandwidth  $\Delta E$  (FWHM) for a given central energy (for example:  $\Delta E = 500\text{meV}$  at  $1000\text{eV}$ ). Often it is more convenient to normalize it as the *resolving power*  $RP = E/\Delta E$ , which has the benefit of being identical when measured in wavelength as well:

$$RP = \frac{E}{\Delta E} = \frac{\lambda}{\Delta \lambda} \quad (2.1)$$

In addition to dispersing the light by wavelength, monochromators must also act to *focus* light from the source, typically onto the exit slit, or onto the focal point of a downstream mirror. The schematic shown in Figure 2.2 is a *plane grating monochromator (PGM)*, where the focussing is accomplished using the two curved mirrors. Other designs use either a curved grating (*spherical grating monochromators*), or subtly change the line spacing of the grooves (*variable line space (VLS) grating monochromators*) to create the required focussing effect and reduce the number of optical elements. We avoid going into detail on focussing and monochromator design here; a good reference is provided in (TODO REF gratings, slits, and mirrors).

Our efficiency calculations in the rest of this thesis assume plane gratings and uniform line spacing; however, when curved gratings are used, the radius of curvature is typically so large – on the order of 10m – that the local changes over a grating surface (a few cm) don’t affect the efficiency. With VLS gratings,

---

<sup>6</sup>For hard x-rays, monochromators use “natural” diffraction gratings consisting of atomic planes in blocks of single crystals, since the inter-atomic spacing is comparable to the short wavelength of the light; these might be analyzed more appropriately using x-ray scattering theory than the electromagnetic approach we take for the man-made structures in this thesis.

the groove spacing may change by a few percent from end-to-end, and we've modelled these situations by averaging the results of multiple efficiency calculations using a set of representative points.

Figure 2.5 is a diagram of a plane grating monochromator, designed by Petersen (TODO REF) for the HE-PGM-3 beamline at BESSY, which became the basis for a lot of soft x-ray beamlines. Many designs offer multiple switchable gratings to let the user optimize between efficiency and resolution, since higher line density gratings are required to maintain the resolving power at higher energies. (As will be shown in Chapter 4, the grating efficiency declines with both increasing line density and increasing energy.) This one use a 366 line/mm grating to cover the energy range between 30eV and 700eV, a 1221 line/mm grating to cover the energy range between 120 and 1900eV.

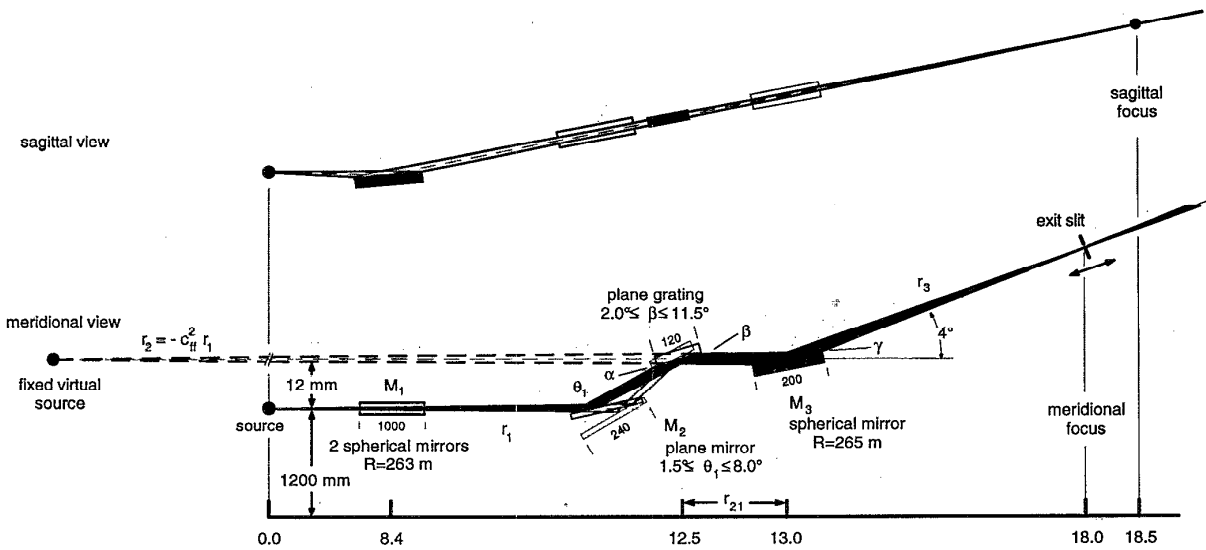


**Figure 2.5:** The Petersen Plane Grating Monochromator, as implemented on the HE-PGM-3 beamline at BESSY. In (TODO REF), Petersen et. al. provide a good overview of monochromator focussing techniques, prior to the widespread adoption of VLS designs.

## Spectrometers

If the goal of a monochromator is to produce monochromatic light, the goal of a spectrometer is to produce a *spectrum* – ie: to resolve the frequency components that exist in an unknown light source and measure their relative intensity. The device in Figure 2.3 is identical to the monochromator shown in Figure 2.2, except that the exit slit has been replaced by an area-sensitive detector. With the grating positioned so that an outgoing diffraction order (typically the 1st order, for best efficiency) lands on the detector, the angular dependence on wavelength puts short wavelengths onto the top of the detector, and long wavelengths onto the bottom of the detector. The intensity profile recorded across the detector surface is a spectrum, although some mathematical correction will need to be done to calibrate the energy axis, by mapping detector positions to diffraction angles, and diffraction angles to energy using the grating equation.

The spectrometer in Figure 2.4 is more representative of those used in soft x-ray applications, where the

low initial levels of fluorescence from the sample and the poor reflectivity of mirrors make it desirable to eliminate as many optical components as possible. Just like monochromators, spectrometers must focus light from the entrance slit – or directly from the source, in the case of slit-less designs – onto the detector. This is accomplished by using spherical gratings and arranging the geometry to exploit the *Rowland Circle* focussing condition discovered by Henry Rowland (TODO REF), or again by using VLS gratings to alter the shape of the focal curve. More information on spectrometer focussing can be found in the M.Sc. thesis by David Muir (TODO REF).

Like monochromators, spectrometer designs usually offer switchable gratings with different line densities and coatings, optimized for different energy ranges as we show in Chapter 5. Figure 2.6 shows a top and side view of the SXF endstation on Beamline 8.0.1 of the Advanced Light Source, a typical “workhorse” spectrometer, which balances moderate resolution with reasonable efficiency. It uses four gratings with groove densities of 600, 1000, and 1500 lines/mm to cover the energy range from 70 to 1200eV, and uses a 40mm wide multi-channel plate detector with an effective spatial resolution between 40 and 80um. Figure 2.7 shows an image recorded by that detector, and the corresponding spectrum.

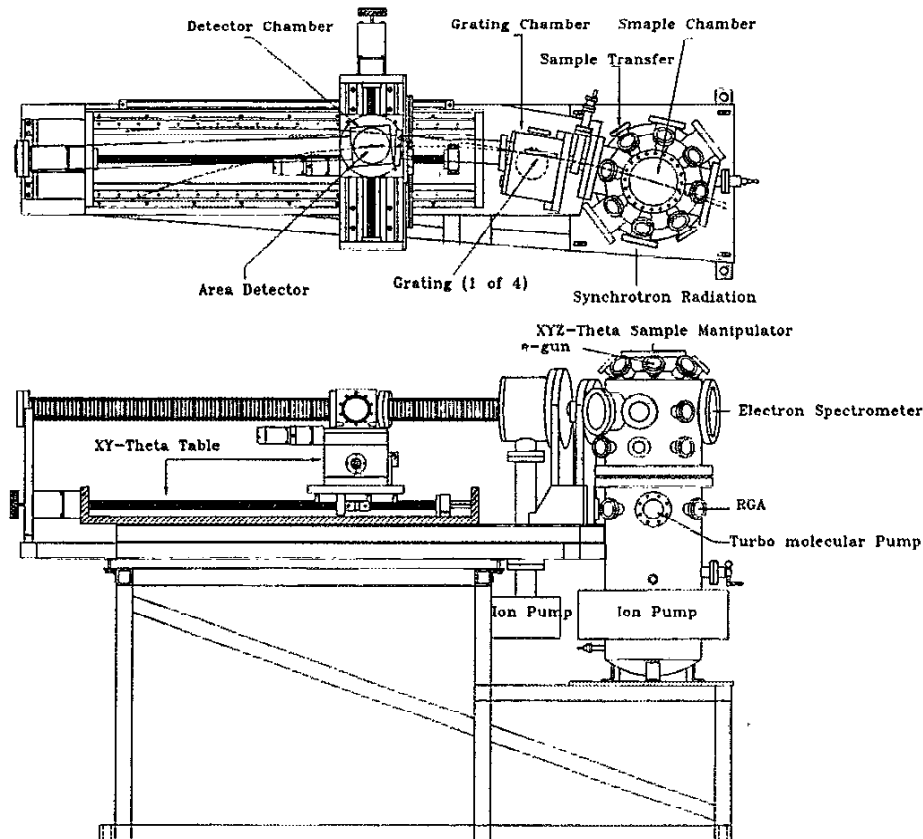


**Figure 2.6:** The SXF endstation spectrometer on Beamline 8.0.1 of the Advanced Light Source – a typical “workhorse” spectrometer. It uses spherical gratings in a Rowland Circle design; four gratings let users choose between higher resolution or higher efficiency at different energy ranges. The resolving power of this machine is compared with other leading spectrometers in Figure 5.1. Source: (TODO REF Jia paper)

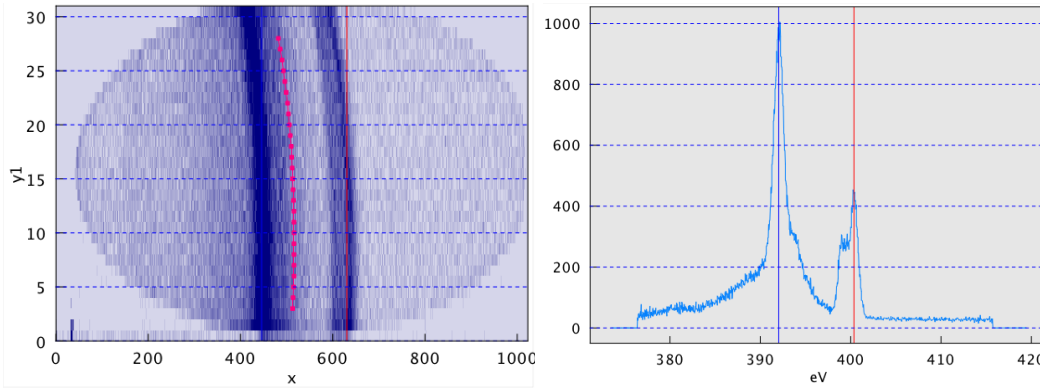


**Figure 2.7:** A detector image and corresponding spectrum produced by the SXF spectrometer in Figure 2.6. (This particular scan is of the nitrogen emission lines in nitrogen-doped zinc oxide.) The curvature of the spherical gratings provides focussing in the dispersion direction ( $x$ -axis), but unfortunately produces a curved image in the perpendicular direction ( $y$ -axis). This curvature is corrected by aligning rows along the red curve when the image is summed to produce the spectrum on the right.

### 2.2.2 Goals for Soft X-ray Instruments

In the design of both spectrometers and monochromators, there are two goals we’ve already mentioned that are important from the experimenter’s perspective:

- The **resolution** is important in order to see details in spectra and probe new science. On a soft x-ray beamline, the monochromator determines the resolution of an absorption scan, and the spectrometer determines the resolution of an emission scan. Both are involved in the experimental resolution of RIXS studies.
- The overall **efficiency** is important because it determines how much light is available, and indirectly how long it takes to generate enough photon interactions to record acceptable statistics. At a minimum, the efficiency must be high enough to produce a signal above the background noise level of the detector. Beyond this threshold, increases in efficiency make it faster to do experiments and let the user accomplish more science in their shift.

Since the probability of an excited atom decaying via fluorescence transitions is so low compared to other decay methods, the initial amount of light available in emission experiments is extremely low. This is further compounded in experiments on doped or dilute samples, when trying to observe the emission lines of the dopant elements. This means that efficiency is especially critical for emission spectroscopy.

What makes these two goals challenging is that they are inherently in tension. To see why, we consider as an example a simple emission spectrometer like the one shown again in Figure 2.8.

The immediate result of a spectroscopy experiment is the image produced along the detector surface. For all detectors – be they photographic film, multi-channel plate detectors, or CCDs – there is an *effective*

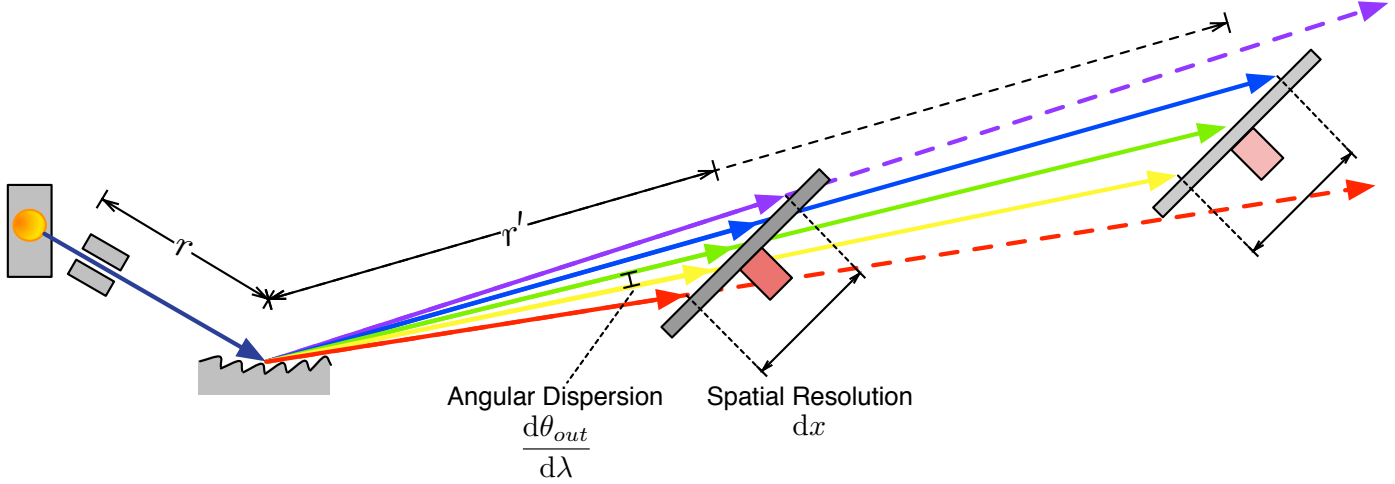


**Figure 2.8:** The detector has an effective spatial resolution  $dx$  which is the minimum distance required to resolve two adjacent incident rays. Except for the  $n = 0$  order, the grating produces an angular dispersion  $d\theta_{out}/d\lambda$ , which is the angular separation between infinitesimally-adjacent wavelengths. To increase the spacing between adjacent wavelengths on the detector, we can either increase the grating-detector distance  $r'$ , or increase the angular dispersion.

*spatial resolution*: the minimum distance along the detector that is required for two adjacent rays to be distinguished. For a given detector, if you wanted to increase the *energy resolution*, you would want to either

1. increase the angular dispersion of the grating – thereby increasing the angular separation between adjacent wavelengths, or
2. you would want to put the detector a long way from the grating, so that over distance the angular dispersion creates a large spatial separation between adjacent wavelengths.<sup>7</sup>

Both of these solutions inherently reduce the *geometric efficiency* of the spectrometer: the fraction of all photons captured by the detector assuming perfect mirror and grating efficiency. In the dispersion direction (or *meridional* direction, vertical in Figure 2.8), the detector will now only capture photons from a smaller energy range; the corresponding reduction in light gathered is an unavoidable tradeoff no matter what scheme is used to increase resolution. However, the second method – increasing the distance from the grating to the detector – reduces the solid angle captured by the detector also in the perpendicular direction (or *sagittal* direction, out of the page), further decreasing the geometric efficiency to an extent which depends on the nature of focussing in that direction.<sup>8</sup> The only way to increase resolution with only the minimum essential reduction in geometric efficiency is by using the first method: increasing the grating’s angular dispersion. By

<sup>7</sup>This is why currently the world’s two highest-resolution emission endstations use 10m- and 50m-long spectrometers; see section TODO.

<sup>8</sup>A complete analysis of focussing criteria would show that, at least for Rowland Circle spectrometers, increasing the source-grating distance requires an increase in both the entrance slit-grating distance, *and* an increase in the grating radius; both of these actions further decrease the geometric efficiency, possibly as a function of the cube of the distance. One could compensate by using larger gratings, but the maximum grating size must be limited to manage spherical aberrations; see (TODO REF).

differentiating the grating equation (3.61) with respect to wavelength (holding the incident angle  $\theta_2$  constant):

$$\begin{aligned}\frac{n\lambda}{d} &= \sin \theta_{2,n} - \sin \theta_2 \\ \frac{n}{d} &= \cos \theta_{2,n} \frac{d\theta_{2,n}}{d\lambda} \\ \frac{d\theta_{2,n}}{d\lambda} &= \frac{n}{d \cos \theta_{2,n}}\end{aligned}$$

we derive an expression for the angular dispersion; it's clear that to create more dispersion, we can either increase the groove density (decrease the groove spacing  $d$ ), or use a higher diffraction order  $n$ . Unfortunately, as will be shown in Chapter 5, both of these actions substantially reduce the *grating efficiency*. As an additional challenge, we can see that the dispersion will be reduced for higher energies, which leave the grating at more normal angles, creating a larger  $\cos \theta_{2,n}$ .

No matter which method is used, resolution and overall efficiency are in conflict. Whether it's a hit to the grating or to the geometry, increasing the resolution demands a reduction in efficiency and vice-versa, the cleverness of the beamline designer being measured in his or her ability to negotiate this compromise.

While this example examined resolution as seen by a spectrometer detector, the same unfortunate principles apply to monochromators as well.

### 2.2.3 Challenges of Soft X-ray Applications

All grating spectrometers, regardless of their wavelength range, are subject to the unavoidable tradeoff between resolution and efficiency. However, the nature of soft x-rays adds an additional set of challenges within this regime, which combine to make efficiency even more important.

#### UHV Compatibility

Because the energy of soft x-ray photons matches the energy of core level electron transitions in all light elements, they are readily absorbed in matter over very short distances. Just passing through (TODO) cm of nitrogen at atmospheric pressure is enough to attenuate a 1000eV beam by (TODO) percent. For starters, this means that all SXS experiments must be done under *ultra-high vacuum* (UHV) conditions, where the beam path has been evacuated of air and other contaminants, ideally to a pressure lower than  $10^{-8}$  torr. This is accomplished by using vacuum chambers and sealed beam pipes, pumped down using turbo-molecular pumps, ion pumps, and/or cryogenic pumps. At these low pressures, most common materials would “out-gas”, boiling off contaminants into the vacuum environment. As a result, chambers and instrumentation must be built using a restricted set of UHV-compatible materials (certain grades of stainless steel and aluminum, copper, gold, and some special ceramics and high-temperature thermoplastics). Anything that comes into contact with the vacuum environment must be carefully cleaned prior to assembly, and it's often necessary to “bake out” the chambers by heating them to temporarily raise the vapour pressure while pumping in order to remove water and other contaminants before eventually attaining UHV levels.

For the experimenter, UHV requirements also apply to samples. Liquid samples and non-UHV-compatible samples must be carefully enclosed and sealed behind thin windows to let the beam in. (Beryllium is often used in this application, due to its strength and relatively low absorption). Loading samples into the vacuum chamber must be done through an airlock, and remote actuators are required to adjust the sample position and the position of optical elements.

## Low Reflectivity and Grazing Incidence

Beamline designers face a more significant challenge when choosing optical elements. The easy absorption of soft x-rays means that mirror and grating surfaces have extremely low reflectivity at these wavelengths – at least at normal incidence. For visible light, the reflectivity of a polished aluminum surface approaches 90%; at 200eV, the reflectivity of the same surface is less than 0.005% (TODO REF [http://henke.lbl.gov/optical\\_constants/mirror2.html](http://henke.lbl.gov/optical_constants/mirror2.html)).

Two approaches are necessary to work around this challenge. Optical coatings need to be selected to avoid absorption edges in the region of interest. For example, carbon and nickel have relatively high peak reflectivities (Figure 4.14), but very strong absorption features at 284eV and 853eV respectively; these coatings would only be appropriate for optical elements used within a narrow wavelength range away from those edges. The absorption edges in heavy materials like gold and platinum are not as strong because they have more electrons (TODO make this more precise and science-y), and as result they have acceptable reflectivity over a wide bandwidth.

Second, mirrors and gratings need to be aligned and used at *grazing incidence* – ie, with the incident light striking them at glancing angles just a few degrees from parallel to their surface. At soft x-ray wavelengths, most materials have a refractive index with a real part *less than* one; the phase velocity of light is actually *faster* than it would be in a vacuum. This allows us to exploit the phenomenon of total internal reflection (TIR), except in this case it becomes a *total external reflection*, since the refractive index is higher in the grating material than it is in the vacuum above it. Just as with conventional TIR in glass and air, we can calculate a critical angle above which total external reflection will occur (See Section ??). For most metals, this turns out to be around 83 to 85 degrees from the surface normal.

## 2.3 REIXS spectrometer project

This thesis – and its motivation to establish a better understanding of diffraction grating efficiency – emerged from a primary engineering goal: to design and build a world-class emission spectrometer for the REIXS beamline at the Canadian Light Source. The REIXS (*Resonant Elastic and Inelastic X-ray Scattering*) beamline is optimized for material science experiments; it offers an elliptically-polarizing undulator to produce a high brightness beam of soft x-ray photons, and a high-resolution monochromator with a flux of  $\sim 10^{13}$  photons/second and a resolution of TODO eV. The beamline has room for two endstations; our task was to

build the emission spectrometer, which will be used for inelastic scattering experiments, while a team from the University of British Columbia built the second endstation used for elastic scattering measurements.

Chapter 5 describes the design process and the resulting optical design of the spectrometer. Used in combination with the work of David Muir on spectrometer resolution (TODO ref), the ability to model grating efficiencies allowed us to optimize the design for an intelligent compromise between these two competing goals. In the process, we discovered an efficiency peak in the 3rd order – typically assumed to be unusable – that prompted us to create an innovative design capable of reaching much higher resolution than would otherwise be possible given the space constraints of the beamline.

Figure ?? is a picture of the REIXS spectrometer as built, in August 2011.












(TODO picture)

## 2.4 Summary: Why Grating Efficiency Matters

Figure 2.9 lists a variety of soft x-ray spectroscopy techniques, and shows the number of gratings in the beam path to the detector for each. Of these techniques, those in *italic text* are possible on the REIXS beamline; the remaining are possible on other beamlines at the CLS. For all of these techniques, the ability to create more efficient gratings would increase the speed of experiments, improve the quality of data, and increase the minimum concentration of samples that can be feasibly studied.

Conversely, during the design phase of these kinds of instruments, the unavoidable tradeoff between resolution and efficiency implies that accurate predictions of the grating efficiency could ironically be used improve *resolution*: by deliberately sacrificing efficiency, designers could push their resolving power to the limit once the efficiency is known to be “good enough”.



	Photon In	Electron In
Electron Out	<i>Near-edge X-ray Absorption Fine Structure (NEXAFS):</i>  <i>electron yield</i>	Auger Electron Spectroscopy (AES)
	Extended X-ray Absorption Fine Structure (EXAFS):  electron yield	
	X-ray Photoelectron Spectroscopy (XPS) 	
Photon Out	<i>Soft X-ray Emission Spectroscopy (SXE)</i>  	<i>Inverse Photoelectron Spectroscopy (IPES)</i> 
	<i>Resonant Inelastic X-ray Spectroscopy (RIXS)</i>  	
	X-ray Excited Optical Luminescence (XEOL)  	
	<i>NEXAFS: fluorescence yield</i> 	

**Figure 2.9:** A variety of soft x-ray spectroscopy techniques, and the number of gratings required in the beam path to accomplish each one. Of these techniques, those in *italic text* are possible on the REIXS beamline using the emission spectrometer endstation. For all these techniques – and particularly those using two gratings – more efficient gratings would increase the speed of experiments, improve the quality of data, and increase the minimum concentration of samples that can be feasibly studied.

## CHAPTER 3

### THEORY: HOW TO CALCULATE GRATING EFFICIENCY

#### 3.1 Introduction of grating theory

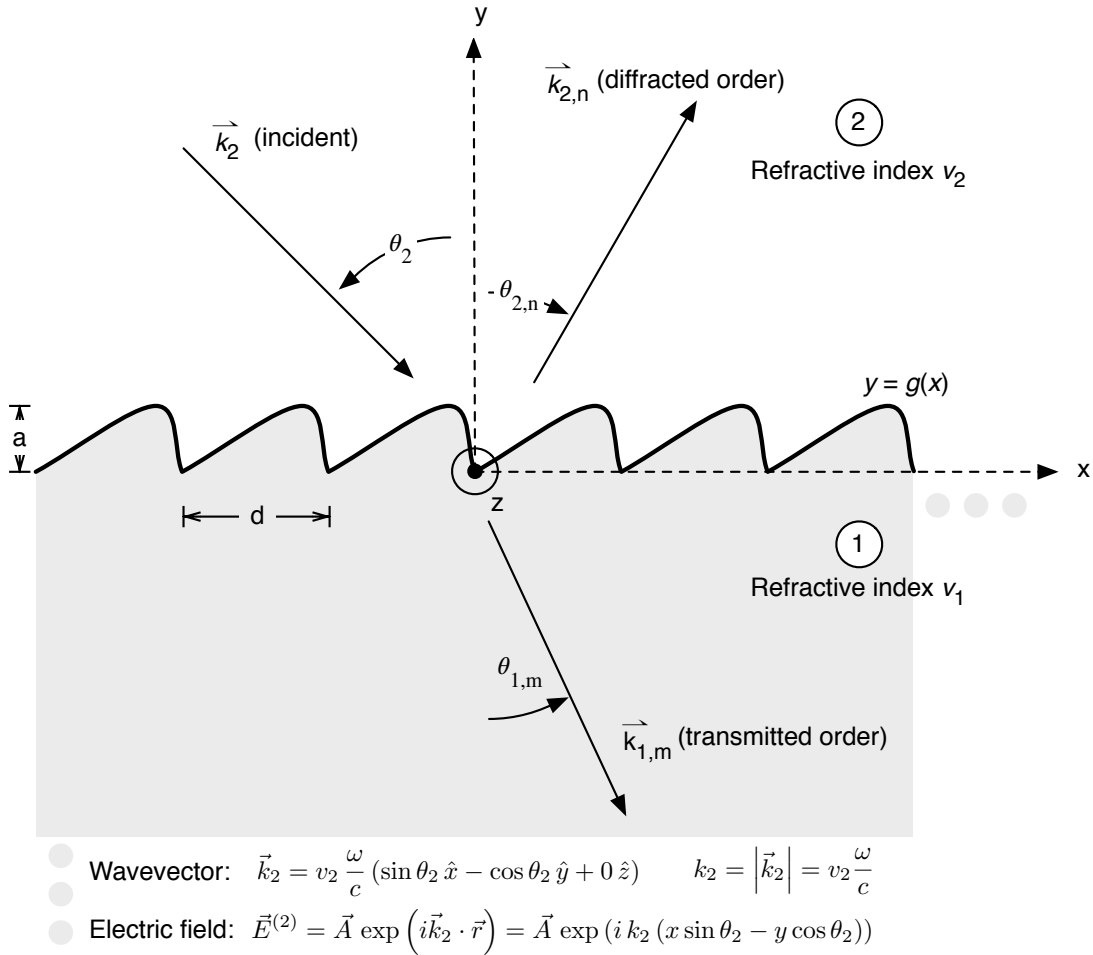


**Figure 3.1:** A one-dimensional grating with in-plane incidence.

For centuries, we've known that gratings reflect and transmit light into a set of discrete angles – called *orders* – where the angles depend on the wavelength (Figure 3.1). A variety of simple proofs have been used to explain this. In undergraduate books, the grating equation is introduced as a consequence of constructive

interference from a linear array of coherent emitters. (This makes sense for a slotted transmission grating, but it's less obvious why an arbitrarily-shaped periodic structure like those shown in Figure TODO would behave the same way.) Other proofs – such as those using Fermat's Principle to minimize an optical path function with a phase offset introduced by the grating [TODO ref] – are general enough to explain the diffraction orders, but they don't say anything about how much light goes into each.

It is only within the last twenty years that mathematical techniques and computational power have advanced enough to accurately model the electromagnetic field of light within and around the surface of a grating, allowing us to actually determine how energy is distributed between the orders, and how much is absorbed within the grating. Although many researchers [TODO ref] have contributed to advancements in numerical grating theory over the last forty years, the most recent breakthroughs have come from the the work of Li [TODO ref] on the factorization of truncated Fourier series, and have been synthesized by Neviere and Popov [TODO Ref, ref].

This chapter lays the groundwork for a full electromagnetic theory describing the interaction of light waves with periodic structures. The notation presented here is consistent with the notation used by Neviere in [TODO ref]. However, before diving into the details of the mathematics, it might be useful to summarize the basic physical principles behind the solution:

1. The theory starts by using the Maxwell equations to derive a 2nd-order wave equation for the electric and magnetic field of the light. According to classical optics, the incoming light can be divided into two independent polarization components; the “Transverse Electric” (TE) component has its *electric* field vector always parallel to the  $z$ -axis in Figure 3.1, and the “Transverse Magnetic” (TM) component has its *magnetic* field vector always parallel to the  $z$ -axis. Due to the beautiful symmetry of the Maxwell equations, it turns out that the wave equation for the electric field in TE polarization is the same as the equation for the magnetic field in TM polarization, and for most of the theory we can use the same mathematics to work with both, referred to as the “general field” or just “the field”.<sup>1</sup> Because the TE and TM polarizations are independent, we can solve the grating problem for both separately, and then combine the diffracted field solutions in proportion to the polarization of the incident light.
2. Because the grating is periodic, we use Fourier series expansions in the horizontal direction to express both the permittivity of the grating material, and the field itself. In the vertical direction, there are three distinct regions:
  - Region 2: above the grooves, where the refractive index is uniform ( $v = v_2$ );
  - Inside the grooves – the “modulated region” – where the refractive index changes as a function of the  $x$  and  $y$  position: it is either  $v_1$  or  $v_2$ ;

---

<sup>1</sup>While the wave equation is the same for both the TE electric field and the TM magnetic field, the boundary conditions for the fields at the grating interface are different and need to be handled separately. This is responsible for the difference in efficiency dependent on polarization.

- Region 1: below the grooves, inside the grating substrate, where the refractive index is again uniform ( $v = v_1$ ).

### 3. Above and below the grooves:

By using the grating as a periodic operator and applying boundary conditions for the field at infinite, we can prove that light is reflected and transmitted at discrete angles, and that a Fourier sum of plane waves known as the Rayleigh Expansion can be used to express the total field which satisfies the wave equation in this region. Each propagating plane wave corresponds to a diffraction “order”, and once we know the angle of the incident light, we can determine the angles of the diffraction orders (Figure 3.2). At this point, the Rayleigh expansion still has unknown coefficients, and we need to determine these coefficients to find out how much energy is diffracted into each order.

### 4. Within the grooves:

However, the field within the grooves depends on the exact shape of the groove profile and the interaction of light within the material. It cannot be simply represented as a sum of plane waves, and the boundary conditions are complicated. There are two leading methods used to handle this. Both express the wave equation using Fourier expansions for the field and for the grating permittivity. (These expansions would theoretically be infinite sums, therefore they need to be truncated to be approximated using computer calculations. Special rules apply for accurately calculating the products of truncated Fourier series, discovered by Li in (TODO ref).)

- (a) In the “Rigorous Coupled Wave” (RCW) approach, the grating groove shape is sliced into thin layers (Figure 4.1) and approximated with vertical walls between layers (the “staircase approximation”). This simplifies the boundary conditions, so that at every layer the wave equation can be converted into a set of simultaneous linear equations and solved algebraically. The effect of each layer on the field is propagated to the next using matrix methods.

This approach is computationally efficient, and has been known to work accurately in TE polarization. However, in TM polarization, the results often don’t match experimental measurements, because the staircase approximation introduces sharp corners and artificially large electric field components at the step boundaries.

- (b) In the “Differential Method” approach, we numerically integrate the wave equation many times using different assumed initial values, to generate a complete orthogonal set of particular solutions. Then we use techniques of linear algebra to solve for the coefficients of the general solution that satisfy the boundary conditions along the grating interface.

5. Finally, most common grating structures consist of one (or often many) stacked layers<sup>2</sup> (Figure 3.4). In classical optics, the *reflection matrix* and *transmission matrix* are conveniently used to propagate an

---

<sup>2</sup>For example, dielectric gratings with a metal coating used for soft X-ray beamlines, gratings with thin-film multilayer coatings, etc.

incoming field through an optical layer. We can generalize this concept to gratings by defining a matrix which maps the Rayleigh coefficients of the incident field to the coefficients of the field that is reflected and transmitted by each layer. The matrices for each layer can then be multiplied together to find the effect of the complete grating; this is known as the “T-matrix” approach. While theoretically sound, the T-matrix becomes unstable in computer calculations because rounding errors introduce instability into diverging exponential functions. An alternative formulation called the “S-matrix” approach defines a matrix at each layer which represents the cumulative effect of *all layers below and including that layer* on the incident field; by definition, this matrix remains bounded and is safe to use for numerical calculations.

### 3.1.1 Simplifying Assumptions

Before we tackle the mathematics of grating theory, this section defines the geometry and terminology we’ll use throughout this text, and introduces some assumptions that simplify the problem. Figure 3.1 shows a side view of a reflection grating, in the following situation:

1. The mean surface of the grating is in the  $x - z$  plane, with the grooves running parallel to the  $z$ -axis. The groove profile is periodic and repeats every distance  $d$  along the  $x$ -axis.
2. The grating is illuminated with a light ray travelling parallel to the  $x - y$  plane (ie: within the plane of the page). This is referred to as “in-plane incidence”, and is typical of how most monochromators and spectrometers are used. (When the incident ray has a component in the  $z$ -direction, the diffraction peaks end up dispersed over the surface of a three-dimensional cone, and this is referred to as “conical mounting”.)

These first two simplifications reduce the grating problem to two dimensions, since the whole system is unchanged by translation along the  $z$ -axis.

Additionally, we assume that:

1. The incident light can be represented as a plane wave, infinite in extent.
2. The grating also stretches forever in the  $x$ - and  $z$ -directions.

Typical gratings used in soft X-ray devices are much much larger (typically: 40 mm) than their groove spacing  $d$  (typically: a few  $\mu\text{m}$ ). As long as they are illuminated with collimated light having a beam width much larger than the groove spacing, both of these assumptions seem reasonable.

Finally, to simplify the electromagnetic field calculations, we assume that

1. The grating material is non-magnetic, with a permeability of  $\mu_0$ .
2. The dielectric constant  $\epsilon$  of the grating material is the same in all directions.

(These last two assumptions are also necessary to keep us within a two-dimensional problem. If the material is non-isotropic, then the dielectric constant  $\epsilon$  becomes a tensor  $[[\epsilon]]$  and the problem requires a full 3D analysis.)

These assumptions make the grating theory much simpler to present in this chapter. However, it should be noted that at the expense of larger matrices and higher mathematical complexity, it is possible to express the same theory in the full three-dimensional case, which enables the analysis of exotic situations like conical mounted gratings, crossed 2D gratings, and non-isotropic materials. [Ref: Neviere Ch. 5] provides a derivation of the full general 3D version.

### A few brief notes on notation:

- Quantities that change depending on the grating region are subscripted to indicate which region they are in. For example,  $k_2$  and  $v_2$  designate the wave vector and refractive index, and  $\theta_{2,n}$  the angle of the  $n$ -th order ray, in Region 2 above the grating. Eventually, we will tackle layered gratings with many numbered regions, and the subscript convention will become very helpful.
- Angles are measured from the surface normal as shown in Figure 3.1. There are two different sign conventions in common use; we will use positive angles for both the incident ray ( $\theta_2$ ) and the diffracted ray ( $\theta_{2,n}$ ) when they are on opposite sides of the surface normal. Transmitted rays ( $\theta_{1,n}$ ) are also measured using positive angles from the  $-y$  axis, as shown in Figure 3.1.<sup>3</sup>

### 3.1.2 Electromagnetic field and polarization

In Figure 3.1, incoming light strikes the grating along wavevector  $\vec{k}_2$  at an angle  $\theta_2$  from perpendicular to the grating plane.

$$\vec{k}_2 = v_2 \frac{\omega}{c} (\sin \theta_2 \hat{i} - \cos \theta_2 \hat{j} + 0 \hat{k}) \quad (3.1)$$

(We use  $v$  to designate the refractive index – in this case, in Region 2 above the grating, which is normally air or vacuum.  $\omega = 2\pi f$  is the angular frequency of the light, and  $c$  is the speed of light in vacuum.)

The incoming light is a travelling electromagnetic plane wave with sinusoidal dependence on time. We can express the electric field vector using the complex exponential form:

$$\vec{E}_{incident} = \vec{A} \exp(i(\vec{k}_2 \cdot \vec{r} - \omega t)) = \vec{A} \exp(i k_2 (x \sin \theta_2 - y \cos \theta_2)) \exp(-i\omega t) \quad (3.2)$$

where the true (physical) field is contained in the real part. Since all fields will have the same harmonic dependence on time, we drop the  $e^{-i\omega t}$  factor from here on. (The scalar  $k_2$  is simply the magnitude of  $\vec{k}_2$ , ie:  $|\vec{k}_2| = v_2 \omega / c$ .)

---

<sup>3</sup>The sign convention for diffraction angles affects the sign in the right-hand side of the grating equation (3.61). In North American literature it is more common to measure all angles positive counter-clockwise from the surface normal; this creates a ‘+’ rather than a ‘−’ in the grating equation.

The electric field vector is always perpendicular to the direction of the wave  $\vec{k}_2$ , but can have an arbitrary polarization determined by  $\vec{A}$ . This can always be expressed as a superposition of two orthogonal components:

- The TE (transverse electric) polarization represents the component of the electric field vector parallel to the  $z$  axis (ie: into the page). For a pure TE wave, the  $E_x$  and  $B_z$  fields are always 0.
- The TM (transverse magnetic) polarization represents the component of the electric field vector in the  $x - y$  plane (ie: the magnetic field vector is along  $z$ ). For a pure TM wave, the  $E_z$  and  $B_x$  fields are always zero.

In general, the grating problem will be solved by applying the Maxwell equations to the incident electric field, according to the boundary conditions imposed by the grating. By solving it separately for each polarization case (TE and TM), we can simplify these equations. In the end, we can superpose the results we calculate for the outgoing fields, weighted based on the actual polarization of the incident light.

### 3.1.3 Maxwell's equations for sinusoidal time-varying fields

Our assumptions in Section 3.1.1 mean that the gratings are not loaded with free charge, or carrying free currents. Therefore, two relevant Maxwell equations are:

$$\nabla \times \vec{E} = -\frac{\partial \vec{B}}{\partial t} \quad (3.3)$$

$$\nabla \times \vec{B} = \mu\epsilon \frac{\partial \vec{E}}{\partial t} \quad (3.4)$$

For sinusoidal time-varying fields, the electric field  $\vec{E}$  is proportional to  $e^{-i\omega t}$ , so the time derivatives reduce to:

$$\nabla \times \vec{E} = i\omega\mu\vec{H} \quad (3.5)$$

$$\nabla \times \vec{H} = -i\omega\epsilon\vec{E} \quad (3.6)$$

or, expressed in Cartesian coordinates:

$$\frac{\partial E_z}{\partial y} - \frac{\partial E_y}{\partial z} = i\omega\mu H_x \quad (3.7)$$

$$\frac{\partial E_x}{\partial z} - \frac{\partial E_z}{\partial x} = i\omega\mu H_y \quad (3.8)$$

$$\frac{\partial E_y}{\partial x} - \frac{\partial E_x}{\partial y} = i\omega\mu H_z \quad (3.9)$$

$$\frac{\partial H_z}{\partial y} - \frac{\partial H_y}{\partial z} = -i\omega\epsilon E_x \quad (3.10)$$

$$\frac{\partial H_x}{\partial z} - \frac{\partial H_z}{\partial x} = -i\omega\epsilon E_y \quad (3.11)$$

$$\frac{\partial H_y}{\partial x} - \frac{\partial H_x}{\partial y} = -i\omega\epsilon E_z \quad (3.12)$$

Since the grating and the incident light are uniform along the  $z$ -axis, all of the partial derivatives with respect to  $z$  are 0. For TE polarization, since  $E_x$  and  $H_z$  are 0, equations (3.7, 3.8, and 3.12) are decoupled into

$$\frac{\partial E_z}{\partial y} = i\omega\mu H_x \quad (3.13)$$

$$-\frac{\partial E_z}{\partial x} = i\omega\mu H_y \quad (3.14)$$

and

$$\frac{\partial H_y}{\partial x} - \frac{\partial H_x}{\partial y} = -i\omega\epsilon E_z \quad (3.15)$$

We can use (3.13) and (3.14) to eliminate  $H_x$  and  $H_y$  in (3.15):

$$\frac{i}{\omega\mu} \frac{\partial^2 E_z}{\partial x^2} + \frac{i}{\omega\mu} \frac{\partial^2 E_z}{\partial y^2} = -i\omega\epsilon E_z \quad (3.16)$$

Note that  $\epsilon$  is a function of position  $\epsilon(x, y)$ , since it changes whether inside the grating or above the grating. Since

$$k^2(x, y) = v^2(x, y) \omega^2 / c^2 = \omega^2 \mu \epsilon(x, y) \quad (3.17)$$

we get a single second-order wave equation in  $E_z$

$$\nabla^2 E_z + k^2 E_z = 0 \quad (3.18)$$

where  $E_z = E_z(x, y)$  and  $k^2 = k^2(x, y)$  are both functions of position.

For the case of TM polarization, the Maxwell equations (3.10, 3.11, and 3.9) reduce to

$$\frac{\partial H_z}{\partial y} = -i\omega\epsilon E_x \quad (3.19)$$

$$-\frac{\partial H_z}{\partial x} = -i\omega\epsilon E_y \quad (3.20)$$

$$\frac{\partial E_y}{\partial x} - \frac{\partial E_x}{\partial y} = i\omega\mu H_z \quad (3.21)$$

and an identical procedure produces the wave equation in  $H_z$ :

$$\nabla \left[ \frac{1}{k^2} \nabla H_z \right] + H_z = 0 \quad (3.22)$$

$$\nabla^2 H_z + k^2 H_z = 0 \quad (3.23)$$

Due to the (near) symmetry of the Maxwell equations, the form of the wave equation is the same for the  $H_z$  field in TM polarization as it is for the  $E_z$  field in TE polarization. To solve the grating problem, we will need to find the solution to this wave equation in the presence of the grating boundary conditions.<sup>4</sup>

---

<sup>4</sup>Although the wave equation is the same, the boundary conditions for electric and magnetic fields are different at the grating boundary where  $\epsilon$  and  $v$  change suddenly – for example, the normal component of the electric field is discontinuous, while the normal component of the magnetic field is continuous. This leads to a difference in the TE and TM efficiency.



### 3.1.4 Periodicity of gratings and fields (aka, pseudo-periodic functions and the Fourier basis)

The periodic nature of the grating grooves immediately hints that we could represent them conveniently using a Fourier series. But can a Fourier expansion also be used to represent the fields  $E_z$  and  $H_z$ ?

Here we define  $u = E_z$  when working in TE polarization, and  $u = H_z$  when working in TM polarization; it represents the “generic field”. The grating can be imagined as an operator  $\mathbb{G}$  that transforms the incident field  $u_i$  into a diffracted field  $u$ :

$$u(x, y) = \mathbb{G} u_i(x, y) \quad (3.24)$$

Because the grating is periodic and extends forever, the operator  $\mathbb{G}$  is invariant (doesn’t change) under translation by a grating period:  $x \rightarrow x + d$ .

$$u(x + d, y) = \mathbb{G} u_i(x + d, y) \quad (3.25)$$

Since the incident light arrives at an angle  $\theta_2$ , this translation will add an extra path distance  $d \sin \theta_2$  to the incident wave  $u_i$ , for a phase change  $e^{ik_2 d \sin \theta_2}$ :

$$u_i(x + d, y) = e^{ik_2 d \sin \theta_2} u_i(x, y) = C u_i(x, y) \quad (3.26)$$

where the constant  $C$  has been matched to  $e^{ik_2 d \sin \theta_2}$ .

Because the set of coupled Maxwell partial differential equations (3.7 - 3.12) is linear, any solution multiplied by a constant  $C$  is still a solution:

$$u(x, y) = \mathbb{G} (u_i(x, y)) \quad (3.27)$$

$$C u(x, y) = \mathbb{G} (C u_i(x, y)) \quad (3.28)$$

$$C u(x, y) = \mathbb{G} u_i(x + d, y) \quad (3.29)$$

but since  $\mathbb{G} u_i(x + d, y) = u(x + d, y)$  also,

$$C u(x, y) = u(x + d, y) \quad (3.30)$$

In other words, the total field translated by one period  $d$  is equal to its untranslated self, multiplied by a complex constant:

$$u(x + d, y) = C u(x, y) = e^{ik_2 d \sin \theta_2} u(x, y) = e^{i\alpha_0 d} u(x, y) \quad (3.31)$$

where we’ve defined

$$\boxed{\alpha_0 \equiv k_2 \sin \theta_2} \quad (3.32)$$

This is known as a *pseudo-periodic* relationship:

$$u(x + d, y) = e^{i\alpha_0 d} u(x, y) \quad (3.33)$$

since a true (strictly) periodic relationship would have the form:

$$v(x + d, y) = v(x, y) \quad (3.34)$$

However, we can easily create such a function by defining  $v \equiv e^{-i\alpha_0 x} u$ . As a legitimately periodic function,  $v$  can be represented as a Fourier series expansion on the grating period  $d$ :

$$v(x, y) = e^{-i\alpha_0 x} u(x, y) \quad (3.35)$$

$$v(x, y) = \sum_{n=-\infty}^{\infty} u_n(y) e^{i2\pi n x/d} \quad (3.36)$$

$$u(x, y) = e^{i\alpha_0 x} \sum_{n=-\infty}^{\infty} u_n(y) e^{i2\pi n x/d} \quad (3.37)$$

If we define

$$\boxed{\alpha_n \equiv \alpha_0 + 2\pi n/d} \quad (3.38)$$

we can express the total field as something that looks *very close* to a Fourier series expansion:

$$u(x, y) = \sum_{n=-\infty}^{\infty} u_n(y) e^{i\alpha_n x} \quad (3.39)$$

This is the Fourier basis for the total field  $u = E_z$  or  $H_z$ , with an infinite number of Fourier coefficients  $u_n$ . (Eventually, we will need to truncate this series to work with it numerically.)

### 3.1.5 Deriving the Grating Equation

Equipped with a Fourier expansion for the total field and a wave equation, we can attempt to solve for the field. Figure 3.1 shows the coordinate system sliced into three regions:

- Region 2: Above the grooves where  $y > a$ , the impedance  $k(x, y)$  is constant and proportional to the refractive index of the air/vacuum:  $k_2(x, y) = v_2\omega/c$ .
- Region 1: Below the grooves where  $y < 0$ , the impedance  $k(x, y)$  is also constant and proportional to the grating's refractive index:  $k_1(x, y) = v_1\omega/c$ .
- Inside the grooves, the impedance is changing as a function of position: whether inside or outside of a groove. We ignore this difficult region for now and try to work with the uniform regions as much as possible.

Where  $k(x, y)$  is constant, the wave equations for both TE (3.18) and TM polarization (3.22) reduce to:

$$\nabla^2 u + k^2 u = 0 \quad (3.40)$$

where  $k = k_1$  above the grating, and  $k = k_2$  below it. If we insert the Fourier expansion for the field  $u(x, y) = \sum u_n(y)e^{i\alpha_n x}$  into the wave equation:

$$\nabla^2 \left( \sum_{n=-\infty}^{\infty} u_n(y)e^{i2\pi n x/d} e^{i\alpha_0 x} \right) + k^2 \sum_{n=-\infty}^{\infty} u_n(y)e^{i2\pi n x/d} e^{i\alpha_0 x} = 0 \quad (3.41)$$

$$e^{i\alpha_0 x} \sum_{n=-\infty}^{\infty} \left( \frac{d^2}{dy^2} + (k^2 - (\alpha_0 + 2\pi n/d)^2) \right) u_n(y)e^{i2\pi n x/d} = 0 \quad (3.42)$$

For this Fourier sum to be equal to zero, all of the coefficients must be zero:

$$\left( \frac{d^2}{dy^2} + (k^2 - (\alpha_0 + 2\pi n/d)^2) \right) u_n(y) = 0 \quad (3.43)$$

$$\left( \frac{d^2}{dy^2} + (k^2 - \alpha_n^2) \right) u_n(y) = 0 \quad (3.44)$$

This is a standard differential equation with the solution

$$u_n(y) = A_n e^{-i\beta_n y} + B_n e^{i\beta_n y} \quad (3.45)$$

where

$$\beta_n = \sqrt{k^2 - \alpha_n^2} \quad (3.46)$$

and  $A_n$  and  $B_n$  are unknown constants to be determined by the boundary conditions.

Special attention must be paid to the square root for  $\beta_n$ , depending on whether we are above or below the grating.

### Above the grating

Above the grating, we are likely inside air or vacuum ( $k = k_2$ ), so the refractive index and  $k$  would be real. Since  $\alpha_n = \alpha_0 + 2\pi n/d$  will increase with  $n$ , there will be a finite number of  $n$  near  $n = 0$  where  $(k^2 - \alpha_n^2)$  will be a positive number. However, there will be an infinite number of  $n$  (approaching  $n \rightarrow \infty$  and  $n \rightarrow -\infty$ ) where  $(k^2 - \alpha_n^2) < 0$ . This creates two possibilities for  $\beta_n$  (which we label  $\beta_n^{(2)}$  because we are in Region 2):

$$\beta_n^{(2)} = \sqrt{k^2 - \alpha_n^2} \quad (k^2 - \alpha_n^2) > 0 \quad (\text{finite occurrences, } \beta_n^{(2)} \text{ real}) \quad (3.47)$$

$$\beta_n^{(2)} = i\sqrt{\alpha_n^2 - k^2} \quad (k^2 - \alpha_n^2) < 0 \quad (\text{infinite occurrences, } \beta_n^{(2)} \text{ complex}) \quad (3.48)$$

Using this solution for the Fourier coefficients  $u_n$ , the total field is:

$$u(x, y) = \sum_{n=-\infty}^{\infty} A_n^{(2)} e^{i\alpha_n x - i\beta_n^{(2)} y} + \sum_{n=-\infty}^{\infty} B_n^{(2)} e^{i\alpha_n x + i\beta_n^{(2)} y} \quad (3.49)$$

This result is remarkable. The total field created above the grating is a finite sum of propagating plane waves (for all  $n$  where  $\beta_n^{(2)}$  is real) and an infinite sum of decaying (when  $\beta_n^{(2)}$  is complex) plane waves.

To expand on this conclusion: The first sum (with  $A_n^{(2)}$  coefficients) are waves travelling in the  $-y$  direction, down toward the grating. For the finite set of  $n$  for which  $\beta_n^{(2)}$  is real, these are non-decaying,

normal waves. There are also an infinite number of exponentially growing waves that explode as  $y \rightarrow +\infty$ , for the remaining  $n$  that cause  $\beta_n^{(2)}$  to be complex.

Similarly, the second sum (with  $B_n^{(2)}$  coefficients) represents waves travelling away from the grating, in the  $+y$  direction. There is a finite set of propagating waves, and an infinite set of exponentially decaying waves that tend to zero as  $y \rightarrow +\infty$ .

The total field will have a unique solution only when the incident field  $u_i$  is totally specified. From the grating setup in Figure 3.1, we know that we only have a single down-going wave, corresponding to the incident plane wave; all of the  $A_n^{(2)}$  for the other propagating waves must be 0. (We label this incident wave as  $n = 0$ .) We also need to reject the non-physical waves that explode as  $y \rightarrow +\infty$ , therefore the expansion of the field *above the grating* simplifies to:

$$u(x, y) = A_0^{(2)} e^{i\alpha_0 x - i\beta_0^{(2)} y} + \sum_{n=-\infty}^{\infty} B_n^{(2)} e^{i\alpha_n x + i\beta_n^{(2)} y} \quad (3.50)$$

The diffraction grating's reflected orders appear out of this expansion as the finite set of  $n$ ,  $\beta_n^{(2)}$ , and  $B_n^{(2)}$  values that create propagating plane waves travelling away from the grating. At this point,  $n$  can now be properly identified with the *diffraction order*. This is known as the *Rayleigh Expansion* for the diffraction field. Figure 3.2 shows this visually and mathematically.

### Below the grating

The field below the grating ( $y < 0$ ) can be expanded using the same technique. One complication is that for grating materials which absorb energy, the refractive index (and hence  $k = k_1$ ) will be complex.<sup>5</sup> In this situation there are two possibilities for the square root  $\beta_n^{(1)} = \sqrt{k_1^2 - \alpha_n^2}$ . The correct choice can be made by requiring that the diffracted waves remain bounded when  $y \rightarrow -\infty$ . The result provides an expansion for the transmitted field, corresponding to the transmitted orders. These are also shown visually in Figure 3.2:

$$u(x, y) = \sum_{n=-\infty}^{\infty} A_n^{(1)} e^{i\alpha_n x - i\beta_n^{(1)} y} \quad (3.51)$$

### The grating equations

These expansions for the reflected and transmitted fields show that as soon as the direction of the incident wavevector is fixed, the outgoing directions of light are determined. For the *reflected* orders, Equation 3.50 gives the  $x$ - and  $y$ -components of the wavevectors:

$$B_n^{(2)} e^{i(k_x x + k_y y)} = B_n^{(2)} e^{i(\alpha_n x + \beta_n^{(2)} y)} \quad (3.52)$$

$$k_x = \alpha_n \quad (3.53)$$

$$= \alpha_0 + \frac{2\pi n}{d} \quad (3.54)$$

$$= k_2 \sin \theta_2 + \frac{2\pi n}{d} \quad (3.55)$$

---

<sup>5</sup>In fact, this is the case for all materials at soft X-ray wavelengths.

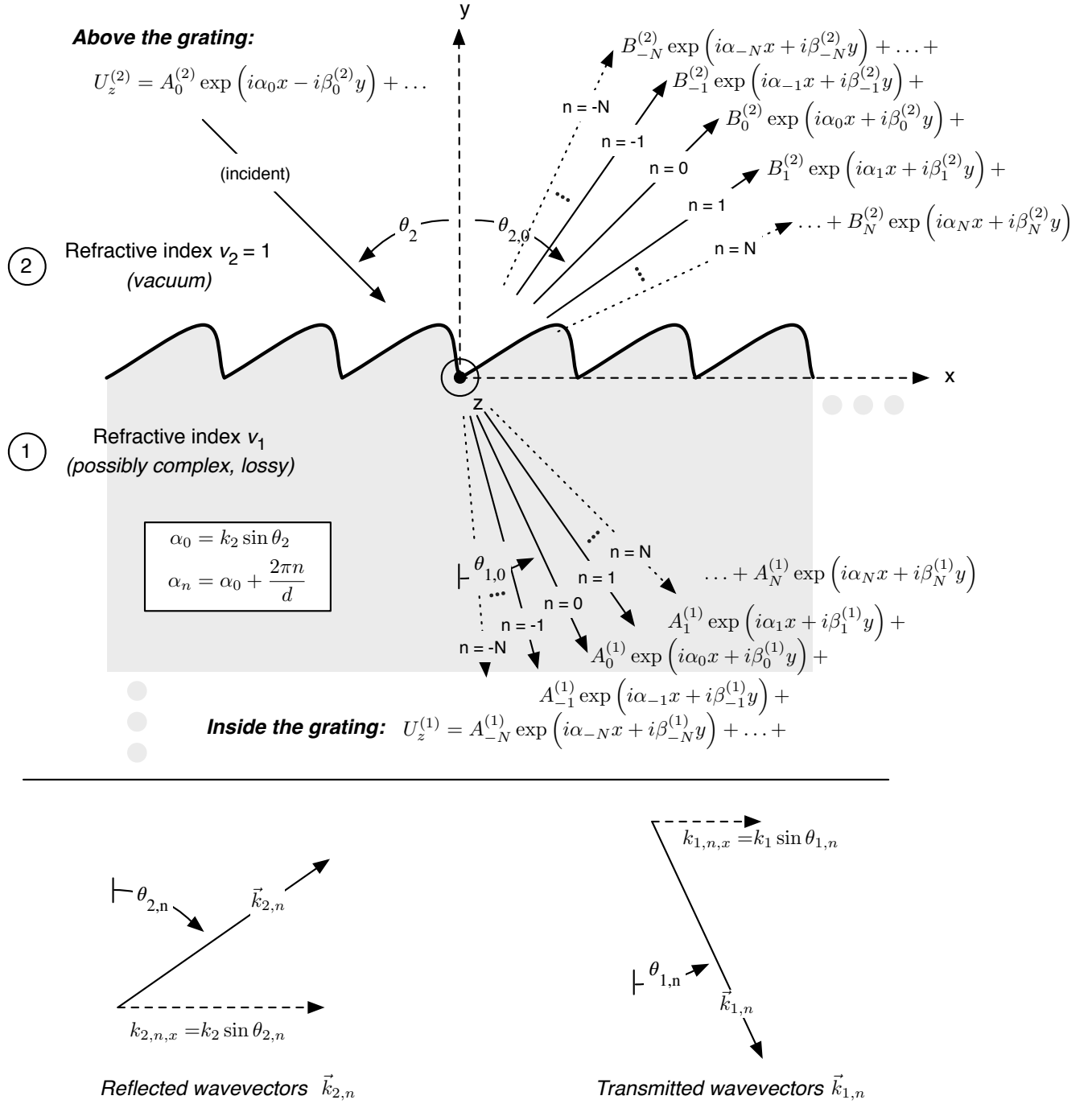


**Figure 3.2:** The Rayleigh expansion describes the electric field (TE polarization) or magnetic field (TM polarization) in homogenous media, above and below the grating. The terms in the expansion include a finite number of propagating plane waves – the diffraction orders – and an infinite number of decaying, or “evanescent” plane waves. From the geometry of the diffracted and transmitted wave vectors, we can derive the grating equation, but we need to solve the  $A_n$  and  $B_n$  coefficients to determine the efficiency of each order.

From the geometry analyzed in Figure 3.2, the  $x$ -component of the outgoing wavevector at angle  $\theta_{2,n}$  is  $k_2 \sin \theta_{2,n}$ . Therefore

$$k_x = k_2 \sin \theta_2 + \frac{2\pi n}{d} = k_2 \sin \theta_{2,n} \quad (3.56)$$

and, after replacing the magnitude of the wavevector above the grating  $k_2 = v_2 \omega / c = v_2 \cdot 2\pi f / c = 2\pi / \lambda$ , the famous grating equation (for reflected orders) is finally:

$$\frac{n\lambda}{d} = \sin \theta_{2,n} - \sin \theta_2 \quad (3.57)$$

(where we've assumed that  $v_2 = 1$  because we are in free space, and  $\lambda$  is also the free-space wavelength.) This is often called the *Fraunhofer Grating Equation*.

When  $n = 0$ , the grating equation reverts to the law of reflection ( $\theta_{2,0} = \theta_2$ , ie: the angle of reflection is equal to the angle of incidence.) This wave corresponds to a classically-reflected wave from a normal surface. The reflected orders that fall *between* the incident wave and the  $n = 0$  reflection are referred to as *inside orders*; using our sign convention for diffraction angles, they correspond to  $n < 0$ . The *outside orders* ( $n > 0$ , see Figure 3.2) are diffracted at angles beyond the  $n = 0$  reflection.

We can also use the same technique to determine the angles of the transmitted orders. Equation 3.51 gives the  $x$ - and  $y$ -components of the transmitted wavevectors:

$$A_n^{(1)} e^{i(k_x x + k_y y)} = A_n^{(1)} e^{i(\alpha_n x + \beta_n^{(1)} y)} \quad (3.58)$$

$$k_x = \alpha_n = \alpha_0 + \frac{2\pi n}{d} = k_2 \sin \theta_2 + \frac{2\pi n}{d} \quad (3.59)$$

From the geometry analyzed in Figure 3.2, the  $x$ -component of the outgoing wavevector at angle  $\theta_{1,n}$  is  $k_1 \sin \theta_{1,n}$ . Therefore

$$k_x = k_2 \sin \theta_2 + \frac{2\pi n}{d} = k_1 \sin \theta_{1,n} \quad (3.60)$$

and, after again replacing  $k_1$ , the magnitude of the wavevector below the grating  $k_1 = v_1 \omega / c = v_1 \cdot 2\pi f / c = v_1 \cdot 2\pi / \lambda$ , the transmission grating equation is:

$$\frac{n\lambda}{d} = v_1 \cdot \sin \theta_{1,n} - v_2 \cdot \sin \theta_2 \quad (3.61)$$

This time, instead of checking for the law of reflection, we can check that when  $n = 0$ , the transmission equation reverts to Snell's law of refraction ( $v_1 \sin \theta_{1,0} = v_2 \sin \theta_2$ ).

**Note: Simplifying  $\beta_n$**

Equations 3.56 and 3.60 provide a useful simplification for  $\beta_n$ . Since

$$k_2 \sin \theta_2 + \frac{2\pi n}{d} = k_2 \sin \theta_{2,n} = k_1 \sin \theta_{1,n} \quad (3.62)$$

we can go back to the expression for  $\beta_n$ , and easily show that

$$\beta_n^{(2)} = \sqrt{k_2^2 - \alpha_n^2} = \sqrt{k_2^2 - (\alpha_0 + 2\pi n/d)^2} \quad (3.63)$$

$$= \sqrt{k_2^2 - (k_2 \sin \theta_2 + 2\pi n/d)^2} \quad (3.64)$$

$$= \sqrt{k_2^2 - (k_2 \sin \theta_{2,n})^2} \quad (3.65)$$

$$= \sqrt{k_2^2 (1 - \sin^2 \theta_{2,n})} \quad (3.66)$$

$$= \sqrt{k_2^2 \cos^2 \theta_{2,n}} \quad (3.67)$$

$$= k_2 \cos \theta_{2,n} \quad (3.68)$$

Similarly, for the transmitted order,

$$\beta_n^{(1)} = k_1 \cos \theta_{1,n} \quad (3.69)$$

## Finishing the grating problem

Based only on Maxwell's equations and an assumption of periodicity, we've shown that a grating reflects and transmits light into a set of discrete angles. Incredibly, this result is fully general – it doesn't depend at all on the shape or nature of the grating profile; all that's required is that it be periodic. Unfortunately, this impressive result still says nothing at all about the *grating efficiency*, or the *amount* of light diffracted into each order. We still don't know anything about the *amplitudes*  $B_n$ ,  $A_n$  of the diffracted plane waves, and to determine these coefficients we'll need to get down and dirty inside the grooves of the grating.

Within the grooves, the wave equations (3.18, 3.22) are much more difficult to solve due to the position-dependence of  $k(x, y)$ . The refractive index (and therefore the impedance  $k$ ) will change whether inside or outside of a groove, and if the grating shape is complicated,  $k(x, y)$  will be a complicated function indeed. Several decades of intense research have produced a handful of methods for solving the full boundary-value problem, all of which are hampered by unique challenges of computational feasibility, numerical stability, and accuracy of approximations. Table (TODO) lists the most common methods, with references and areas of applicability.

Some methods are only applicable in specific cases. For example, for certain particular groove profiles, there exist coordinate transformations (“conformal mappings”) which simplify the boundary conditions so they can be solved analytically. In the following sections, we present an overview of two *general* methods which can handle arbitrary groove profiles. Before getting there, however, we take a closer look at defining grating efficiency.

## 3.2 Defining Grating Efficiency

In spectroscopy applications, the experimenter typically illuminates a grating with light and uses a single outgoing order ( $n \neq 0$ ) to resolve the light by wavelength. If they are concerned about optimizing the amount

of light delivered to their experiment, the “efficiency” question that matters to them is, “*How much light do I get out of the grating (in the useful order), compared to how much light went in?*” Fundamentally, this depends on how much energy is absorbed in the grating itself, and how energy is distributed between orders.

We can define the grating efficiency for a single order quite rigorously in the same way. For electromagnetic plane waves, the *Poynting Vector* represents the energy flux (or energy per unit area,  $\text{W/m}^2$ ) carried by the wave:

$$\vec{S} = \vec{E} \times \vec{H} \quad (3.70)$$

This gives the instantaneous energy flux, which will oscillate in time with the wave. The *time-averaged Poynting vector* gives the average flux delivered over a full period of the wave. For harmonic waves, this turns out to be

$$\bar{S} = \frac{1}{2} \text{Re} \left( \vec{E} \times \vec{H}^* \right) \quad (3.71)$$

where  $\vec{H}^*$  denotes the complex conjugate of  $\vec{H}$ .

We define the grating efficiency formally as *the ratio of the total time-averaged Poynting flux – through a surface parallel to the mean grating plane – of the outgoing order ( $\bar{S}_n^{(2)}$ ) relative to the incident wave ( $\bar{S}^{(2)}$ )*. Figure 3.3 highlights the surface  $Q_2$  used for reflected efficiencies ( $e_n^{(r)}$ ), which spans one grating period  $d$  in the  $x$ -direction, and has unit length in the  $z$ -direction. For defining transmitted efficiencies  $e_n^{(t)}$ , we use a similar surface  $Q_1$  at  $y \leq 0$ .

$$e_n^{(r)} \equiv \frac{\iint_{Q_2} \bar{S}_n^{(2)} \cdot \hat{y} \, dz dx}{\iint_{Q_2} \bar{S}^{(2)} \cdot \hat{y} \, dz dx} \quad (3.72)$$

$$e_n^{(t)} \equiv \frac{\iint_{Q_1} \bar{S}_n^{(1)} \cdot \hat{y} \, dz dx}{\iint_{Q_1} \bar{S}^{(2)} \cdot \hat{y} \, dz dx} \quad (3.73)$$

It turns out that this definition for efficiency can be nicely expressed in terms of the coefficients in the Rayleigh expansion for the reflected and transmitted fields (3.50, 3.51), so that if we can solve for these coefficients, we’ll have determined the grating efficiency:

### Reflected Efficiencies

We know that the incident and diffracted orders are plane waves, so the magnetic field  $\vec{H}$  is related to the electric field  $\vec{E}$  as

$$\left| \vec{H} \right| = \frac{\left| \vec{E} \right|}{Z_2} \quad (3.74)$$

where  $Z_2 = v_2 Z_0$  is the impedance of the space above the grating (usually free space, so  $v_2 = 1$  and  $Z_2 = Z_0 = 377\Omega$ , the impedance of free space). Based on the Rayleigh expansion for the outgoing field



*Time-averaged Poynting vectors:*

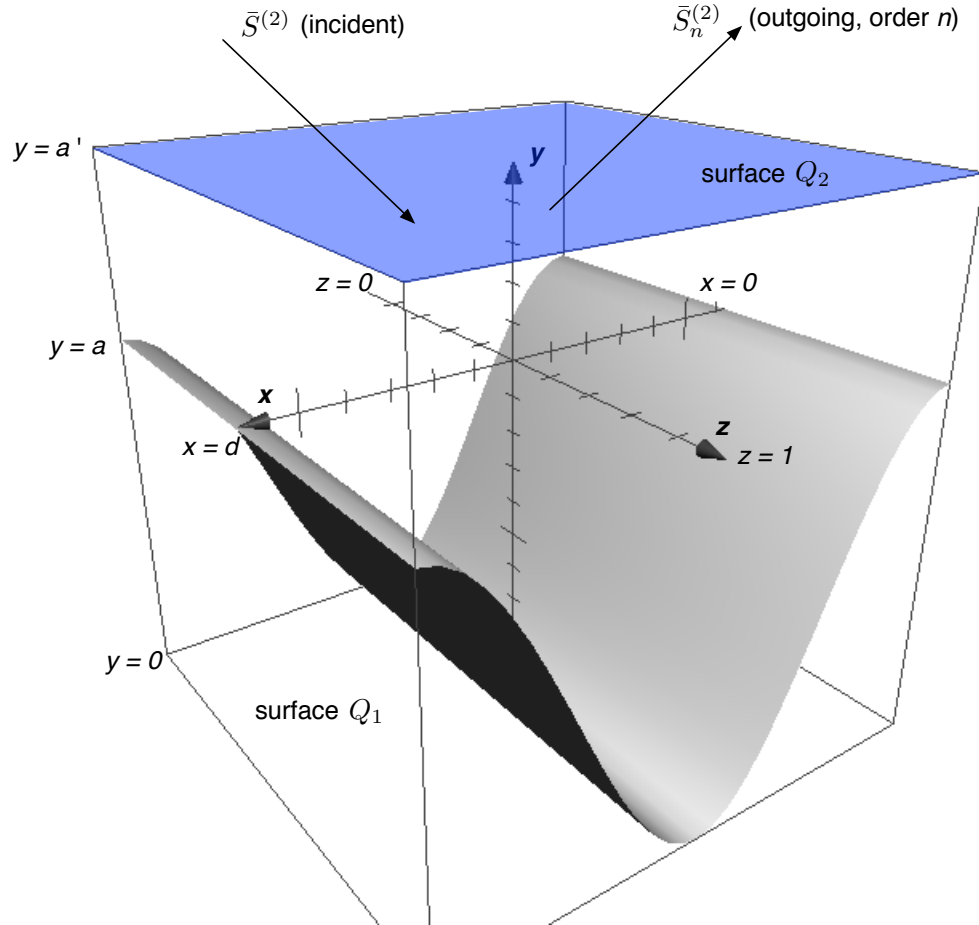


**Figure 3.3:** The total electromagnetic flux through this highlighted area ( $Q_2$ ) is used to define the grating efficiency of a diffraction order  $n$ , as the ratio of the flux of the diffracted wave  $\bar{S}_n^{(2)}$  compared to the incident wave  $\bar{S}^{(2)}$ .

(equation 3.50), the magnitude of the time-averaged Poynting vector for the *reflected order* is therefore

$$|\bar{S}| = B_n^{(2)} B_n^{(2)*} \eta_2 \quad (3.75)$$

where we've defined  $\boxed{\eta_2 \equiv 1/(2Z_2)}$  in the case of TE polarization, and  $\boxed{\eta_2 \equiv 2Z_2}$  for TM polarization. The direction of the vector is along the propagation direction, ie: at an angle  $\theta_{2,n}$  to the  $y$ -axis, therefore the integrated flux through the surface is:

$$\iint_{Q_2} \bar{S}_n^{(2)} \cdot \hat{y} \, dz dx = \int_0^d \int_0^1 \bar{S}_n^{(2)} \cdot \hat{y} \, dz dx \quad (3.76)$$

$$= B_n^{(2)} B_n^{(2)*} \eta_2 d \cos \theta_{2,n} \quad (3.77)$$

For the incident wave, the integrated flux is similarly

$$\iint_{Q_2} \bar{S}^{(2)} \cdot \hat{y} \, dz dx = A_0^{(2)} A_0^{(2)*} \eta_2 d \cos \theta_2 \quad (3.78)$$

and so the reflected efficiency in order  $n$  is:

$$e_n^{(r)} = \frac{B_n^{(2)} B_n^{(2)*} \cos \theta_{2,n}}{A_0^{(2)} A_0^{(2)*} \cos \theta_2} \quad (3.79)$$

We can simplify this somewhat by choosing a unit amplitude for the incident field, ie:  $A_0^{(2)} = 1\text{V/m}$  for the TE electric field, or  $1\text{A/m}$  for the TM magnetic field. Also, since  $\beta_n^{(2)} = k_2 \cos \theta_{2,n}$ , we can simplify this to

$$e_n^{(r)} = B_n^{(2)} B_n^{(2)*} \frac{\beta_n^{(2)}}{\beta_0^{(2)}} \quad (3.80)$$

## Transmitted Efficiencies

Gratings used in the soft X-ray regime are always used in reflection, due to the high absorption of materials at these wavelengths. However, since we're working on a general theory with application to all gratings, we can go through the same process for simplifying the transmitted efficiencies.

Again, we define  $\boxed{\eta_1 \equiv 1/(2Z_1)}$  in TE polarization, and  $\boxed{\eta_1 \equiv 2Z_1}$  in TM polarization, where  $Z_1 = v_1 Z_0$  is the impedance of the grating substrate material. The same integrations over the surface  $Q_1$  give the ratio between the total transmitted and incident fluxes:

$$e_n^{(t)} = \frac{A_n^{(1)} A_n^{(1)*} \cos \theta_{1,n} \eta_1}{A_0^{(2)} A_0^{(2)*} \cos \theta_2 \eta_2} \quad (3.81)$$

In this case, the difference in impedance above and below the grooves causes  $\eta_1$  and  $\eta_2$  to remain in the formula, so the final simplification depends on polarization:

$$e_n^{(t)} = A_n^{(1)} A_n^{(1)*} \frac{\beta_n^{(1)}}{\beta_0^{(2)}} \quad (\text{TE Polarization}) \quad (3.82)$$

$$= A_n^{(1)} A_n^{(1)*} \frac{\beta_n^{(1)}}{\beta_0^{(2)}} \left( \frac{v_2}{v_1} \right)^2 \quad (\text{TM Polarization}) \quad (3.83)$$

### 3.3 Solving for efficiency

- Solving: Requires periodic representation of refractive index: only true at fixed (y). Needs computational methods

- key set of differential equations to solve...  $d^2 E_n / dy^2 + k^2 E_n = 0$

#### 3.3.1 Numerical Challenges

##### Integration of growing exponentials

- Integrating growing exponentials: floating point rounding error leads to runaway [reference: Neviere: S-matrix; Somebody: R-matrix]

##### Truncation of Fourier expansions

- Must truncate Fourier expansion. Problem in TM case: makes field discontinuous, where should be continuous. [reference: Li, FFF]

#### 3.3.2 Applying boundary conditions within the groove region

- Highlighted methods for dealing with boundary conditions in groove region:

- RCWA: split into thin layers and make rectangular
- Differential method
- Table of methods, areas of applicability, and references

#### 3.3.3 Handling stacks of gratings

### 3.4 X Rays and materials: how do they interact?

(Especially: lossy metals) - Characterized: atomic scattering factor -  $i$  \*complex refractive index\*

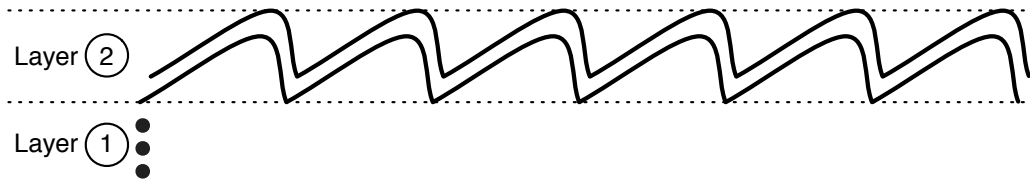
FIGURE 2e: plot of real and imaginary components... Metals at 100-1000eV.

- RI Derived from Henke Data
- Reference CXRO calculator
- Note: total external reflection (overcome notoriously absorbing materials via grazing incidence)

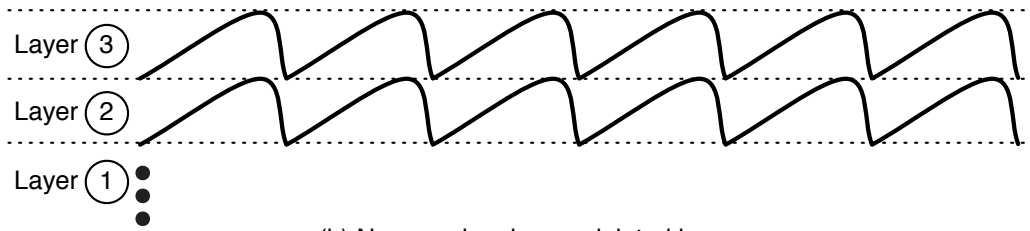
Next chapter: look at the how this is applied, and what we can learn about grating efficiency using the theory

REMAINING QUESTIONS: numerical integration of WHAT. (A: 2nd order in TE; 1st-order in TM. Eqn II.2')

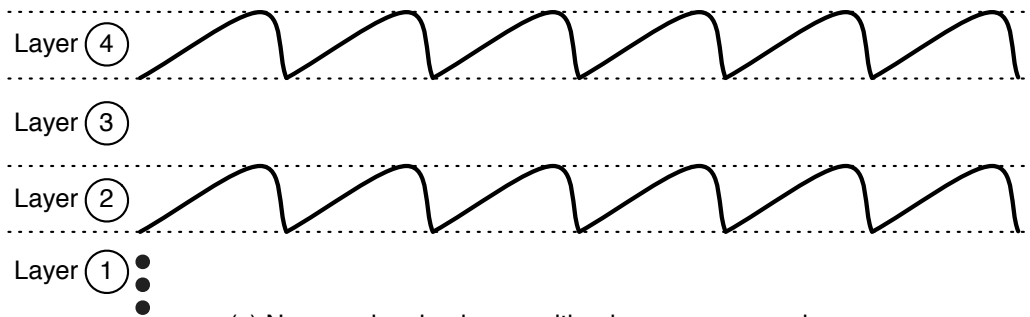
How to get coefficients for  $k^2(x,y)$ ?



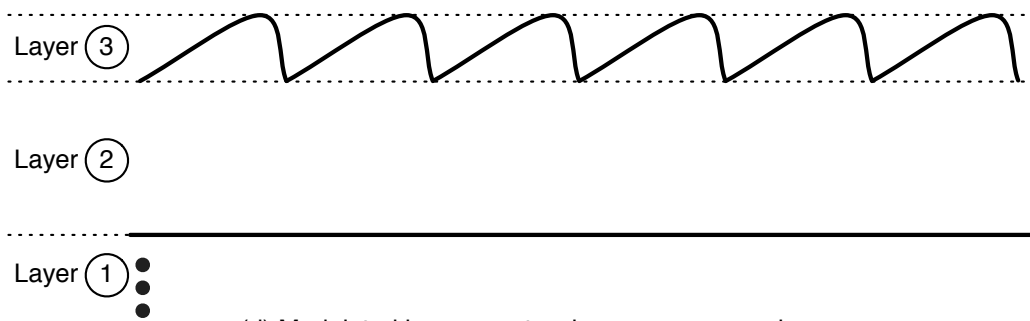
(a) Overlapping modulated layers



(b) Non-overlapping modulated layers



(c) Non-overlapping layers with a homogenous region



(d) Modulated layer over two homogeneous regions  
(ex: grooves ruled into a metal-coated dielectric blank)

**Figure 3.4:** Arbitrarily-complicated structures can be handled by dividing the grating into layers, where each layer is either homogenous (constant refractive index), or modulated (with a refractive index that changes periodically as a function of  $x$  at any given height  $y$ ).

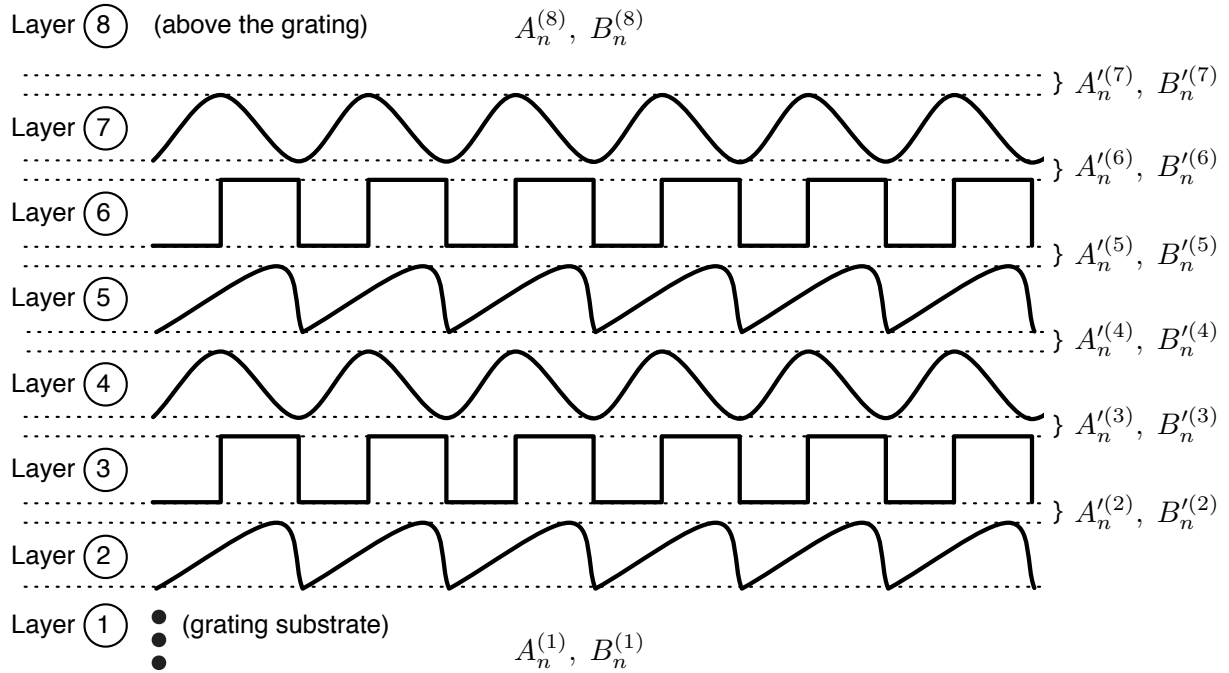


**Figure 3.5:** Modulated layers in a complicated stack of gratings. In between every layer, we can insert an imaginary, infinitely-thin homogenous layer where the Rayleigh expansion applies. The  $A'_n$  and  $B'_n$  expansion coefficients connect the boundary conditions between layers. Within each layer, the Rayleigh expansion does not apply – inside the grooves, the field cannot be represented as a simple sum of plane waves – and numerical methods are required to approximate it.

## CHAPTER 4

# IMPLEMENTATION OF THEORY: WHAT PEOPLE AND I DID TO IMPLEMENT THE THEORY USING COMPUTERS

Introduction: yadda yadda yadda (TODO)

### 4.1 Methods

#### 4.1.1 Rigorous Coupled Wave method: GSolver

TODO

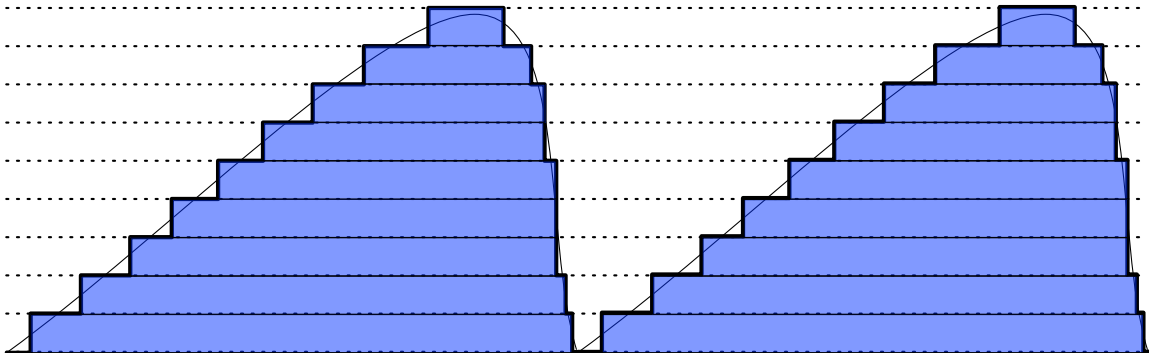


**Figure 4.1:** The RCW method approximates every real grating as a stack of rectangular gratings, where the boundary conditions are easy to solve and the problem can be reduced to algebraic methods.

#### 4.1.2 Differential method: Gradif by Michel Nevieri

TODO

### 4.2 Improving the usability and efficiency of calculation methods

The Canadian Light Source purchased the Gradif code from Professor Nevieri and made it available for this project. However, there were two challenges involved in applying the code:

1. The code itself is an iteration on old Fortran program that provides no user interface. Instead, to calculate an efficiency data point for a grating at just one energy, approximately 30 numbers must be entered into a blank screen, with no prompts, in the correct order. These numbers define the grating geometry, the coating/layer thicknesses, the incidence conditions, the integration parameters, and also the complex refractive indices of the layers and the substrate.<sup>1</sup> As a result, using this program requires a time-consuming and error-prone process.
2. In the event of an error made during the data entry process, one of many grating parameters could end up outside the narrow region of convergence where the code is able to numerically integrate a solution successfully. When this happens, the program runs forever in an infinite loop, with no feedback that the calculation has failed. This region of convergence is not well established, so even when data entry errors are avoided, it's possible for a user to specify a valid grating that is – for example – too deep to be calculated. Without user feedback, it's impossible to know if the calculation is still running successfully, or if it has failed into this infinite loop.

To beat these two challenges, we built a web-based graphical interface, and carefully modified the Fortran source code to detect convergence failures.

#### 4.2.1 Visual interface to the Gradif code

Figure 4.2 shows a screenshot of the graphical user interface (GUI) that we built to help us perform efficiency calculations quickly and efficiently. The interface serves as a wrapper to generate input for the Gradif code, manages running a set of calculations, and extracts the results.

The interface was implemented as a web-based application, so it can be used from anywhere through a browser, without having to distribute the Gradif code or install anything on a person's individual computer. Users describe the grating parameters and application scenario through a form that prompts them for the necessary information based on the type of grating (Figure 4.2). The results automatically generate a plot, and users can also download data tables of their calculations. These tables are also archived so they can be retrieved later.

It supports the following features:

- **Grating Types**

The interface supports rectangular, blazed, trapezoidal, and sinusoidal grating profiles; it prompts for the geometry parameters that are required in each case.

- **Order and Polarization**

Users can configure which inside and outside orders should be calculated, as well as specify the polarization of the incident light: TE, TM, or natural light (un-polarized).

---

<sup>1</sup>These last two values will change as a function of photon energy, since the refractive index varies with wavelength, so we need to look them up for each data point.

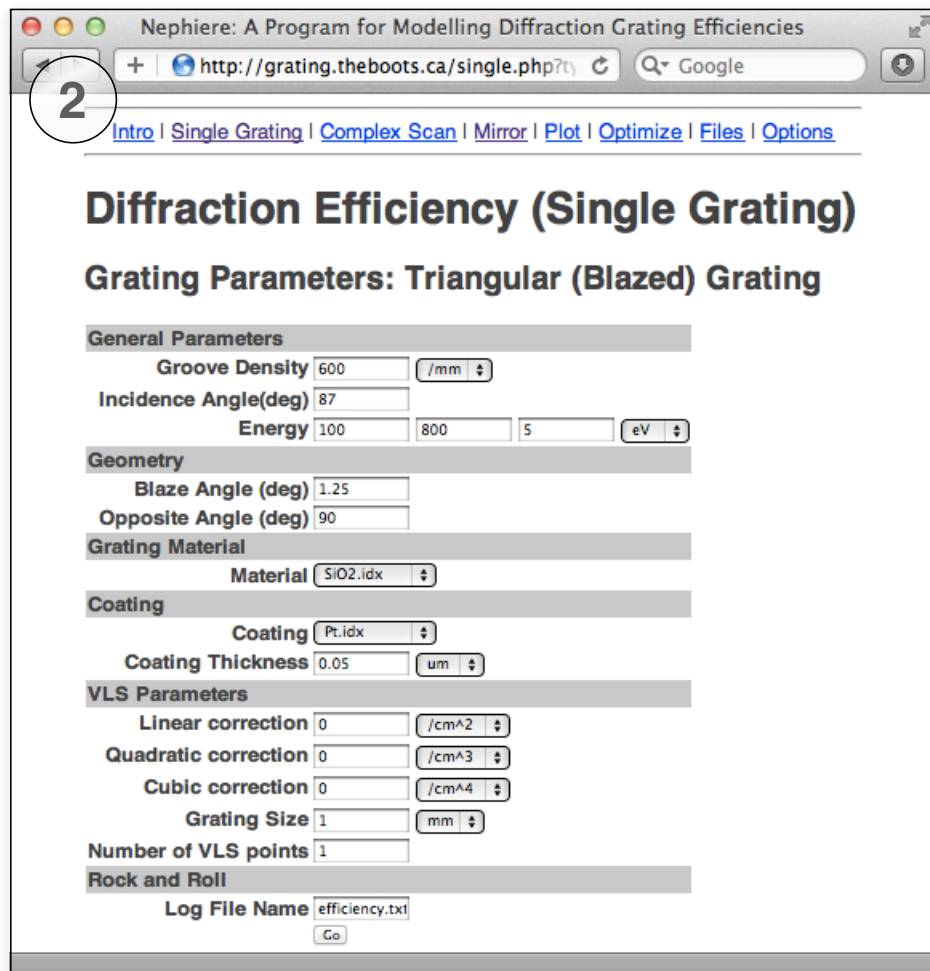
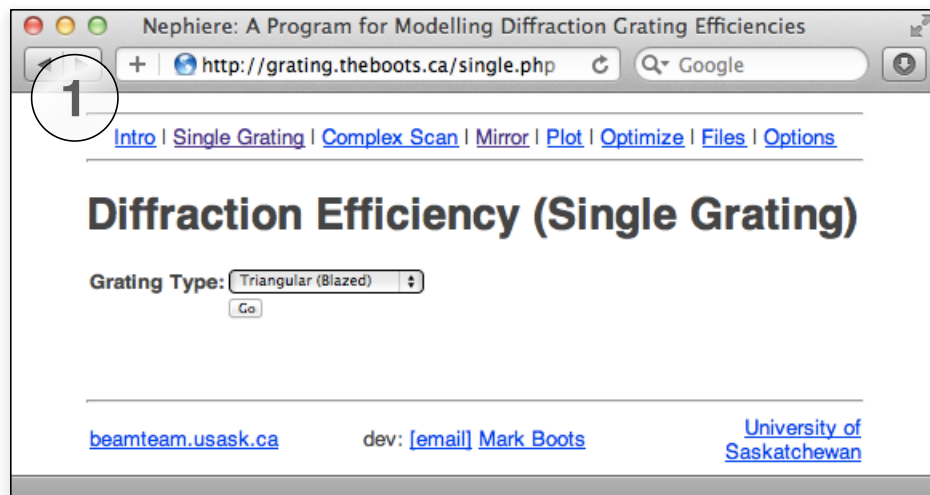


**Figure 4.2:** This web application provides a graphical user interface for calculating grating efficiencies. Forms prompt users for the grating parameters...



- **VLS Gratings**

To model variable line space gratings, the interface accepts the VLS parameters in conventional notation (linear, quadratic, and cubic corrections) and uses these to calculate the groove density and corresponding efficiency at a user-determined number of points along the grating surface; the overall efficiency is taken as an average of these.

- **Efficiency plots as a function of wavelength**

The simplest way to use the interface generates a plot of the efficiency in the desired orders as a function of wavelength, holding all the other parameters constant (Figure 4.3). This is the most typical use-case for testing how a grating would perform in a beamline.

- **Complex scans over arbitrary grating parameters**

The interface also offers flexibility to test arbitrary relationships along incidence angle, energy, geometry, and other parameters. This feature is most efficiently used in conjunction with a spreadsheet or other data analysis program to fill in the grating parameters and interpret the data tables that are produced.

- **Database of Optical Materials and Refractive Index**

We also developed a database of common grating substrate and coating materials, so that the interface can automatically look up their complex refractive index as a function of photon energy. This information was calculated using the semi-empirical Henke data tables of the x-ray atomic form factor (TODO ref). The current library is valid from 30eV to 10 000eV, but is known to have limited accuracy in the immediate neighborhood of absorption edges.

- **Mirror Reflectivity**

As an additional tool for beamline designers, we implemented the ability to calculate the reflectivity of a simple mirror using any of the materials in the refractive index database. Mirror reflectivities are computed as a function of incidence angle and photon energy using the complex Fresnel equations (TODO ref Modern Optics), and are subject to the same options for polarization.

- **Control of Numerical Precision**

An ‘Options’ page (Figure 4.4) allows users to configure the numerical precision used in the calculations. The two critical factors are the number of integration steps used in the numerical integration of the particular solutions for the  $A_n^{(m)}$  and  $B_n^{(m)}$  coefficients at each layer, and the number of Fourier coefficients  $N$  used before the sum is truncated. The defaults we chose ( $N = 31$ ; 401 integration steps) have been found to produce accurate results reasonably quickly across the entire soft x-ray range, as long as the coating thickness is less than 0.5um. However, prudent designers should still do convergence tests for any high-stakes results, by repeating the calculations and comparing against efficiencies computed using larger values. This technique can also be used to find the minimum number of Fourier coefficients that are required before the results start to disagree. (This can help to optimize the computation speed before running a large number of calculations on similar gratings at similar wavelengths.)

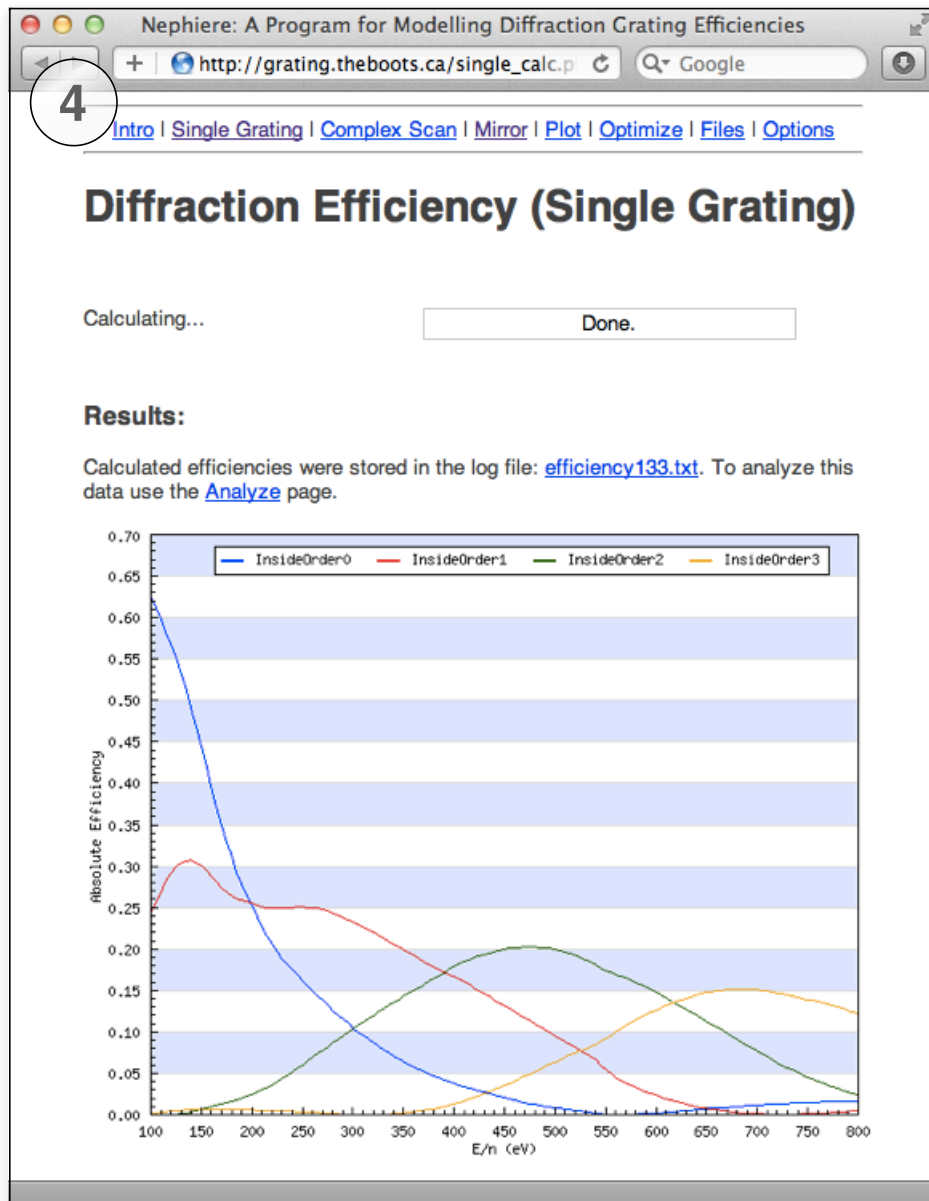
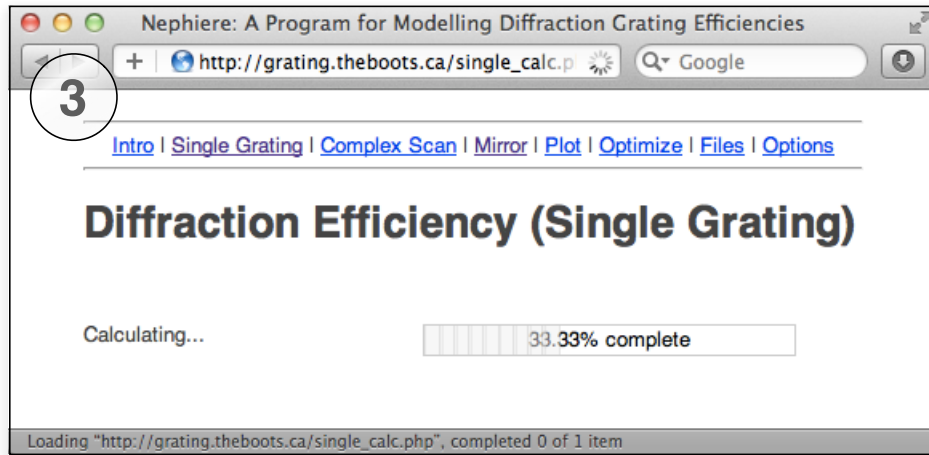


**Figure 4.3:** This web application provides a graphical user interface for calculating grating efficiencies. The results are plotted, and users can download a text-based table for further analysis.

### 4.2.2 Detecting convergence failures

The Fortran code that makes up the Gradif program was written using a 1970's-era programming approach, including prodigious use of global variables and GOTO statements. (These two features are now heavily discouraged in modern programming methodologies.) As a result, the code is hard to trace, but we were able to insert a counter to detect when a numerical integration fails to converge after multiple attempts. This allows the calculation to exit with an error message, rather than run indefinitely.

### 4.2.3 Open Source, Open Access, and Future Work

Since we released the user interface under an ‘open-source’ license, it can be upgraded or enhanced by anyone with an interest in the beamline design community. Julian Miller, a summer student in the metrology department at the CLS, recently created an updated version of the interface to support multi-threaded calculations and add more options for incidence configurations. To the original ‘constant incidence angle’ mode, he added a ‘constant included angle’ mode, used in many monochromators, which tilts the grating as a function of photon energy to maintain a constant angle between the incident and outgoing beam in the desired order. Since every grating efficiency calculation (at a single energy) is independent, they can be run in parallel; this takes advantage of modern multi-core processors, and dramatically speeds up the creation of a user’s plot or data set. In the future, this could be extended even further to spread calculations over a cluster of computers, or on distributed hardware in a ‘cloud computing’ network.

Because the user interface runs as a web application, it can be (and has been) accessed by beamline designers from all over the world. As one example, it was used by Professor Coryn Hague to improve the design of a new beamline for the SOLEIL synchrotron (TODO find ref). The calculations can be requested and retrieved by anyone from anywhere, but they all run on a single server computer at the University of Saskatchewan. Unfortunately, the Gradif code itself is not open source, and while we are licensed to run it on this machine, recent communications from Professor Nevieri indicate that he is unhappy with this level of open access to results produced using his Gradif engine. As a result, we have temporarily disabled public access.

In the future, we plan to completely re-implement the core engine for calculating efficiencies, according to the theory outlined in this thesis. This will allow us to optimize the the computation speed by employing per-calculation multi-threading and a modern high-performance programming language. This will also allow us to distribute a completely open version of the whole system, un-encumbered by licensing issues. Finally, we plan to combine this with Julian’s work and other upgrades to the usability of the web interface.

Nephier: A Program for Modelling Diffraction Grating Efficiencies

http://grating.theboots.ca/options.php

[Intro](#) | [Single Grating](#) | [Complex Scan](#) | [Mirror](#) | [Plot](#) | [Optimize](#) | [Files](#) | [Options](#)

## Options

**Numerical Accuracy**

Number of Integration Steps ('0' for automatic)

Number of Fourier Coefficients

Number of Internally-propagating Wavefronts

**Orders of Interest**

Inside Orders

Outside Orders

**Polarization**

Polarization

**Output**

Working Folder

Log Filename

**Set Options**

[beamteam.usask.ca](http://beamteam.usask.ca) dev: [\[email\]](#) [Mark Boots](#) [University of Saskatchewan](#)

**Figure 4.4:** This ‘Options’ page configures the numerical precision of the calculations, the diffraction orders of interest, and the polarization of the incident light. It also sets some other house-keeping options for where users want to store their data.

## 4.3 General trends and factors affecting efficiency

With these tools in-hand, we move on to the next question: What can we learn from them about the efficiency of gratings, especially those used in the soft x-ray regime?

This section looks at the theoretical effects caused by changes to grating parameters: groove profile, shape (depth, duty cycle, blaze angle, etc.), line density, coating material, coating thickness, and incidence angle. We can think of the grating efficiency as a scalar function of this many-dimensional parameter space, but it's impossible to capture its complexity in a simple analytical equation. None the less, the results of this section should give beamline designers an understanding of trends along each dimensions within this space, and how to apply these trends to the optimization of gratings.

We attempt to isolate the effects of each parameter as much as possible. However, many parameters are linked together so that they cannot be made independent. For example, as we show in Section 4.3.1, gratings with triangular profiles have an optimal *blaze angle* which aligns the outgoing diffraction order with the specular reflection for maximum efficiency. For this type of grating, changing only the groove density will change the outgoing diffraction angle, and therefore change the optimal blaze angle. Simply plotting the efficiency as a function of groove density while holding all other parameters constant would confuse the blaze effect with the density effect; instead, we correct for this by adjusting the angle to keep the grating “on-blaze” as we vary the groove density in Figure 4.12.

### 4.3.1 Effect of Grating Profile: Groove Shape

As we showed in Chapter 3, any kind of periodic groove structure will have a diffraction effect, regardless of the nature of the groove shape. However, the grating efficiency – particularly in the order the experimenter wants to use – depends substantially on the groove shape.

Five common groove profiles are shown in Figure 4.5: a classic rectangular profile, a triangular profile (also known as a “sawtooth” or “blazed” pattern), a trapezoidal profile, a sinusoidal profile, and an approximated triangular profile.

### Grating Manufacturing Techniques

These types of profiles emerged largely as a consequence of grating manufacturing techniques. Henry Rowland invented a method for machining long, precise screws (TODO ref), and this enabled him to create a “ruling engine” (Figure 4.6) for mechanically scratching fine parallel lines into a layer of metal on a substrate material. His version was much more accurate than previous machines because it self-compensated for systematic errors in the screw pitch, and his efficient production of high-quality gratings “revolutionized spectroscopy” (TODO <http://www.aip.org/history/gap/Rowland/Rowland.html>). Today, there are several extremely precise ruling engines around the world, using diamond tips and interferometric position feedback to mechanically engrave

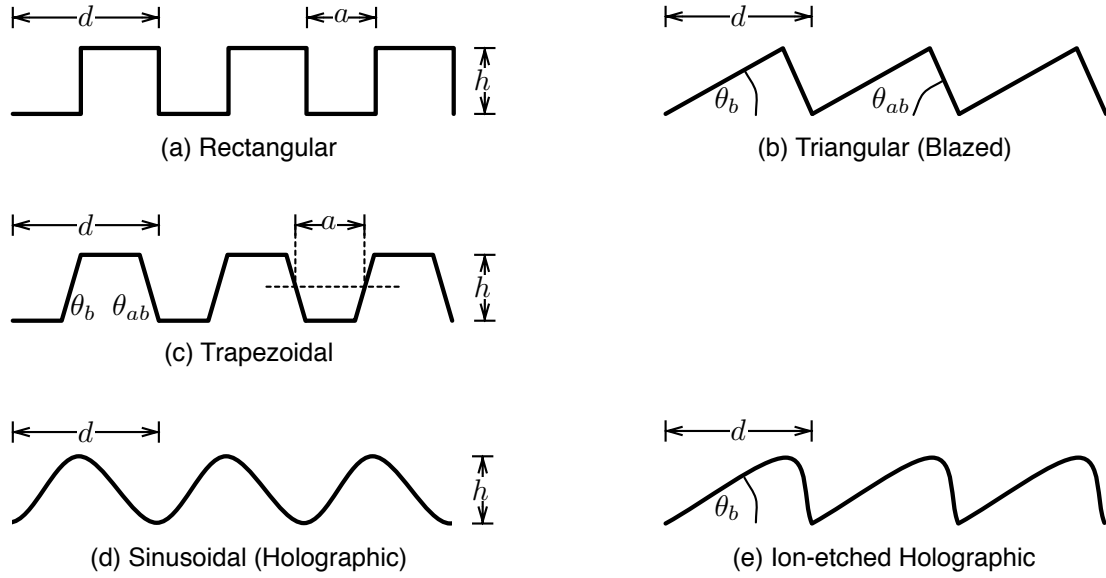


**Figure 4.5:** 5 common groove profiles and their geometry parameters. The rectangular profile (a) and triangular profile (b) are idealized versions of those produced by mechanical ruling. The trapezoidal profile (c) is usually produced accidentally while trying to rule a rectangular profile with an imperfect ruling tip. The sinusoidal profile (d) is the natural shape produced by holographic ruling; the result can be ion-etched to approximate a triangular profile (e).

groove densities approaching 3 000 lines/mm.<sup>2</sup>

The rectangular and triangular profiles in Figure 4.5 are a consequence of the shape of mechanical ruling tips. The trapezoidal profile is often produced accidentally when attempting to rule a rectangular profile with a non-ideal tip, as was the case for the gratings shown in Figures 4.20 and 4.21.

The setup and operation of mechanical ruling engines is a long, elite, and painstaking process; for gory details, see (TODO REF <http://gratings.newport.com/information/handbook/chapter3.asp>) by the Newport Corporation, which operates three ruling engines. To reduce the cost of ruled gratings, often a “master grating” is ruled mechanically and then used to create a mould for replicating other gratings; the groove shape is transferred using a thin layer of liquid resin which is hardened while in contact with the master grating surface (Figure 4.8).<sup>3</sup>

A more recent technique was invented in the late 1960s for manufacturing gratings faster and with more repeatability. It uses two sources of coherent light to project a holographic interference pattern of regular standing waves onto a grating master. The grating master consists of a photoresist material that is either strengthened or weakened by exposure to light. After the master has been exposed to the interference pattern for a sufficient time, it is bathed in a developer chemical, which washes away either the exposed or unexposed parts, leaving behind a sinusoidal relief pattern that corresponds to the original intensity of light (TODO

<sup>2</sup>The Michelson ruling engine at the Newport Corporation can rule up to an astonishing 10 800 lines/mm.

<sup>3</sup>The gratings used for the REIXS spectrometer were all master gratings. They were ruled directly into a smooth gold coating on top of a quartz grating blank, and then top-coated with an evaporated platinum or nickel surface.

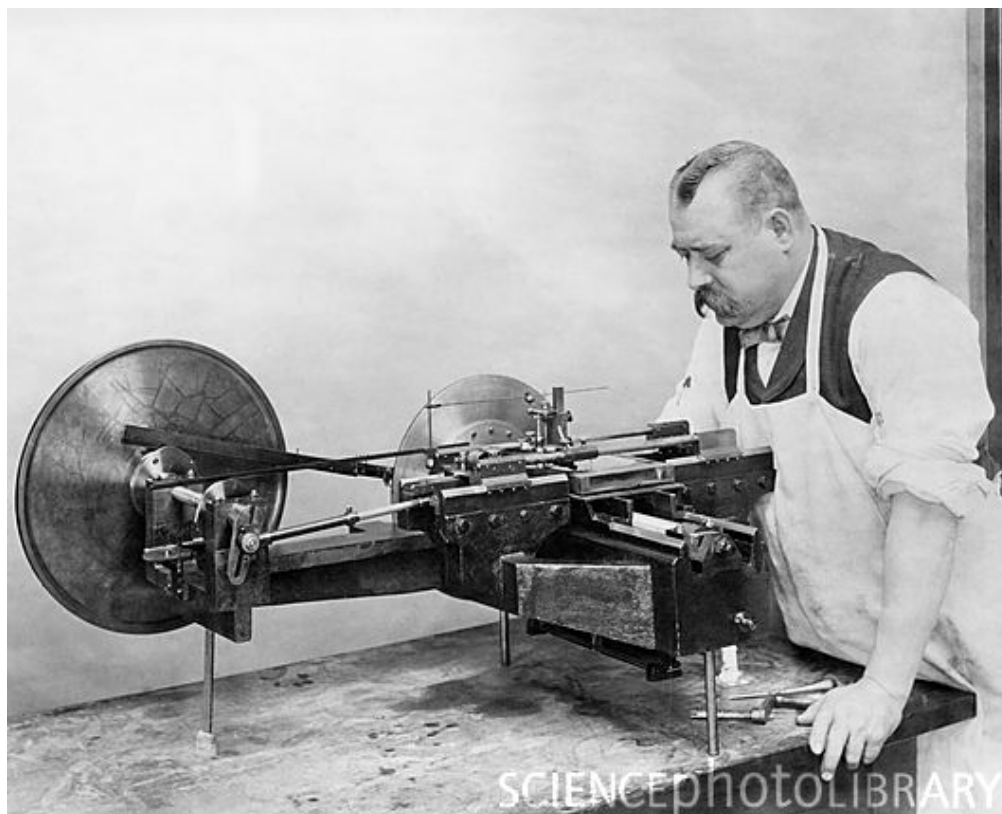


**Figure 4.6:** Henry Rowland's ruling engine, mechanically engraving a grating under the operation of his instrument maker Theodore Schneider. Photographed at Johns Hopkins University, Baltimore.  
**Image credit:** EMILIO SEGRE VISUAL ARCHIVES/AMERICAN INSTITUTE OF PHYSICS/SCIENCE PHOTO LIBRARY (TODO ref <http://www.sciencephoto.com/media/150151/enlarge>)

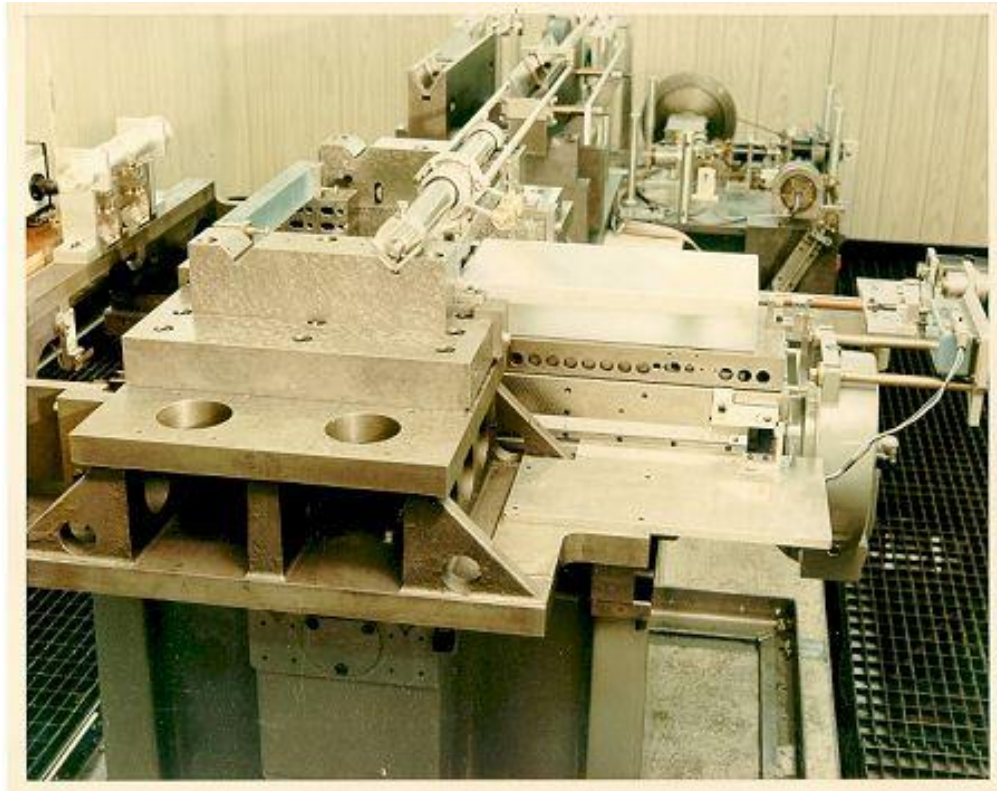


**Figure 4.7:** The MIT ‘B’ ruling engine, now owned and operated by Richardson Gratings (a division of the Newport Corporation). It can rule gratings up to 420 mm wide, with grooves up to 320 mm long. The maximum groove density is 1500 lines/mm. Equipped with a servo system for advancing the grating carriage and interferometric feedback using frequency-stabilized lasers, it is the most accurate ruling engine in the world. To control for thermal expansion of the engine, the room temperature is controlled to 0.005°C; the system even compensates for changes in room air pressure since a change of just 2.5 mm of mercury will affect the refractive index of air (and therefore the interferometer wavelength) by one part per million. The entire engine is suspended from springs to dampen vibrations between 3Hz to 60Hz, which could otherwise be transmitted to the diamond tip. **Image credit:** DIFFRACTION GRATING HANDBOOK (TODO REF).



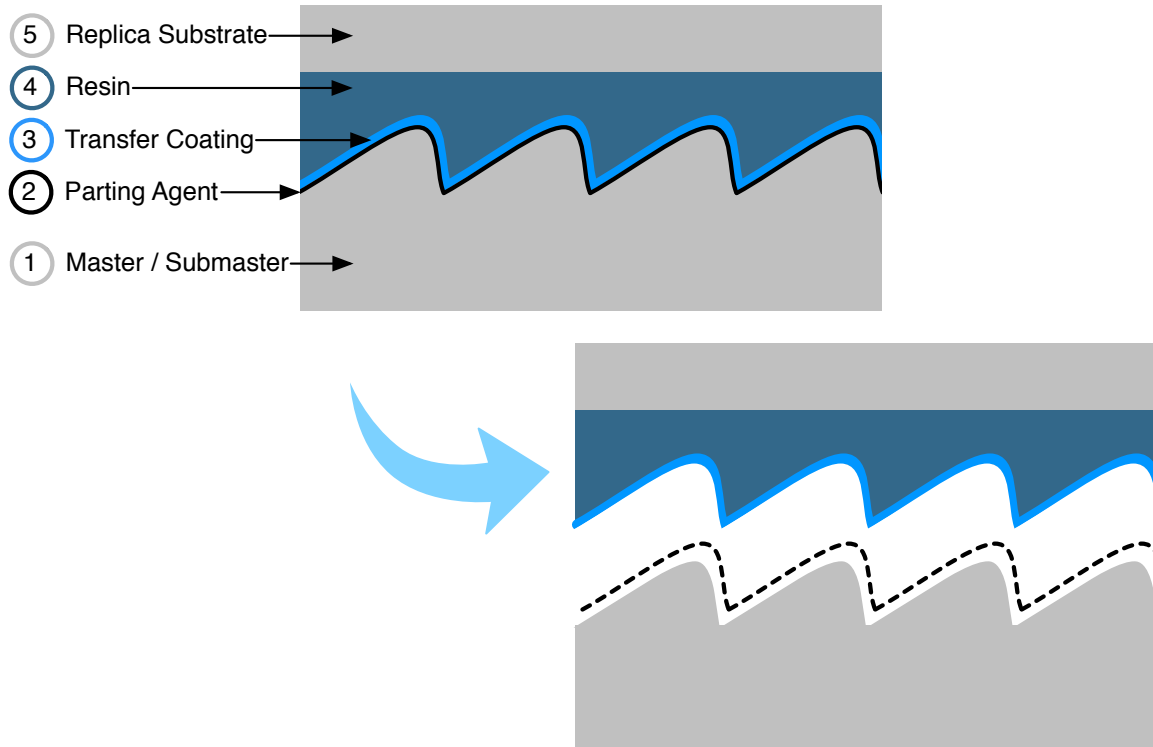


**Figure 4.8:** Master gratings can be replicated using a resin which hardens while in contact with the master (or subsequently, a submaster replicated from the first master). First, a parting agent (2) is applied to the surface of the master; it must be thin and uniform otherwise it will affect the profile. A metallic (aluminum or gold) coating about 1 $\mu$ m thick is then applied above the parting agent; this coating will eventually end up as the top surface of the replicated grating, and is called the *transfer coating* (3). Finally, the replica blank (5) is cemented from above using a resin ( $\sim 10\mu$ m thick) that hardens under UV exposure or over time (4). Once the resin is cured, the gratings are separated at the parting agent layer, leaving the hardened resin in the shape of the grooves, with the metal coating adhered to the top. This will produce a mirror image of the master grating; to create a perfect replica, this first replica needs to be replicated again. **Image credit:** DIFFRACTION GRATING HANDBOOK (TODO REF).

REF S. Lindau, "The groove profile formation of holographic gratings," Opt. Acta 29, 1371-1381 (1982).).

The last groove profile shown in Figure TODO represents an attempt to turn holographically-ruled sinusoidal gratings into triangular gratings using ion etching to partially eat away the groove surface while holding the finished photoresist master at an angle to the ion beam (TODO REF <http://www.tandfonline.com/doi/abs/10.1080/71381>). Another technique for pseudo-blazed holographic gratings is known as Sheridan's Method (TODO REF N. K. Sheridan, "Production of blazed holograms," Appl. Phys. Lett. 12, 316-318 (1968).), which uses a transparent photoresist, exposed to the intersection of a coherent light source with its reflected self (Figure 4.9). Because the master is inclined relative to the interference pattern, the intensity profile is asymmetric and produces a lopsided sinusoidal shape.

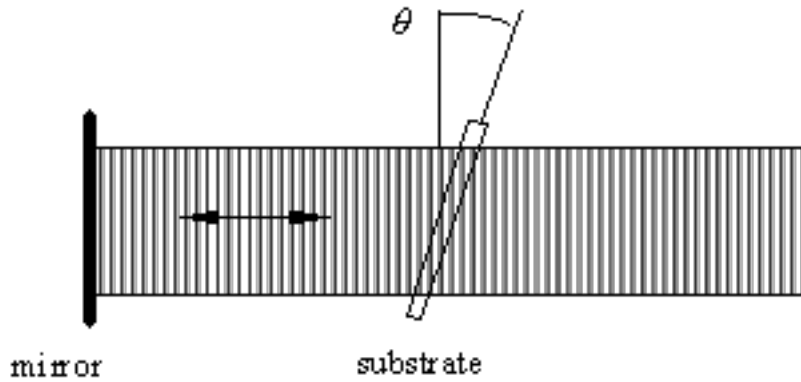


**Figure 4.9:** The Sheridan technique for recording pseudo-blazed holographic gratings uses a single light beam reflected back on itself to make a regular interference pattern of standing waves. The master substrate consists of a *transparent* photoresist material which is hardened or weakened by exposure to the light. By placing the substrate at an angle  $\theta$  to the light path, the light and dark fringes are stretched out parallel to the grating surface; additionally, the angled incidence creates a lopsided sinusoidal intensity pattern that mimics blazed gratings. **Image credit:** DIFFRACTION GRATING HANDBOOK (TODO REF).

## Profile Geometry

Figure 4.5 shows the parameters that describes that describe the geometry of each profile. In addition to the groove spacing  $d$ , rectangular gratings are characterized by a groove depth  $h$  (or duty cycle) and a groove width  $a$ . Ruled triangular gratings are described by their blaze angle  $\theta_b$ ; ideally the opposite angle (or "anti-blaze angle"  $\theta_{ab}$ ) would be  $90^\circ$  but often it ends up closer to  $60^\circ$  or even  $30^\circ$ . Trapezoidal gratings are described by a groove depth  $h$ , a groove width  $a$ , and their blaze and anti-blaze angles  $\theta_b$  and  $\theta_{ab}$ . Sinusoidal gratings are fully described by just their groove depth  $h$ , and an assumption of a sinusoidal variation  $y(x) = y_0 + \frac{h}{2} \sin(2\pi x/d)$ .

## Blazed Optimization for Triangular Gratings

The triangular profile in Figure 4.5 (b) is much more than an accidental artifact of mechanical ruling. This shape is optimal for concentrating as much energy as possible into a single order, and therefore boosting the grating efficiency in that order. Intuitively, we might imagine that to increase efficiency, we should line up the direction of classical “reflection” off the majority of the grating surface with the direction of the diffracted ray. Still thinking classically, we might also want to minimize shadowing in the corners of the grooves.

The ideal blazed grating meets both of these criteria. By carefully choosing a blaze angle  $\theta_b$  we can – at least at one wavelength of interest – line up the specular reflection of the angled surface with the diffraction direction in order  $n$ . Using the law of reflection from geometric optics ( $\theta_{\text{incident}} = \theta_{\text{reflected}}$ ), we can easily<sup>4</sup> derive the optimized condition for a blazed grating. From the geometry in Figure 4.10, where  $N'$  is normal to the angled surface:

$$\theta_{\text{incident}} = \theta_{\text{reflected}} \quad (4.1)$$

$$\theta_2 - \theta_b = \theta_{2,n} + \theta_b \quad (4.2)$$

$$\theta_{2,n} - \theta_2 = -2\theta_b \quad (4.3)$$

Applying a trigonometric identity to the grating equation (3.61):

$$n\lambda/d = \sin \theta_{2,n} - \sin \theta_2 \quad (4.4)$$

$$\frac{n\lambda}{2d} = \cos \left( \frac{\theta_{2,n} + \theta_2}{2} \right) \sin \left( \frac{\theta_{2,n} - \theta_2}{2} \right) \quad (4.5)$$

$$\frac{n\lambda}{2d} = \cos \left( \frac{\theta_{2,n} + \theta_2}{2} \right) \sin (-\theta_b) \quad (4.6)$$

$$(4.7)$$

or

$$\theta_b = -\arcsin \left( \frac{n\lambda}{2d \cos \left( \frac{\theta_{2,n} + \theta_2}{2} \right)} \right) \quad (4.8)$$

Textbooks and resources on beamline design universally provide this derivation and formula for the optimal blaze angle  $\theta_b$  (TODO ref: CXRO x-ray data book, diffraction grating handbook, gratings slits and mirrors). Using efficiency calculations, we’ve confirmed that this intuitive argument is a very good approximation for what happens in the full electromagnetic picture; the actual ideal blaze angle is usually slightly but insignificantly lower. For a 1200 line/mm grating used at an incidence angle of 88 degrees with 400eV photons in the first inside order ( $n = -1$ ) (Figure ??), Equation 4.8 would recommend a blaze angle of 1.67°. We used this as the starting point to conduct a software optimization using efficiency calculations, and were only able to increase the 1st order efficiency from 16.2% to 16.8% by reducing the blaze angle from 1.67° to the optimal 1.46°.

---

<sup>4</sup>Setting up a ruling engine to correctly and accurately engrave this angle is another story...

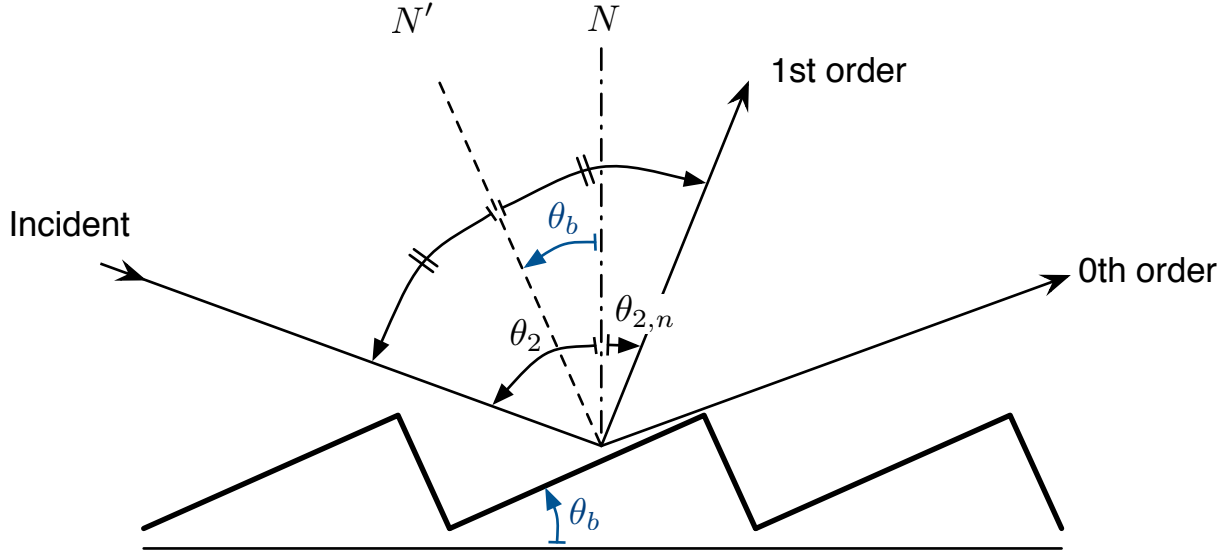


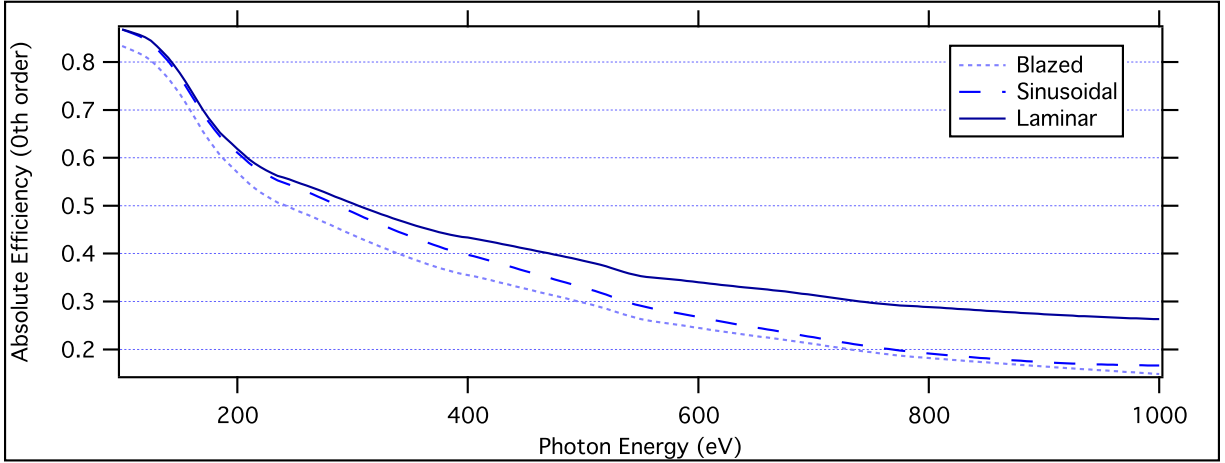
**Figure 4.10:** In the blazed condition, the desired order diffraction angle – in this case, 1st order – is aligned with the direction of specular reflection off the groove surfaces.

Because the blaze angle depends on the  $n\lambda$  term in the grating equation, a grating optimized for a wavelength  $x$  in 1st order will also be optimized for a wavelength  $x/2$  in 2nd order (or, in terms of energy, optimization for  $x$  eV in 1st order would imply optimization for  $2x$  eV in 2nd order). We can confirm this for the blazed grating in Figure 4.11, where the 1st-order efficiency peak occurs at 450eV, and the 2nd order efficiency peak occurs near 900eV.

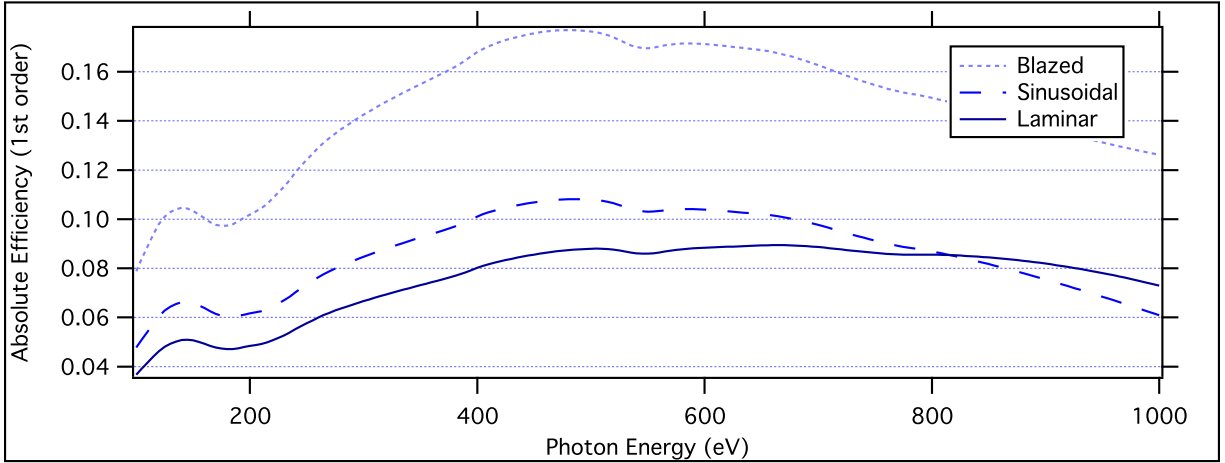
### Efficiency Comparison of Common Profiles

For comparison, Figure 4.11 shows the 0th order, 1st order, and 2nd order efficiency for three common grating profiles: blazed, sinusoidal, and rectangular (commonly referred to as *laminar*). All three gratings have a groove density of 1200 lines/mm, are shown at an incidence angle of 88 degrees, and have had their geometry optimized for maximum efficiency in 1st-order with 400eV photons. (The coating is platinum, and the substrate is quartz [SiO<sub>2</sub>].) The blazed grating was optimized by adjusting the blaze angle; the sinusoidal grating by adjusting the groove depth, and the rectangular grating by adjusting the groove depth and assuming a duty cycle of 50%.

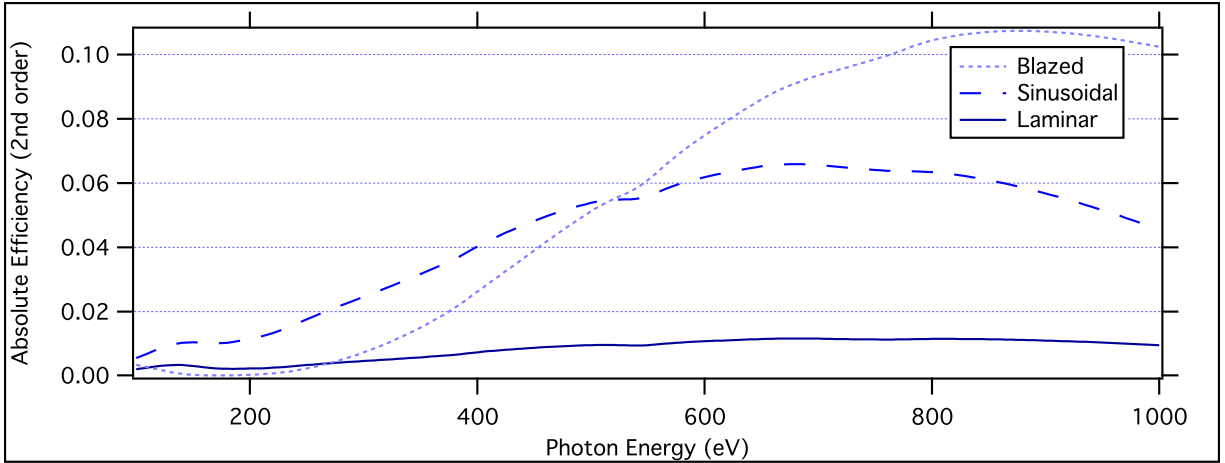
The blazed profile is substantially superior to both the sinusoidal and laminar alternatives. In first order, even though the efficiency curve peaks near the design energy of 400eV, the performance is better across the entire range from 100eV to 1000eV (and beyond). The blaze effect causes this curve to be shifted up in energy by a factor of 2 in 2nd order, so that again the blazed grating out-performs the other profiles, but only above 500eV. The sinusoidal grating has relatively flat efficiency across the energy range, even though it still shows the energy-dependence of its optimization for 400eV. (We've chosen a platinum coating for these demonstrations since its reflectivity is relatively constant across the energy range; see Figure 4.15. The small



(a) 0th Order



(b) 1st Order



(c) 2nd Order

**Figure 4.11:** 0th order, 1st order, and 2nd order efficiency of three different groove profiles, all optimized for use at 400eV. The blazed grating is superior in both 1st and 2nd order. All gratings: 1200 lines/mm, Platinum coating. Blazed:  $1.46^\circ$  angle,  $60^\circ$  anti-blaze angle. Sinusoidal: 13.7nm groove depth. Laminar (rectangular): 9.6nm groove depth, 50% duty cycle.

universal dip in efficiency at 180eV is due to a drop in the Pt reflectivity here.)

### 4.3.2 Effect of Groove Density

Because the groove density directly affects the angular dispersion, using a higher-density grating is the most direct path to designing a higher-resolution instrument (Section 2.2.2). Unfortunately, Figure 4.12 shows that increasing the groove density universally decreases the grating efficiency in all orders except the 0th order, even when the remaining parameters are adjusted to keep the grating optimized. This turns out to be true, not only in this example for two grating profiles, but as a general principle. Intuitively, we can argue that as the groove density approaches infinite, the grating will look more and more like a flat mirror – with microstructure becoming smaller and smaller. Therefore, it makes sense that the amount of light in the 0th-order specular reflection will increase at the expense of the diffracted orders.

Figure ?? explores the groove density effect in more detail, with an efficiency spectrum for a series of blazed gratings from 300 lines/mm to 2700 lines/mm, all optimized for 400eV at 88° incidence. (TODO: Comment on width of blazing peak? Does blazing become less pronounced at higher groove densities?)

TODO generate 3e-2. (3e-2.xls for data)

### 4.3.3 Effect of Coating Thickness

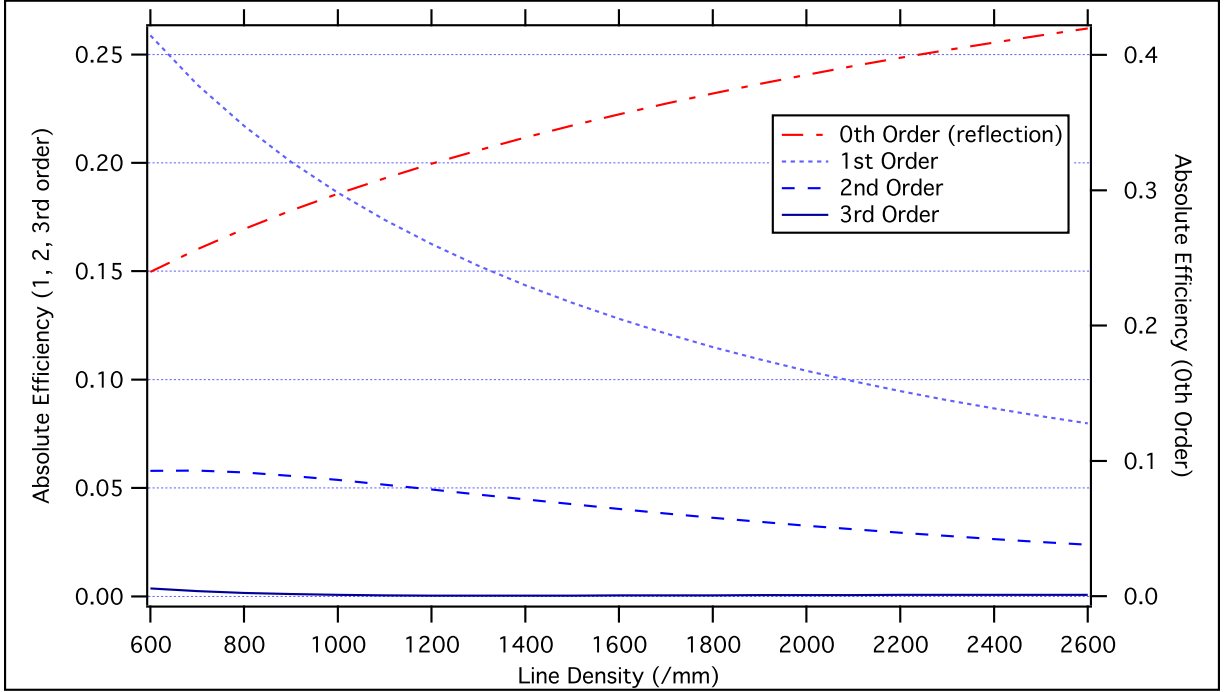
Gratings intended for use in soft x-ray instruments are manufactured on precision-ground blanks, usually consisting of fused quartz (SiO<sub>2</sub>) or other amorphous glasses. The insulating (dielectric) blank is coated in a layer of metal, where the smoothness of the surface is absolutely critical. Often gold is used as a first coating, since it can be applied with very low roughness, and because it provides a soft layer in which to rule the grooves. If another type of coating is required (such as nickel and platinum, in our case), these coatings are applied on top of the gold after ruling.

The required thickness of the coating is another question that can be answered by efficiency calculations. Thin coatings can be applied more smoothly than thick ones (TODO ref Gratings Slits and Mirrors), so the question is: how thick must a coating be for a given photon energy and incidence angle, so that photons are fully reflected or absorbed before reaching the substrate interface? If the coating is too thin, the absorption characteristics of the glass oxide substrate will start to show up in the efficiency spectrum.

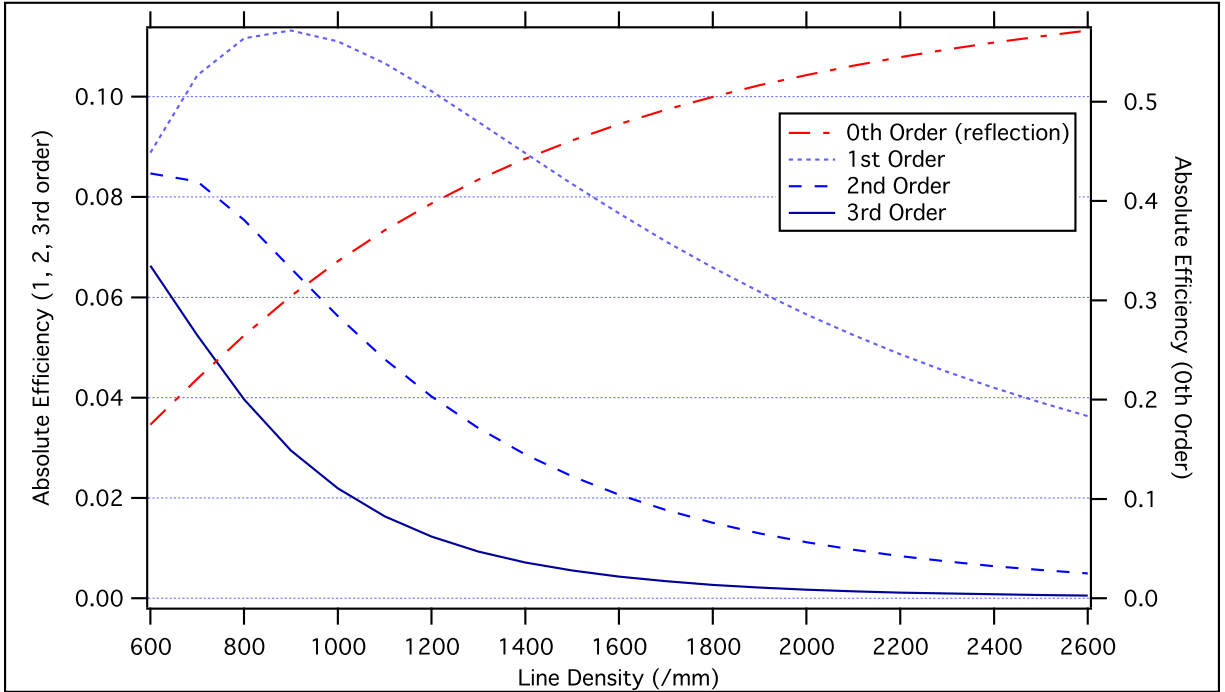
Figure 4.13 shows calculations for various thicknesses of platinum coatings above an SiO<sub>2</sub> substrate, compared with a theoretical solid platinum grating of infinite thickness. The 0.5nm and 1nm coatings show the oxygen absorption edge at 525eV, as well as significantly reduced reflectivity over the whole energy range. The 5nm layer shows a thin-film interference effect that actually boosts the efficiency above 600eV.<sup>5</sup> As we should expect, at a thickness of 50nm and above, the coated gratings become indistinguishable from an infinitely-thick platinum substrate.

---

<sup>5</sup>The sharp peak in this spectrum at 525eV might be anomalous; the Henke data – from which we derive the complex refractive index for all these materials – is admittedly not accurate in the immediate vicinity of absorption edges.

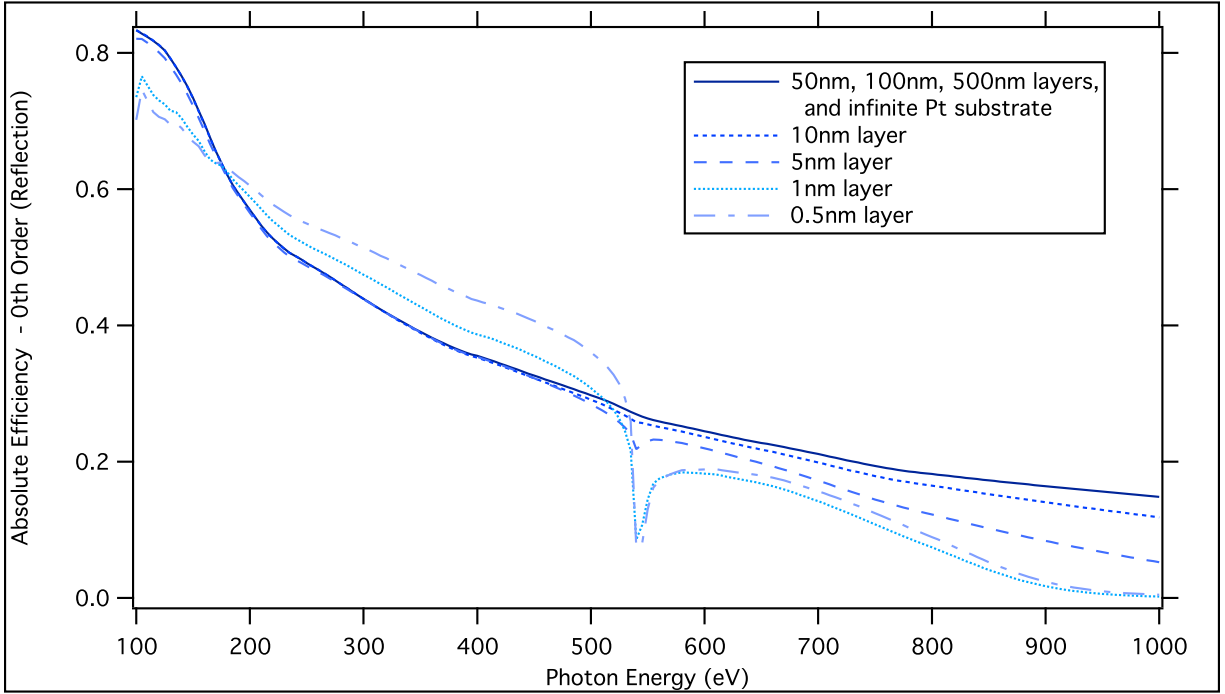


(a) Blazed grating, maintaining the blaze condition as the groove density changes.  
Platinum coating, 88-degree incidence, 400eV photon energy.

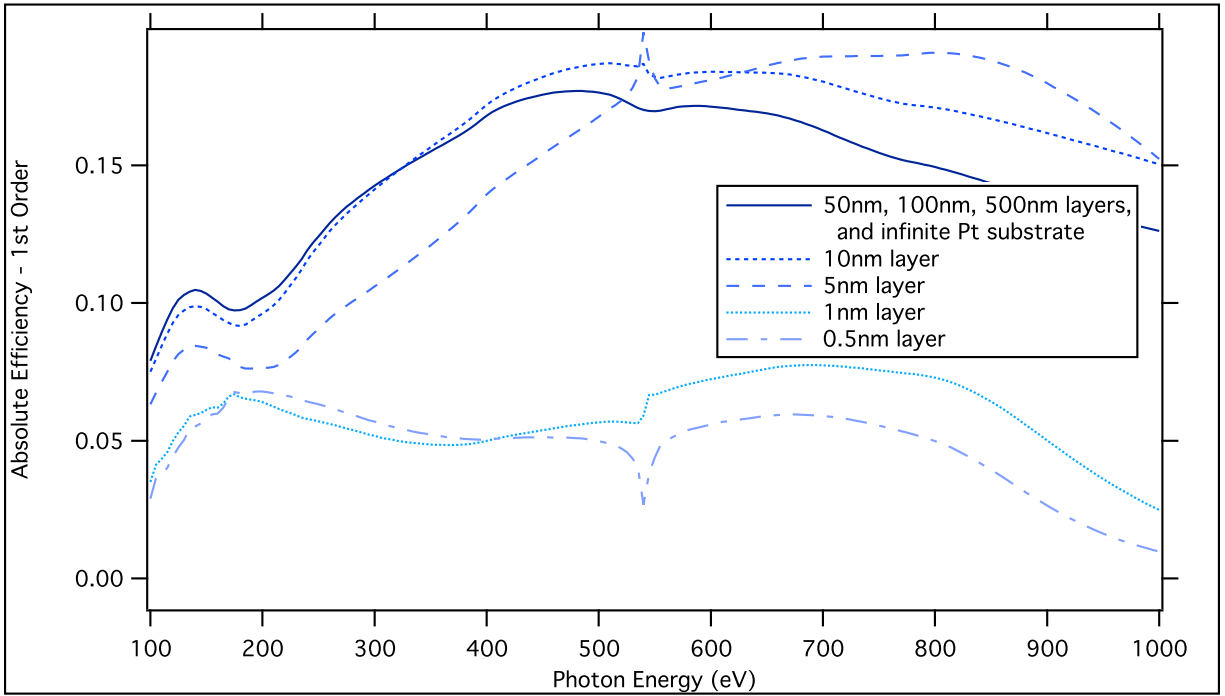


(b) Sinusoidal grating. Groove depth optimized at 1200 lines/mm; maintaining the depth-to-period ratio as the line density changes. Platinum coating, 88-degree incidence, 400eV photon energy.

**Figure 4.12:** Increasing the groove density always decreases the diffraction efficiency – at least for all the useful orders ( $n \neq 0$ ). In these plots, we've tried to control for inter-related factors: For the blazed grating in (a), the blaze angle has been adjusted with the groove density (using Equation 4.8) to maintain the on-blaze condition. In (b), the sinusoidal grating depth was optimized at 1200 lines/mm, and then the depth-to-period ratio was maintained across changes to the groove density.



(a) 0th Order



(b) 1st Order

**Figure 4.13:** In the soft x-ray regime under grazing incidence, metal-coated dielectric gratings are indistinguishable from pure metal gratings... as long as the coating is thicker than  $\sim 20\text{nm}$  (although the exact thickness depends on the material, photon energy, and incidence angle). These calculations show Pt coatings of varying thickness over an  $\text{SiO}_2$  substrate, as well as an infinitely thick pure Pt grating. (Blazed grating, 1200 lines/mm,  $1.46^\circ$  blaze angle,  $88^\circ$  incidence).



In general, the required minimum thickness will depend on the photon energy, incidence angle, and the x-ray form factor of the coating material – all of which affect the x-ray penetration depth. These results show that for thin coatings, the efficiency calculations are able to rigorously incorporate the effects of interference and absorption at the interface with the substrate.

#### 4.3.4 Comparison of coating materials

All materials suffer from inherently low reflectivity at soft x-ray energies. Even when gratings are used at grazing incidence, designers must carefully choose coating materials to maximize efficiency considering the desired wavelength range of the instrument. (This becomes particularly frustrating when a material with otherwise high reflectivity has an absorption edge right in the middle of the region of interest.)

To help in selecting materials, Figures 4.14 and 4.15 show several possibly grating coatings: carbon, nickel, gold, platinum, and iridium. (Figure 4.14 shows the reflectivity of a plain mirror made out of these materials over the energy range from 100 to 1000eV, at 88° grazing incidence. Figure 4.15 compares the mirror reflectivity with the 0th order and 1st order efficiency of a sinusoidal grating, which had its groove depth optimized for 400eV.)

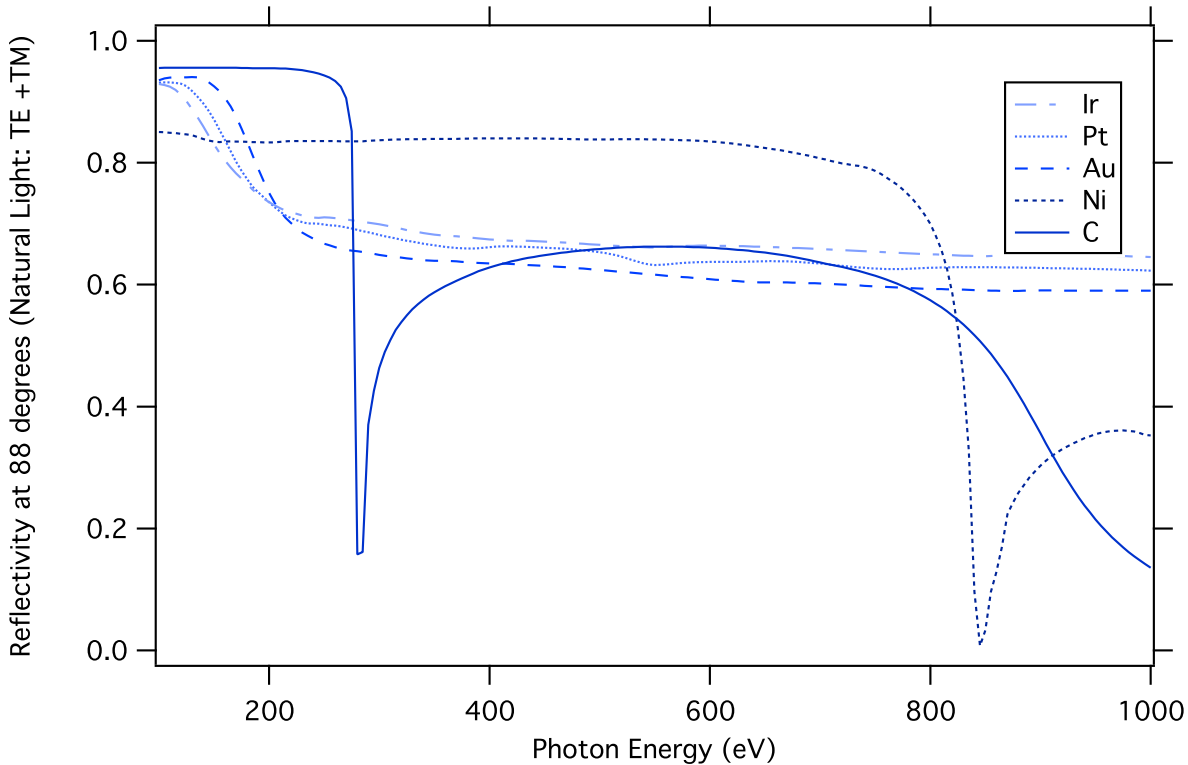


**Figure 4.14:** The reflectivity of a pure mirror at grazing incidence (88°), as a function of photon energy. Lighter elements like carbon and nickel have the highest peak reflectivity, but have strong absorption features. Heavier metals, particularly those within the platinum group, have reasonable reflectivity over the entire soft x-ray region of interest. Up to 200eV, Gold has a higher reflectivity than Pt and Ir.

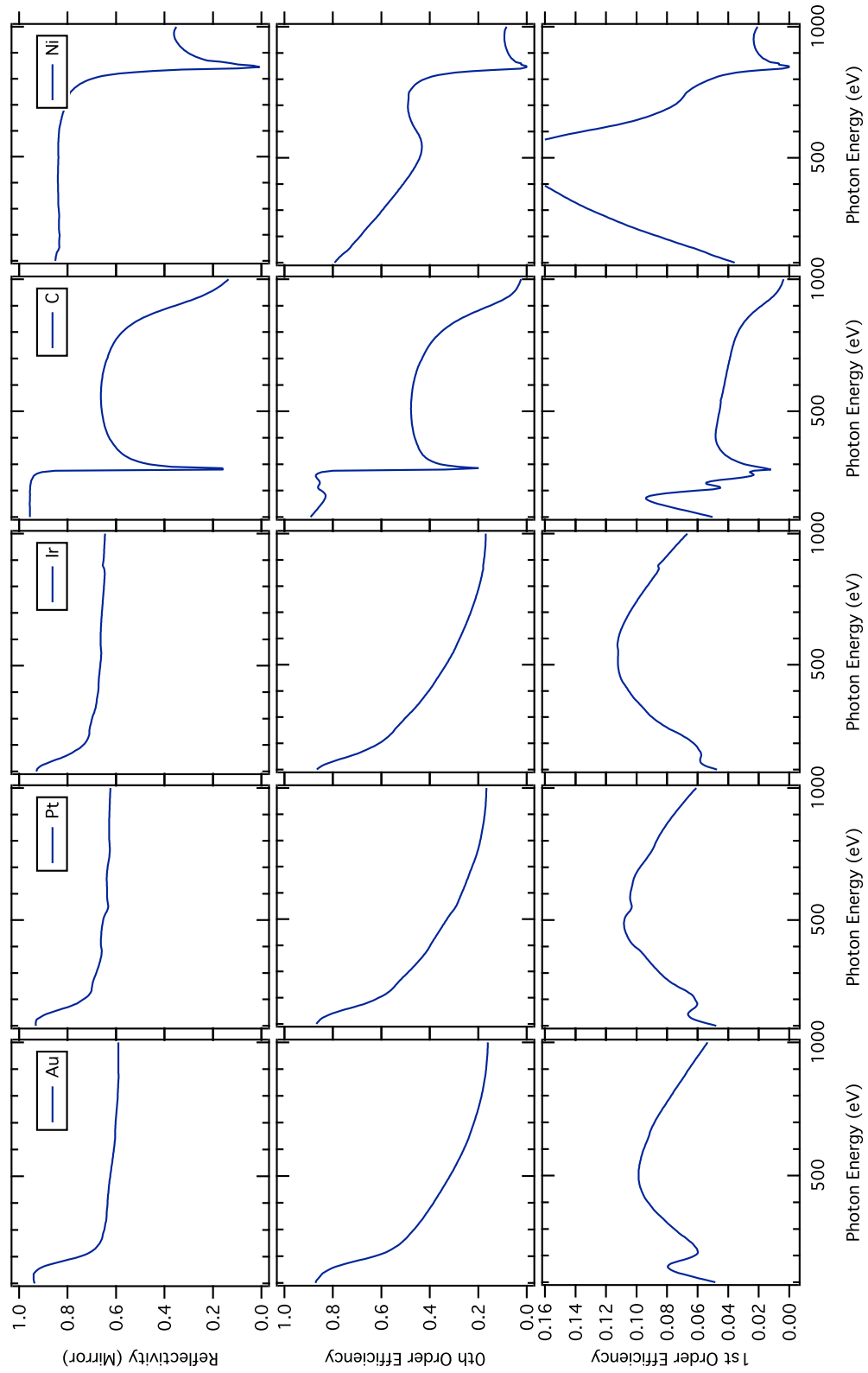


**Figure 4.15:** A comparison of the mirror reflectivity, 0th order, and 1st order efficiency for different coating materials, as a function of photon energy. (Gratings: Sinusoidal profile,  $88^\circ$  incidence angle, 1200 lines/mm, 13.7nm groove depth) Note that the 1st order efficiency has energy-dependent features that aren't visible in the simple reflectivity.

The heavy precious metals (Au, Pt, Ir) are commonly chosen for grating coatings because they have a relatively constant reflectivity over this energy range. This is because their core-level electrons are so tightly bound that their strongest absorption features occur well above the soft x-ray range. (For example, the Pt K 1s absorption edge is at 78.4 keV.) Their outer-shell electrons fall within the soft x-ray range (for example, the platinum N and O transitions), but these absorption features aren't nearly as strong, and therefore don't seriously affect the reflectivity. Gold has better reflectivity than Pt and Ir below 200eV, and also has the previously-mentioned desirable property of being easy to apply smoothly and rule mechanically. Above 200eV, platinum has been the de-facto choice for high-energy wide-bandwidth gratings for many years. Iridium (and rhodium, not shown) actually have even better reflectivity and corrosion resistance than platinum, and are becoming standard coating options with some manufacturers.

In contrast, carbon and nickel offer much higher reflectivity over some parts of this energy range, but unfortunately have strong absorption features right in the middle. The carbon K 1s absorption edge at 284eV makes it restricted to, but excellent for, low-energy applications. The nickel L<sub>2</sub>/L<sub>3</sub> edges don't occur until 870/853 eV, and Figure 4.15 seems to suggest that nickel would be the clear winner over much of the soft x-ray range. This prompted us to use it for two of the REIXS spectrometer gratings, with one obvious but unforeseen consequence (Section ??).

Not shown in these plots, silicon also has a very high reflectivity up to its L<sub>2</sub>/L<sub>3</sub> absorption edge at 100eV. Therefore, bare (uncoated) SiO<sub>2</sub> mirrors are often used for extreme ultra-violet (EUV) and very low-energy soft x-ray beamlines (TODO REF Gratings, Slits and Mirrors); Si-coated gratings might be useful here as well.

### 4.3.5 Effect of photon energy / wavelength

The energy-dependence (or wavelength-dependence) of grating efficiency has been shown in many of the previous plots, where we've displayed the efficiency as a function of photon energy. However, it's impossible to completely isolate this relationship because the photon energy is inherently coupled to the grating efficiency in multiple ways. For starters, the complex refractive indexes of the coating and substrate vary as a function of energy. However, the photon energy also determines the angle of the outgoing diffraction orders, which can be seen in both the Rayleigh expansion for the total field, and in the simplified grating equation (Equation 3.61). Therefore, optimizations for geometry parameters that depend on angle – like the blaze angle and groove depth – are inherently coupled to the photon energy. The plots in Figure ?? highlight this by showing the difference between the energy-dependent reflectivity of a plain flat mirror, versus the more complicated diffraction efficiency.

### 4.3.6 Effect of incidence angle

In the soft x-ray regime, the real part of the refractive index for most metals is less than unity. This means that the phase velocity for light in the material is actually *faster* than the speed of light in a vacuum.<sup>6</sup> As mentioned in Section ??, we can exploit this lucky phenomenon to increase the reflectivity of gratings and mirrors by using them at grazing incidence to create a “*total external reflection*”.

Total internal reflection (TIR) happens in conventional materials when a light ray travels from a slower optical medium (refractive index  $n_1$ ) toward a faster optical medium (refractive index  $n_2 < n_1$ ). Snell’s law of refraction would relate the angles of the incident ( $\theta_1$ ) and transmitted ( $\theta_2$ ) waves:

$$n_1 \sin \theta_1 = n_2 \sin \theta_2 \quad (4.9)$$

$$\sin \theta_2 = \frac{n_1}{n_2} \sin \theta_1 \quad (4.10)$$

By choosing an incident angle  $\theta_1$  for which there is no possible solution to  $\theta_2$ , we can ensure that there is no transmitted wave – the incident wave must be completely reflected.

$$\frac{n_1}{n_2} \sin \theta_1 > 1 \quad (4.11)$$

This will happen for all incident angles  $\theta_1$  beyond a critical angle:

$$\theta_{\text{critical}} = \arcsin\left(\frac{n_2}{n_1}\right) \quad (4.12)$$

The same situation happens when light from the (slower) vacuum is incident on the (faster) medium of the grating. Here the vacuum refractive index is  $n_1 = 1$ , and the real part of the grating refractive index (which gives the propagation velocity) is  $\tilde{n}_2 < 1$ . (For example, at 410 eV, the real part of the refractive index of gold is  $\tilde{n}_2 = 0.99425$ .) We can therefore calculate the critical angle for *total external reflection*; for incident angles larger than this, there should be no transmitted wave into the grating:

$$\theta_{\text{critical}} = \arcsin(\tilde{n}) \quad (4.13)$$

(where  $\tilde{n}$  is the real part of the coating’s complex refractive index.) Critical angles for the coatings in Figure 4.15 at 410eV are given in Table 4.17.

The concept of TER is just another intuitive approximation for what happens in the full electromagnetic picture, but Figure 4.16 does confirm that the grating efficiencies in the 0th, 1st, and 2nd inside orders are indeed extremely low below platinum’s critical incidence angle of  $83.3^\circ$ . This figure shows the effect of incidence angle on efficiency for several different geometry profiles. We might expect that as the incidence angle becomes more and more grazing, the efficiency should increase continuously...and that is certainly true for the  $n = 0$  order. However, this turns out to be not true for the remaining orders; *there is actually*

---

<sup>6</sup>The non-zero imaginary part of the refractive index ensures that the transmitted wave decays and is absorbed, therefore Einstein’s speed limit is not violated.

**Table 4.1:** Critical incidence angles for “total external reflection” at 410 eV for the grating coatings shown in Figure 4.15.

Material	$\theta_{\text{critical}}$ for TER ( $^{\circ}$ )
Carbon (C)	85.92
Nickel (Ni)	83.20
Gold (Au)	83.85
Platinum (Pt)	83.32
Iridium (Ir)	83.10

*an optimal incidence angle below  $90^{\circ}$  where efficiency is maximized.* At first glance, it might seem like this is an accidental side-effect of the blazed optimization; since the optimal blaze angle depends on the incidence angle, it might have been possible that all the gratings in Figure ?? had their geometry optimized for a sub- $90^{\circ}$  incidence angle. However, by exploring the effect of incidence angle on efficiency over a range of blaze angles, Figure 4.19 dispels this idea; it shows that for  $n \neq 0$  orders, there is indeed an optimal incidence angle, which depends only on the groove density and the energy.

Figure 4.19 contains a take-away message for instrument designers: if an arbitrary incidence angle is required for some external reason, the blaze angle can be adjusted to optimize for that incidence. However, in the absence of constraints, there does exist a unique optimal incidence angle (and corresponding blaze angle), typically between  $87^{\circ}$  and  $88^{\circ}$ , where the efficiency reaches an absolute maximum.

TODO: test with groove density. Does it depend on diffraction eqn?

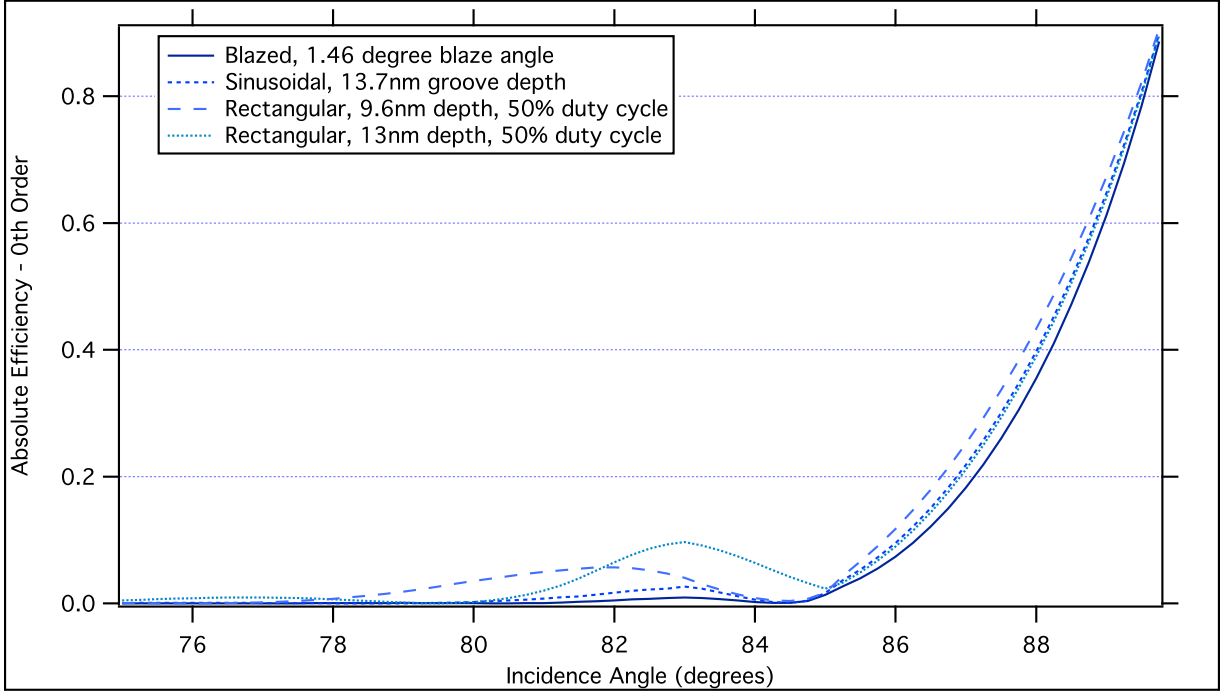
### 4.3.7 TODO Applications to beamline and instrument design

- Observation: blaze angle and groove depth can be used to optimize efficiency for a constrained incidence angle. However, while 0-order reflectivity increases with grazing incidence, there IS an optimal incidence angle (usually between 87 and 88 degrees), which does not depend on the grating material, and depends somewhat on the incident energy (increases with energy).

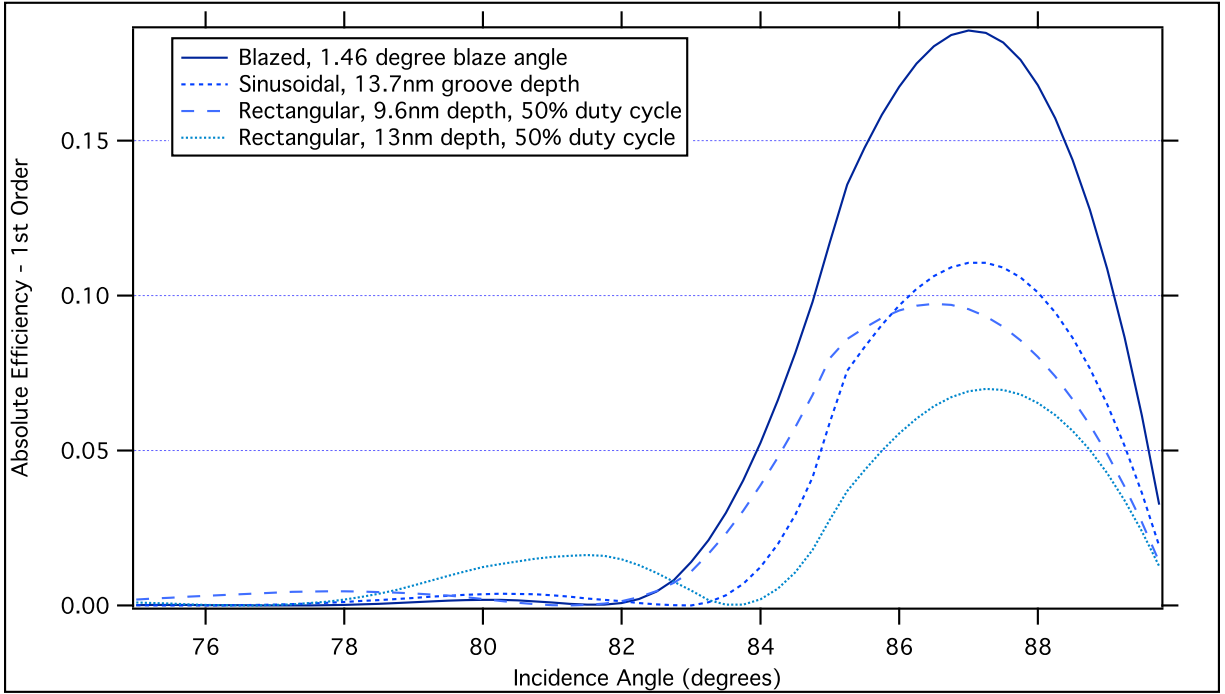
Practical application: This optimal incidence angle provided the starting point for the incidence angles used in the REIXS spectrometer, and explains why the lower-energy gratings (LEG, IMP) use lower (more normal) incidence angles than the high-energy gratings. TODO if time: determine way to calculate optimal incidence angle. Is this just a TE or TM effect? NO... te and tm behave the same.

Highlighted conclusions: - blazed is idea for narrow energy range and constant incidence angle. In case of spectrometer, definitely the right choice. For mono... No constant incidence angle. Still better than sinusoidal if not? Find out.

- Optimal incidence angle
- always blazed: (show whether better than sinusoidal for CII monochromator)



(a) 0th Order



(b) 1st Order

**Figure 4.16:** The effect of incidence angle on diffraction efficiency for various grating profiles. While the 0th order efficiency/reflectivity always increases as the incident light becomes more grazing, there is an optimal incidence angle below  $90^\circ$  for higher-order light. The critical angle for total external reflection in Platinum is  $83.3^\circ$ ; clearly both the 0th-order and 1st-order efficiency drop off significantly below this angle. (Gratings: 1200 lines/mm, platinum coating, 400 eV; blaze angles and profiles as indicated.)

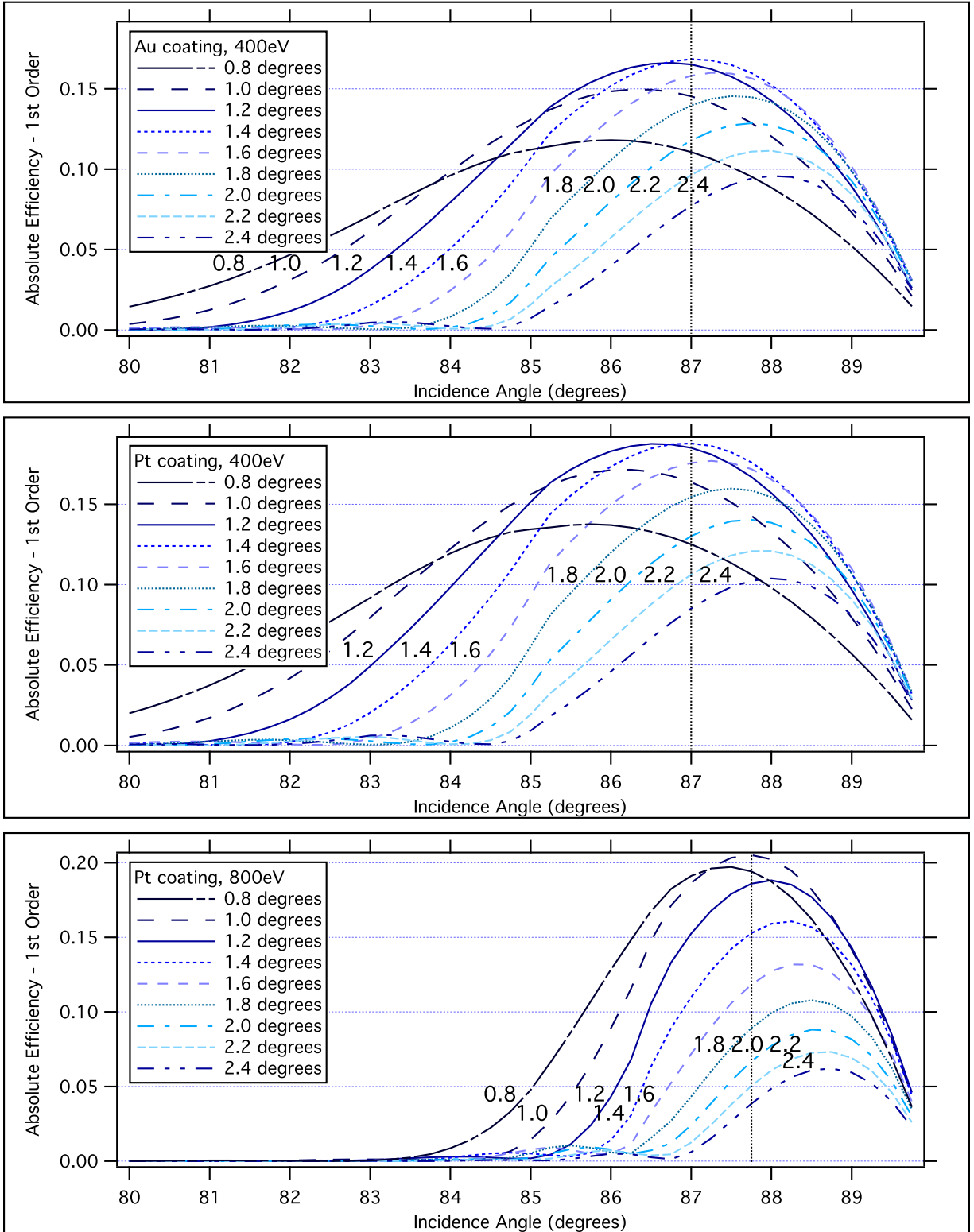


**Figure 4.17:** While the blaze angle can always be used to tune a grating for a required incidence angle, there is still a particular *optimal* incidence angle that – when combined with a corresponding optimized blaze angle – would produce the highest achievable efficiency. This optimal angle doesn't seem to depend on the material, but only on the groove density and energy. (Gratings: all 1200 lines/mm; coatings, blaze angles, and energies as indicated.)

- consider 3rd order rather than increasing groove density (manuf. limit) – next chapter.
- blazed gratings: when optimizing for low energies (near 100eV): create narrow efficiency peaks. when optimized for higher energies, the peaks are wider and the gratings can be more general.

## 4.4 Validation: comparison of theory to experimental results

The previous section provides some recommendations to beamline designers based on this theoretical survey of the factors affecting grating efficiency. For these results to be trustworthy, we need confirmation that the theoretical methods in Chapter 3 – and the software implementation described in this chapter – accurately describe gratings in the real world. We go onward in Chapter 5 to use these tools to design the gratings and optical layout for the REIXS beamline spectrometer; before starting this project, we clearly needed our own validation of the software’s accuracy.

The published literature on grating efficiency does not contain many measurements of real-world grating efficiency, partly due to the difficulty of completing these measurements, and partly because – on receiving brand new gratings – most beamline builders would rather install them as quickly as possible and start doing their own science, rather than spend time on another beamline characterizing the gratings. We were able to find one study by M. Bowler at the SRS light source (TODO REF Bowler) with a recent set of efficiency measurements done on four gratings, representing three different types of grating profiles, which turned out to be ideal for comparing with theoretical calculations. The gratings consisted of one blazed grating with 1440 lines/mm, one laminar grating with 600 lines/mm, and two attempted-laminar gratings that ended up with trapezoidal sides of approximately  $57^\circ$ . All of the gratings were well-characterized by the manufacturer after ruling, allowing for accurate geometry inputs into the theoretical calculations. (The study also conducted efficiency calculations using the differential method, but we duplicated these calculations as a double-check on our implementation.)

Figures 4.18 through 4.21 show the experimental measurements from (TODO REF), combined with our own calculations of the grating efficiency. Table ?? provides the geometry parameters, derived from the manufacturer’s measurements.

### Note on incidence angle

Unlike the constant incidence angle efficiency curves we’ve been using up to this point, these gratings were designed for use in constant-included-angle monochromators, where the deviation angle ( $\theta_2 + \theta_{2,n}$ ) between the incident beam and the useful order  $n$  is held constant. Therefore, these plots show the efficiency as a function of energy, with an incidence angle that also varies according to this constraint as a function of energy along the  $x$ -axis.

Of particular interest are the 1st and 2nd order results for the blazed grating in Figure 4.18, since we quickly chose blazed gratings for the design in Chapter 5. The close agreement between theoretical and



measured efficiency shown here gives us a high degree of confidence in applying the grating software to optimize real-world beamlines.

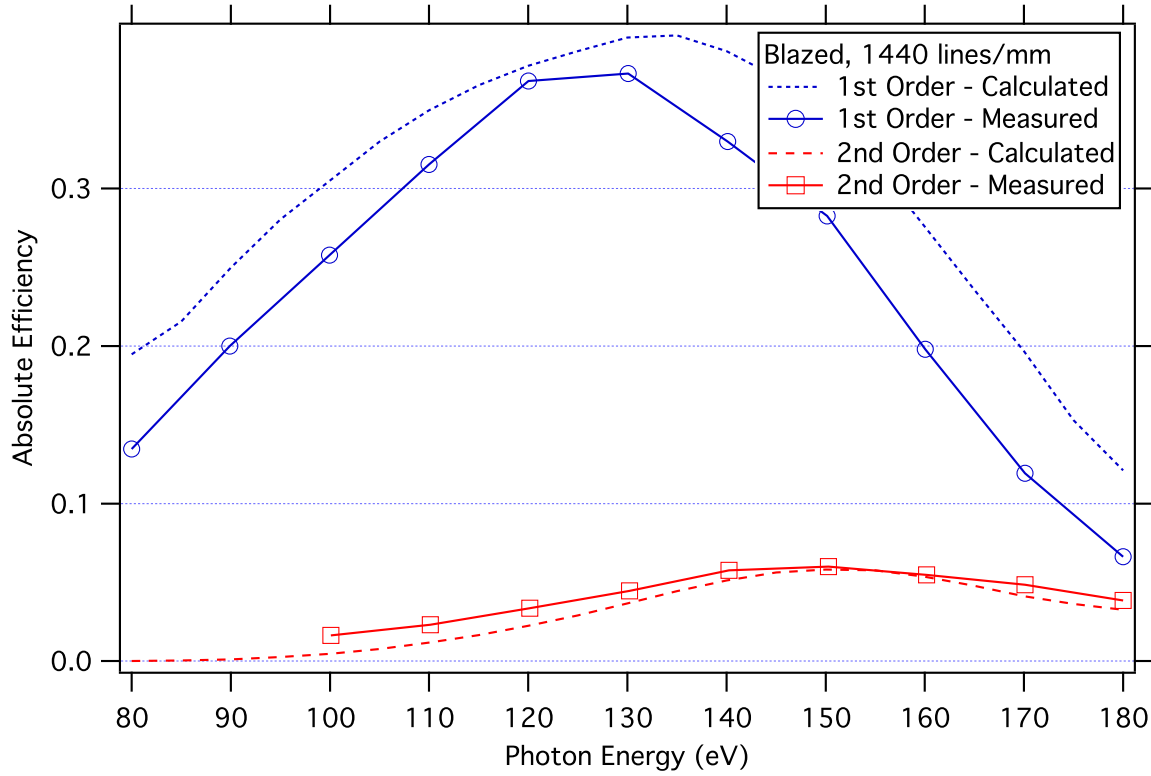


**Figure 4.18:** Comparison of grating efficiency calculations to diffractometer measurements. Blazed grating, 1440 lines/mm, 2.2° blaze angle, 12.8° anti-blaze angle. Incidence: 160° constant included angle to the 1st inside order.

[compare with GSolver results?]

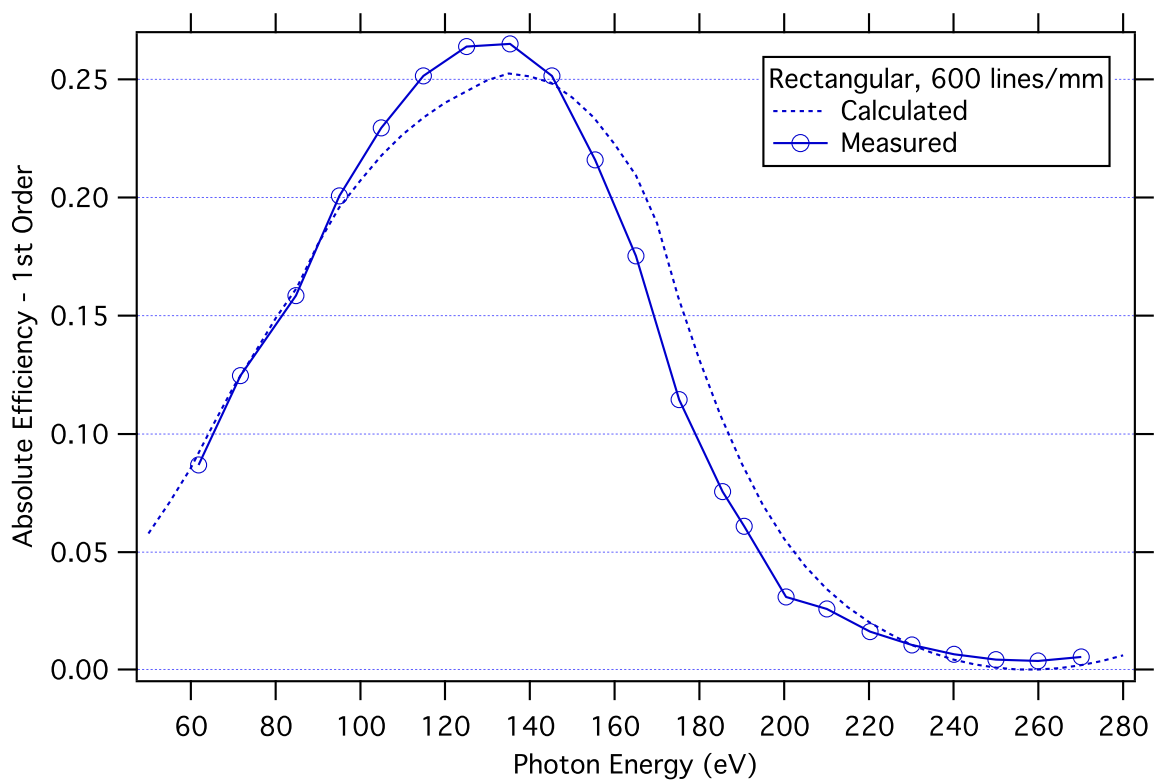


**Figure 4.19:** Comparison of grating efficiency calculations to diffractometer measurements. Rectangular grating, 600 lines/mm, 22.2 nm depth, 0.833  $\mu\text{m}$  valley width. Incidence:  $167^\circ$  constant included angle to the 1st inside order.

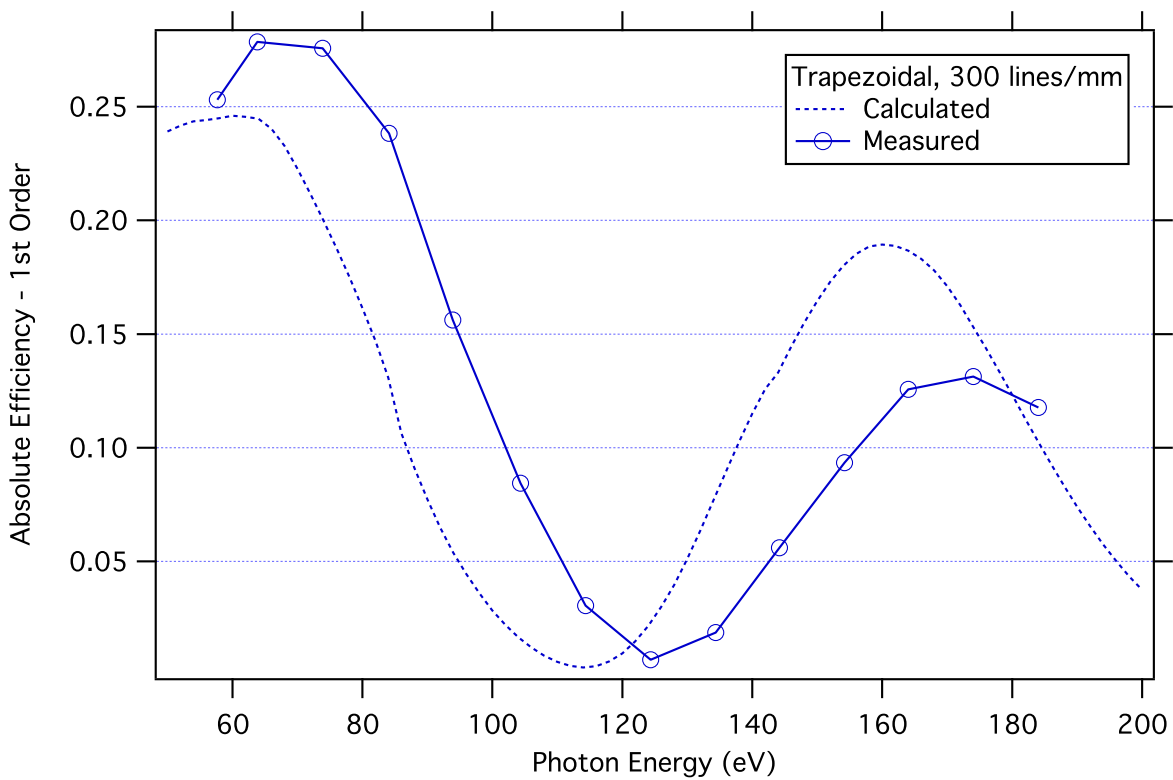


**Figure 4.20:** Comparison of grating efficiency calculations to diffractometer measurements. Trapezoidal grating, 300 lines/mm,  $57^\circ$  side angles, 49.3 nm depth, 2.46  $\mu\text{m}$  valley width. Incidence:  $167^\circ$  constant included angle to the 1st inside order.

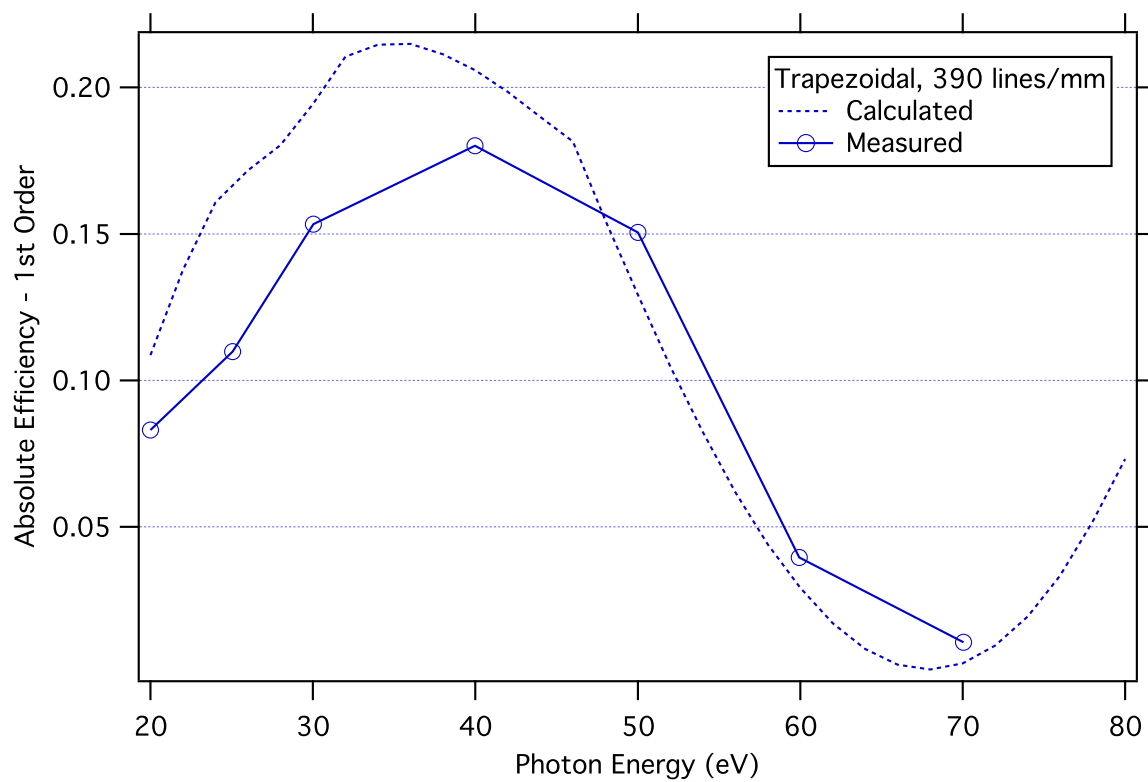


**Figure 4.21:** Comparison of grating efficiency calculations to diffractometer measurements. Trapezoidal grating, 390 lines/mm,  $57^\circ$  side angles, 54 nm depth, 1.39  $\mu\text{m}$  valley width. Incidence:  $160^\circ$  constant included angle to the 1st inside order.

## CHAPTER 5

# DESIGN: HOW DAVID AND I APPLIED THESE TOOLS TO MAKE THE REIXS OPTICAL DESIGN

## 5.1 Application to spectrometer design

### 5.1.1 Design Goals: (simultaneously)

- Highest resolution: "Resolution, Eres, is a measure of smallest amount by which two energies can differ and still be distinguished (or re- solved) by a given spectrometer."
  - Fast experiments (high efficiency) -
- Reference: Stated goals from David's thesis

### 5.1.2 Comparative examples

- High-res beamline at SLS; - BL8 (workhorse); - commercial XES350

FIGURE 4a: comparison of resolution, REF david's thesis

## 5.2 Design Process

- Iterative design process with David: jointly address factors affecting resolution  
describe overlapping factors...

TABLE 4b: Factor, effect on resolution, effect on efficiency

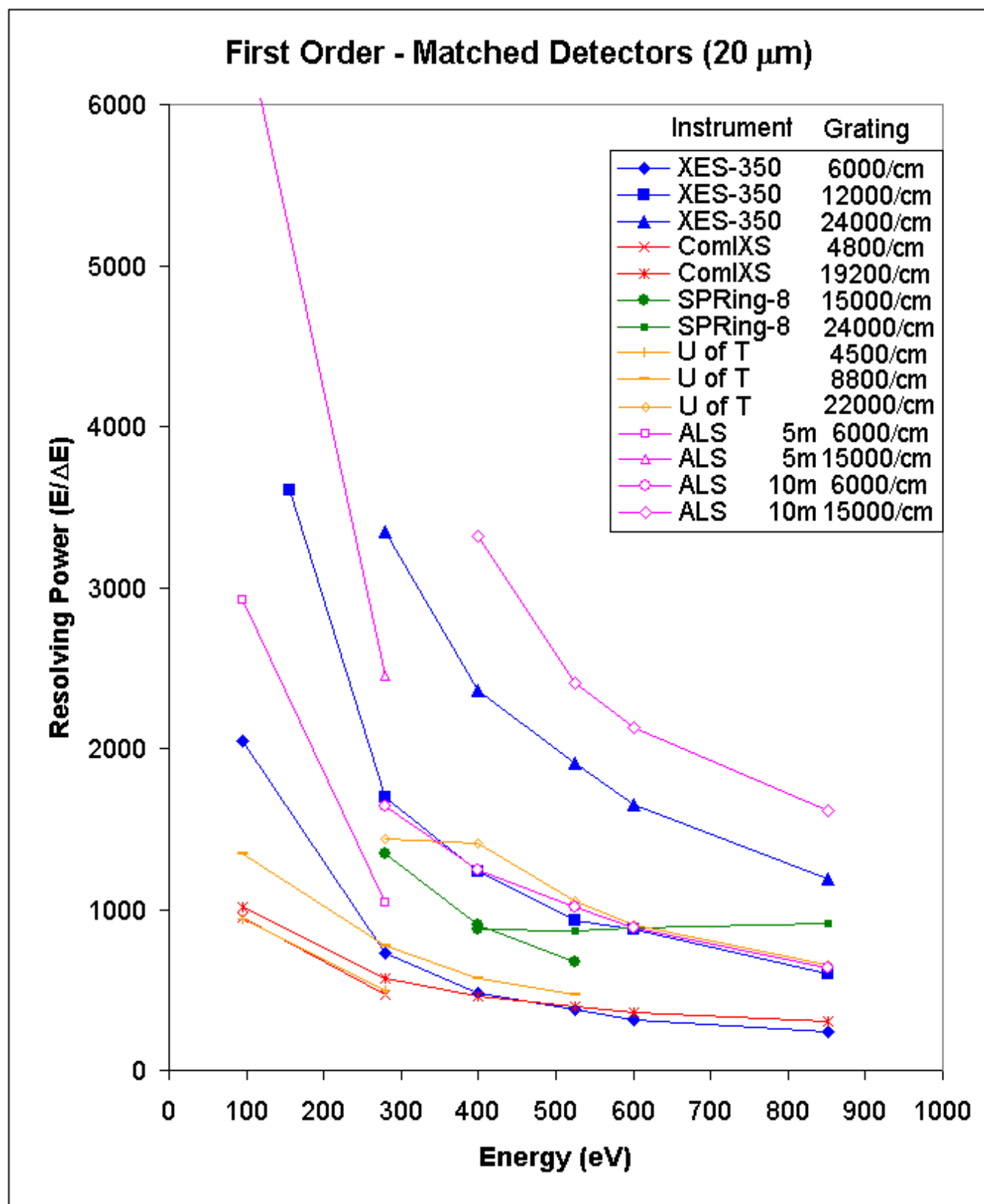
### 5.2.1 Justification of Design choices:

#### Ruled vs holographic gratings

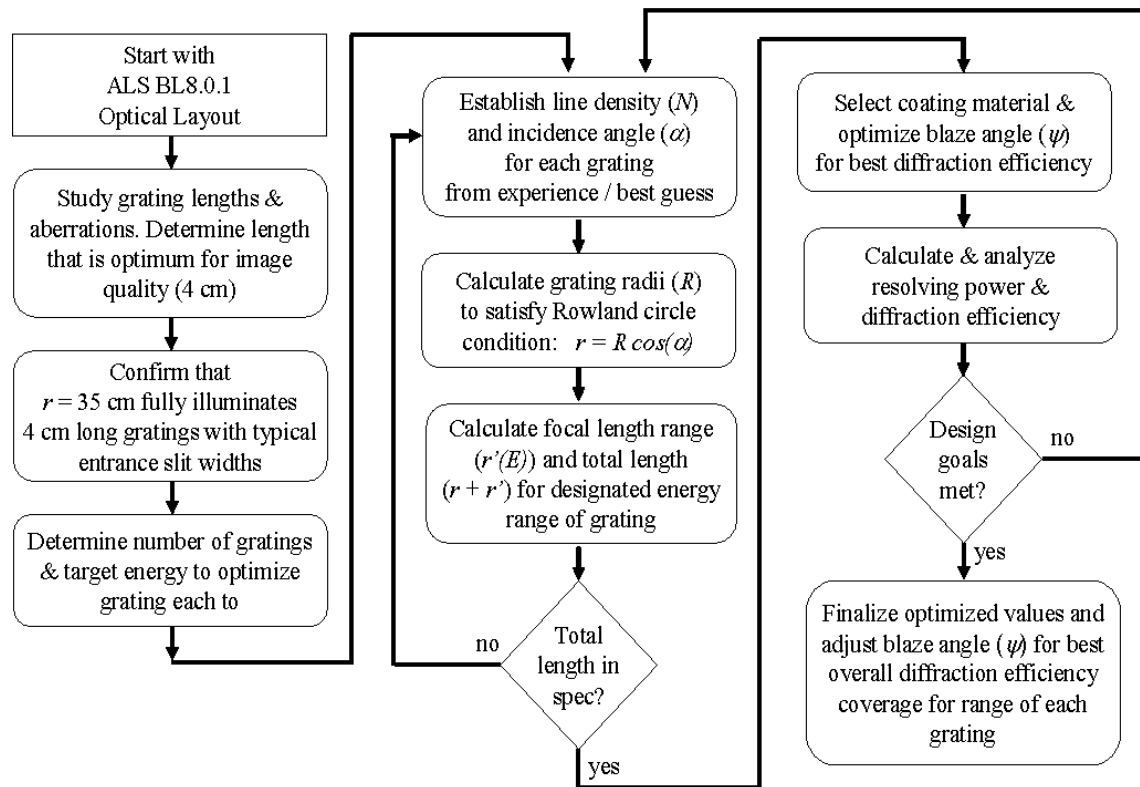
- manufacturing errors - holo: can't get true blaze profile... can reduce from sinusoidal using ion etching

FIGURE 4d: common ruling errors (ideal grating; blaze angle off; ion-etched blaze; ruled blaze with large apex; ghosting)

- ruled: susceptible to "ghosting" from higher-order structure; lower upper limit on groove density; difficult and long to manufacture with precision ruling engine. Still not true sawtooth with 90degree top corner.



**Figure 5.1:** Resolving power performance comparison of existing spectrometer designs, calculated with all detectors having a 20  $\mu\text{m}$  pixel size. The legend specifies the spectrometer and grating choice (size and/or line density). [Source: David Muir M.Sc. thesis.]



**Figure 5.2:** Approximation of the process used to design the optics of the REIXS spectrometer. [Source: David Muir M.Sc. thesis.]

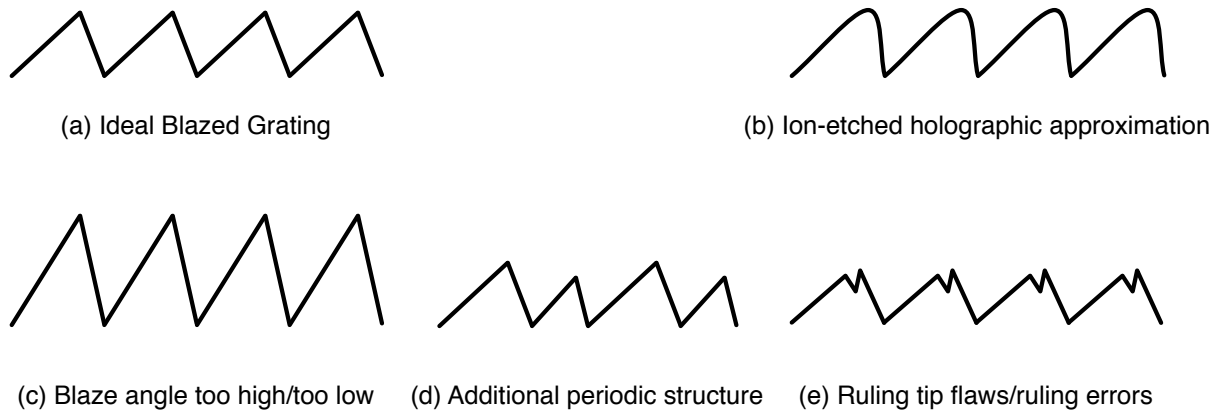


**Figure 5.3:** Common errors in the manufacture of ruled and holographic gratings. Holographic exposure creates a sinusoidal profile; subsequent ion-etching (b) can only approximate a triangular profile. Ruled gratings can suffer from blaze angle errors (c), or errors due to the shape and/or depth of the diamond tip (e). If the ruling engine introduces periodic errors in the groove position, this additional structure (d) creates additional diffraction peaks (ghosts).

## Rowland vs. VLS design

just reference david's thesis - VLS: flat focal curve, minimize aberrations, compact design but lose spatial resolution for the same grating density. Examples require extremely high-res CCD detectors just to maintain average resolution. Also: aberrations can only be fully corrected around a single energy. Also, lose flexibility to operate in higher orders for more resolution, since the VLS optimizations depend on the order, and behave erratically outside of that. [cite: Table 3.3] Figure 5.1

## blazed vs. trapezoidal/sinusoidal

- Not using dielectric multi-layer gratings (reason: tuned for excellence at single energy)

## 5.3 High-resolution (3rd order) design

### 5.3.1 Options for reaching extreme resolution:

- increase groove dens... manufacturing limit; serious drop in efficiency. - long detector distance (increased radius)... reduction in geometrical efficiency due to longer source-grating. [alternative: proposed design that alex reviewed: uses collecting mirror] - Our Novel approach: attempt usage of specially-designed blazed gratings in 3rd order. (immediately see by differentiating grating equation with respect to wavelength: effect of order on resolution) - Highlight: only known design in the world to do this. Why? Maybe we'll find out ; ) - effect on geometric efficiency:  $r$  (source grating)

DATA 4e: triple-groove dens. vs. long-distance [scaled by geometric efficiency] vs. 3rd-order design. [note: triple-groove density would be impossible to rule]

Alternative options to increase resolution

- We were constrained at maximum machine size. Even if you could make it bigger, would it be better?
- - Increasing  $R$ : - Need to maintain  $\alpha$  (efficiency) -  $r$  and  $r'$  increase - First geometric efficiency hit: increase entrance arm... would need to increase grating size, but this increases cost; also limit on grating size because spherical aberrations become even more significant with grating size— $\propto 1/r^2$

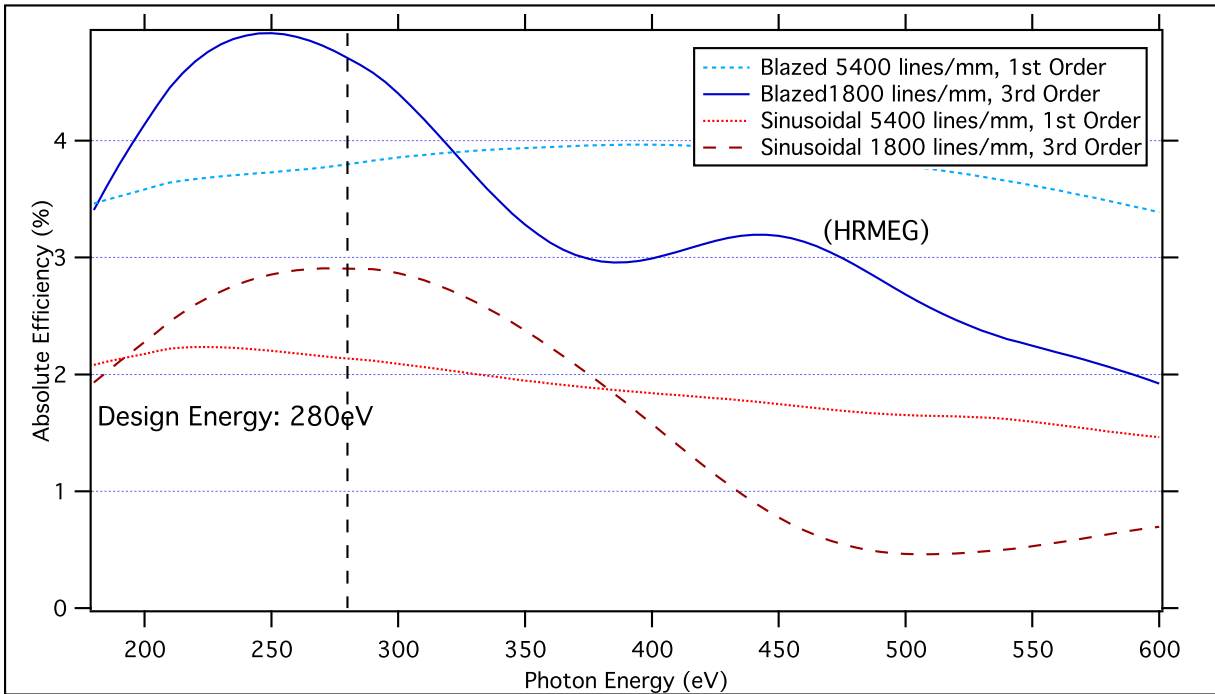
- second geometric efficiency hit: increase exit distance. Only include sagittal; assume reduction in geometric efficiency due to detector catching smaller solid angle as inherent in increasing resolution. - spherical grating: by increasing  $R$ , also decreasing sagittal focussing

TODO: Why is there a peak at 87 in the incidence curve? Does it depend on material?

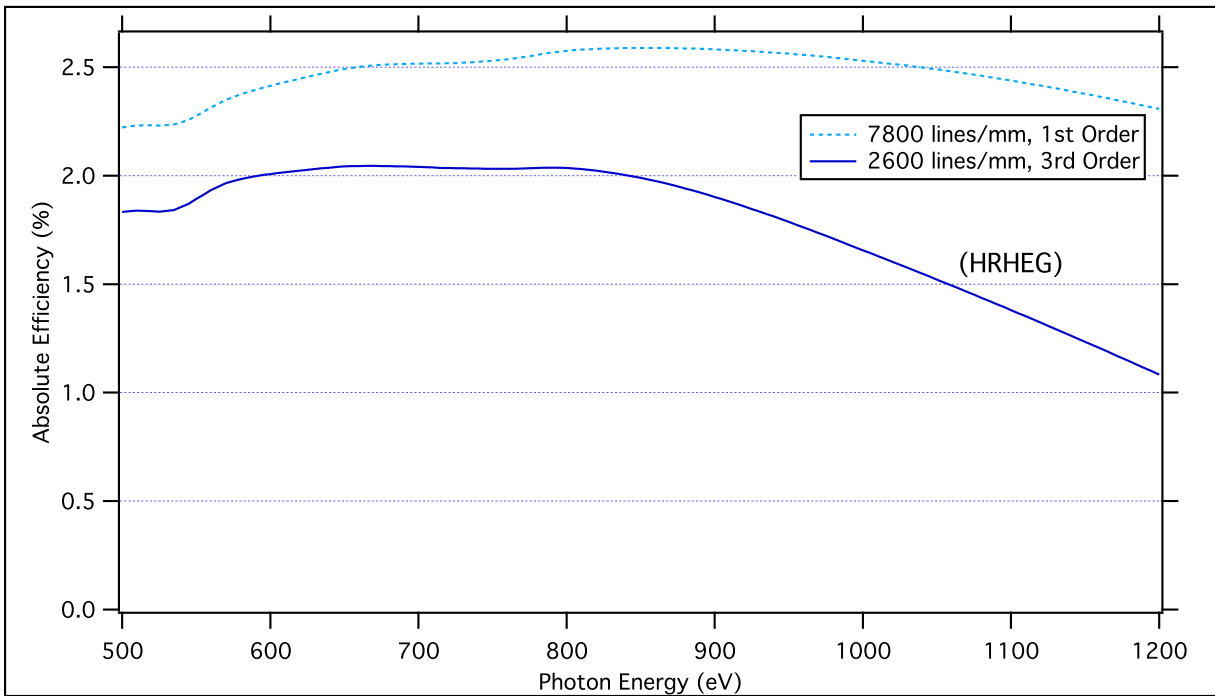
## 5.4 Coating choices:

- DATA 4f: plot reflectivities over range for: Au, C, Ni, Pt, Ir, Ag, etc [use DATA 3g] - Choices within regions of interest





(a) The 3rd-order HRMEG (1800 lines/mm), and an equivalent-resolution 1st-order grating (5400 lines/mm - impossible to manufacture). The 3rd-order efficiency advantage persists even for sinusoidal gratings without the blazing advantage.



(b) The 3rd-order HRHEG (2600 lines/mm), and an equivalent-resolution 1st-order grating (7800 lines/mm - impossible to manufacture).

**Figure 5.4:** todo todo todo

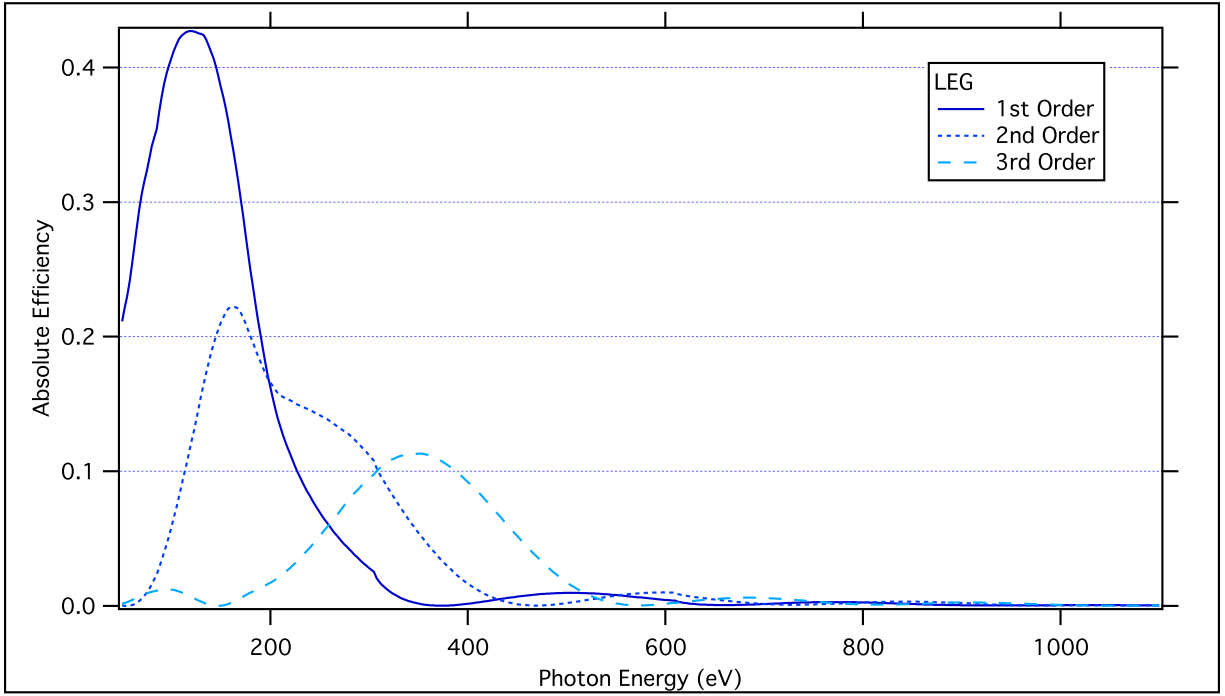
## 5.5 Optimization

simple hill-climbing [with constraints]

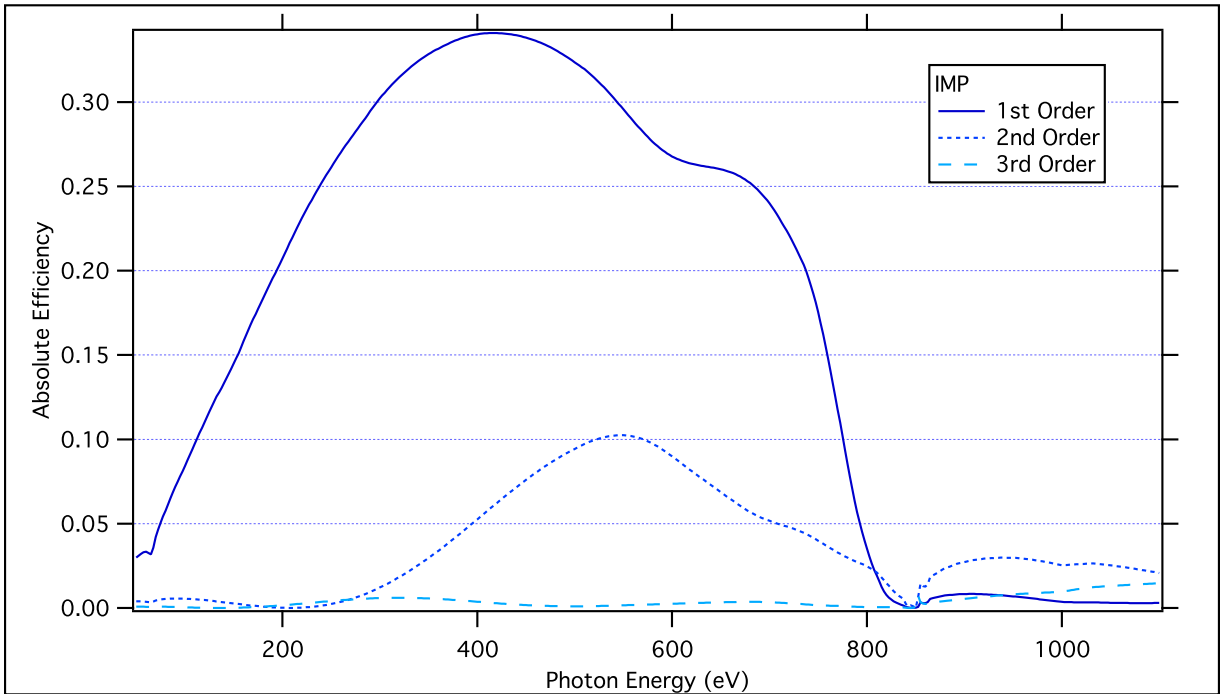
## 5.6 Summary of Final Design

- Key performance parameters - TABLE 4g: Resolution and efficiency at emission edges of interest
  - DATA 4h: efficiency plots for each grating

Note: effect of blazing: profound at low energies and low groove densities. Less pronounced "humps" at higher energies and groove densities. EXPLORE: Optimize an LEG for 800eV. Still humps? Effect due to groove dens, energy, or incidence? [LEG is low on all of those]

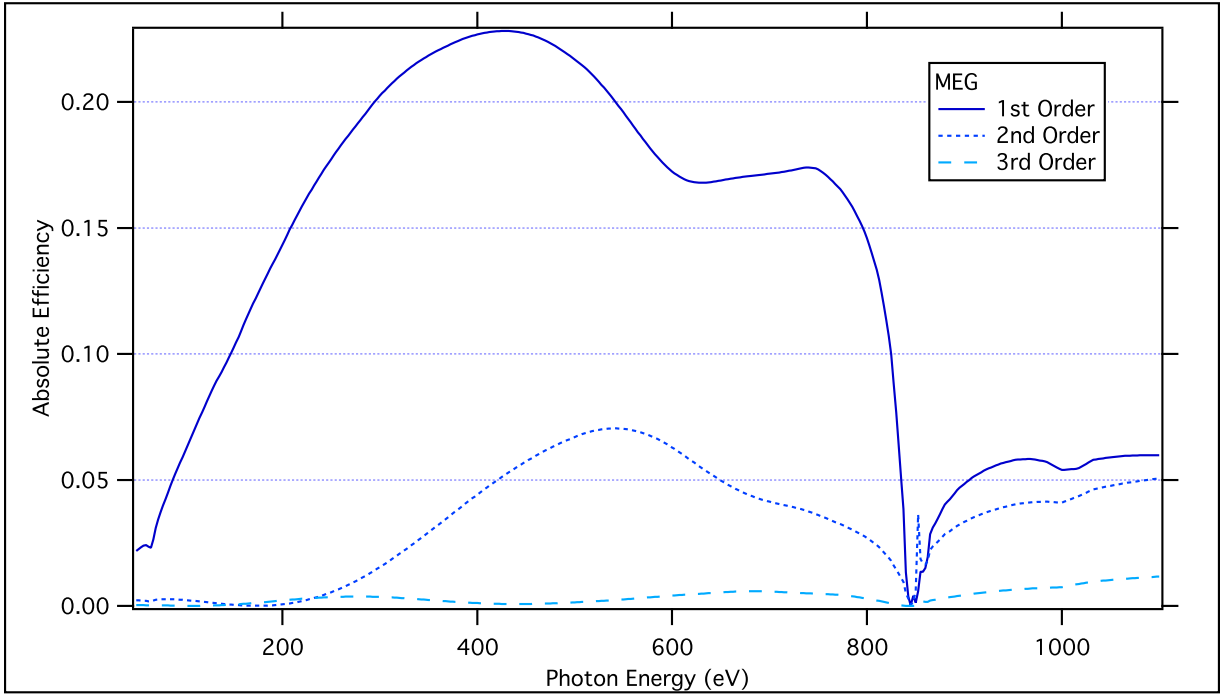


(a) Low Energy Grating (LEG): 600 lines/mm, 1.85 deg. blaze angle, Au coating, for 86 deg. incidence

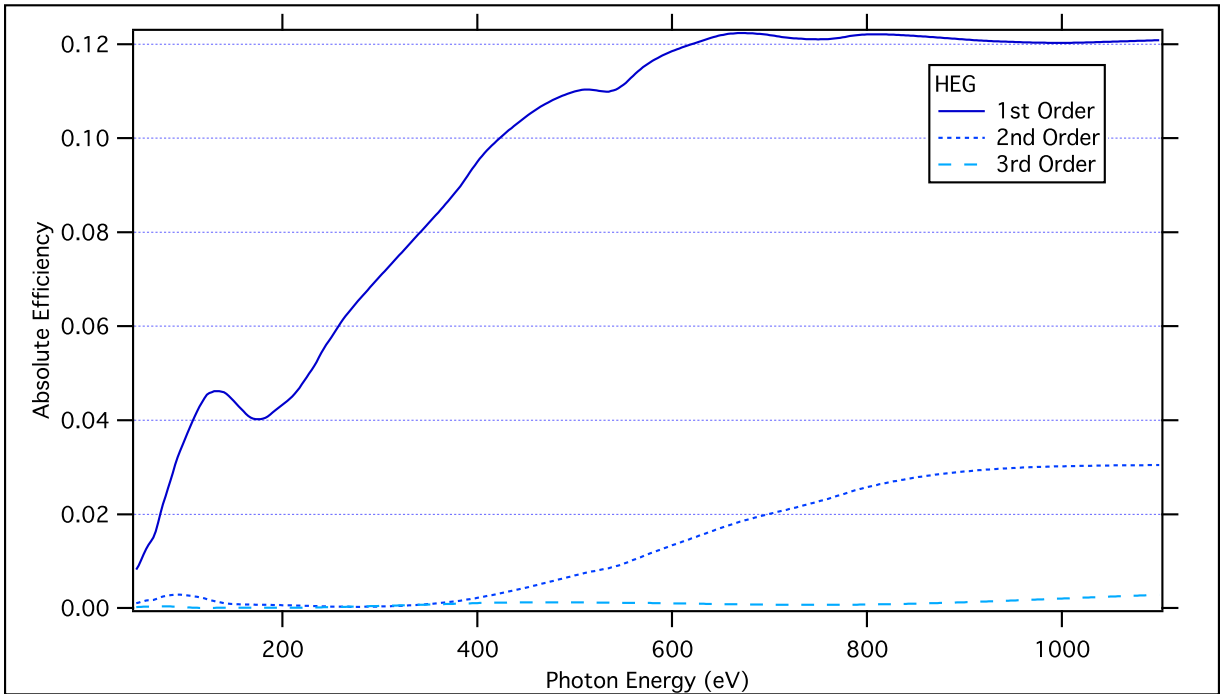


(b) Impurity Grating (IMP): 900 lines/mm, 1.11 deg. blaze angle, Ni coating, for 87 deg. incidence

**Figure 5.5:** Theoretical diffraction efficiency for the Low Energy Grating and Impurity Grating, as designed

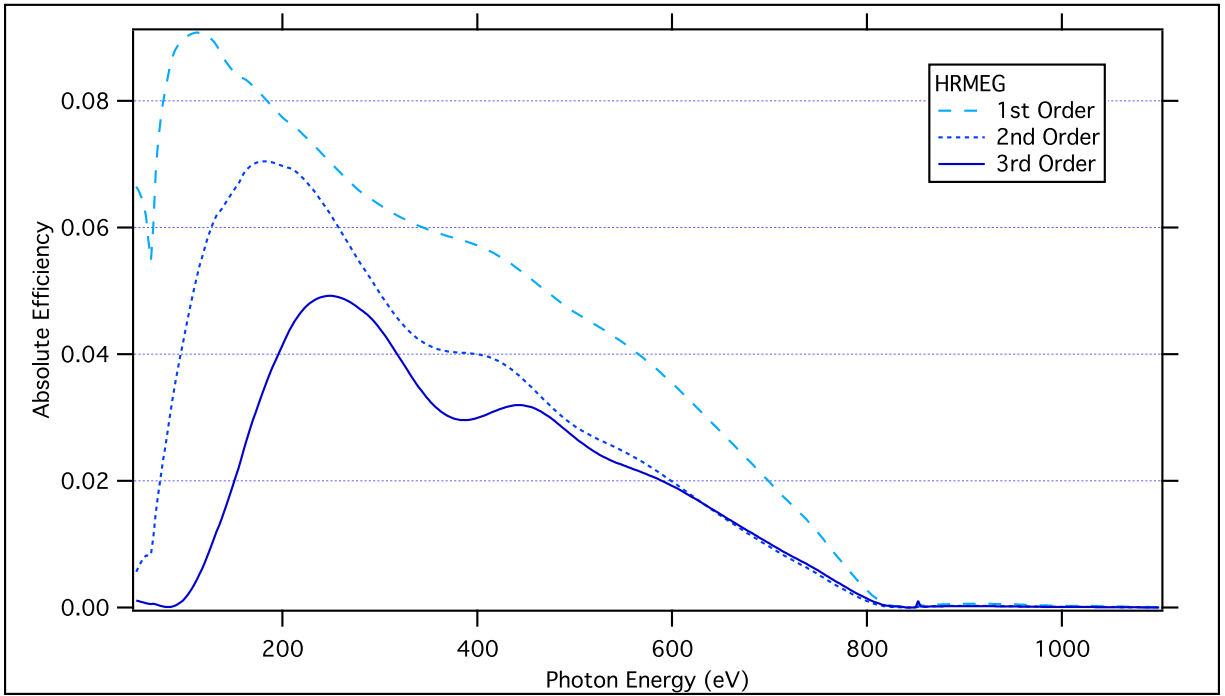


(a) Medium Energy Grating (MEG): 1200 lines/mm, 1.48 deg. blaze angle, Ni coating, for 88 deg. incidence

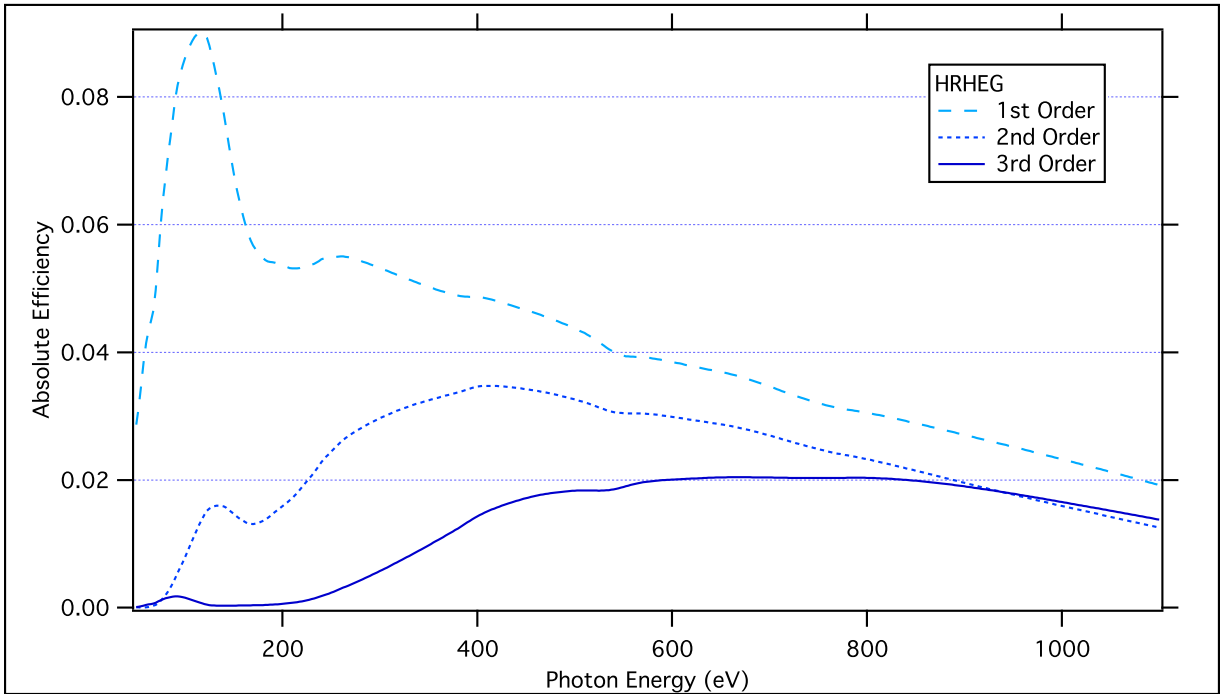


(b) High Energy Grating (HEG): 2000 lines/mm, 1.52 deg. blaze angle, Pt coating, for 88 deg. incidence

**Figure 5.6:** Theoretical diffraction efficiency for the Medium Energy and High Energy Gratings, as designed



(a) High-res Medium Energy Grating (HRMEG): 1800 lines/mm, 4.85 deg. blaze angle, Ni coating, for 88 deg. incidence



(b) High-res High Energy Grating (HRHEG): 2600 lines/mm, 4.05 deg. blaze angle, Pt coating, for 88.25 deg. incidence

**Figure 5.7:** Theoretical diffraction efficiency for the High Resolution Gratings, optimized to be used in 3rd order.

## CHAPTER 6

# CHARACTERIZATION: HOW WE MEASURED THE ACTUAL GRATING PERFORMANCE, AND ACCOUNTED FOR DIFFERENCES

## 6.1 AFM measurements of manufactured grating profile

[locate all]

challenge: blaze angle numerical measurements... requires calibration of z-axis.

## 6.2 Diffractometer measurements of actual grating efficiency

### 6.2.1 Beamline 6.3.2 Diffractometer

- describe machine

TODO: get paper and cite: [http://ieeexplore.ieee.org/xpl/freeabs\\_all.jsp?arnumber=4994440](http://ieeexplore.ieee.org/xpl/freeabs_all.jsp?arnumber=4994440)

FIGURE 5b: picture of diffractometer tank with gratings positioned

- If you know groove density: can position to detector to correct angle as you scan energy. Otherwise, need to scan angle to find diffraction peak, and take eff. there.

DATA 5c: example angle scan at energies of interest

DATA: 5d example energy scan known groove density

- mono: higher-order light contamination. Uses filters in front of end station

## 6.3 Real-world grating effects

### 6.3.1 Stray Radiant Energy

<http://gratings.newport.com/information/technotes/technote9.asp>

#### Surface roughness

(scattering: uniform decrease in efficiency) Other way to think about: periodic structures with *many* frequency components. Diffract all over the place.

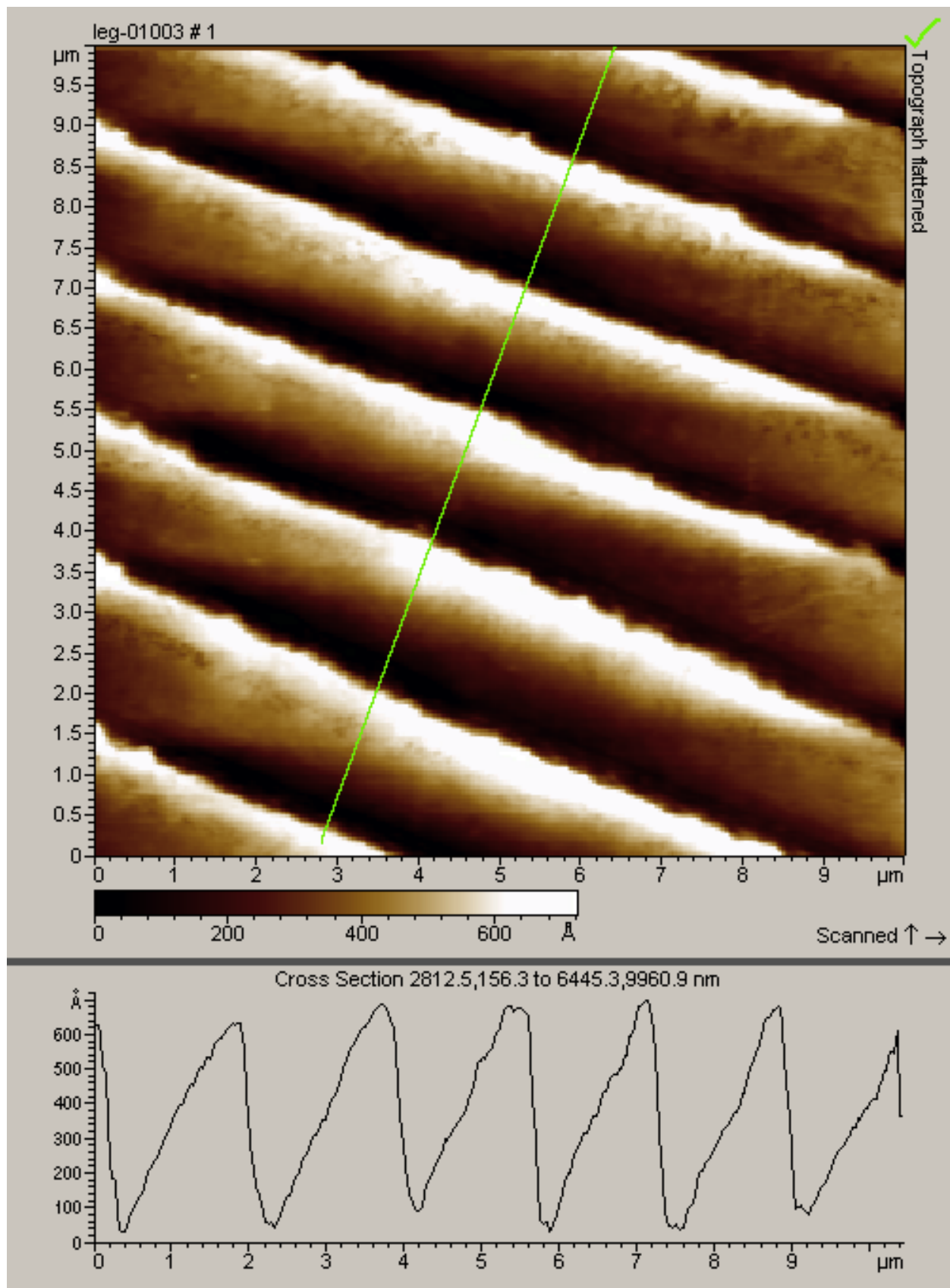


**Figure 6.1:** The Low Energy Grating has a smooth regular profile, shown in this example image measured using an Atomic Force Microprobe (AFM).

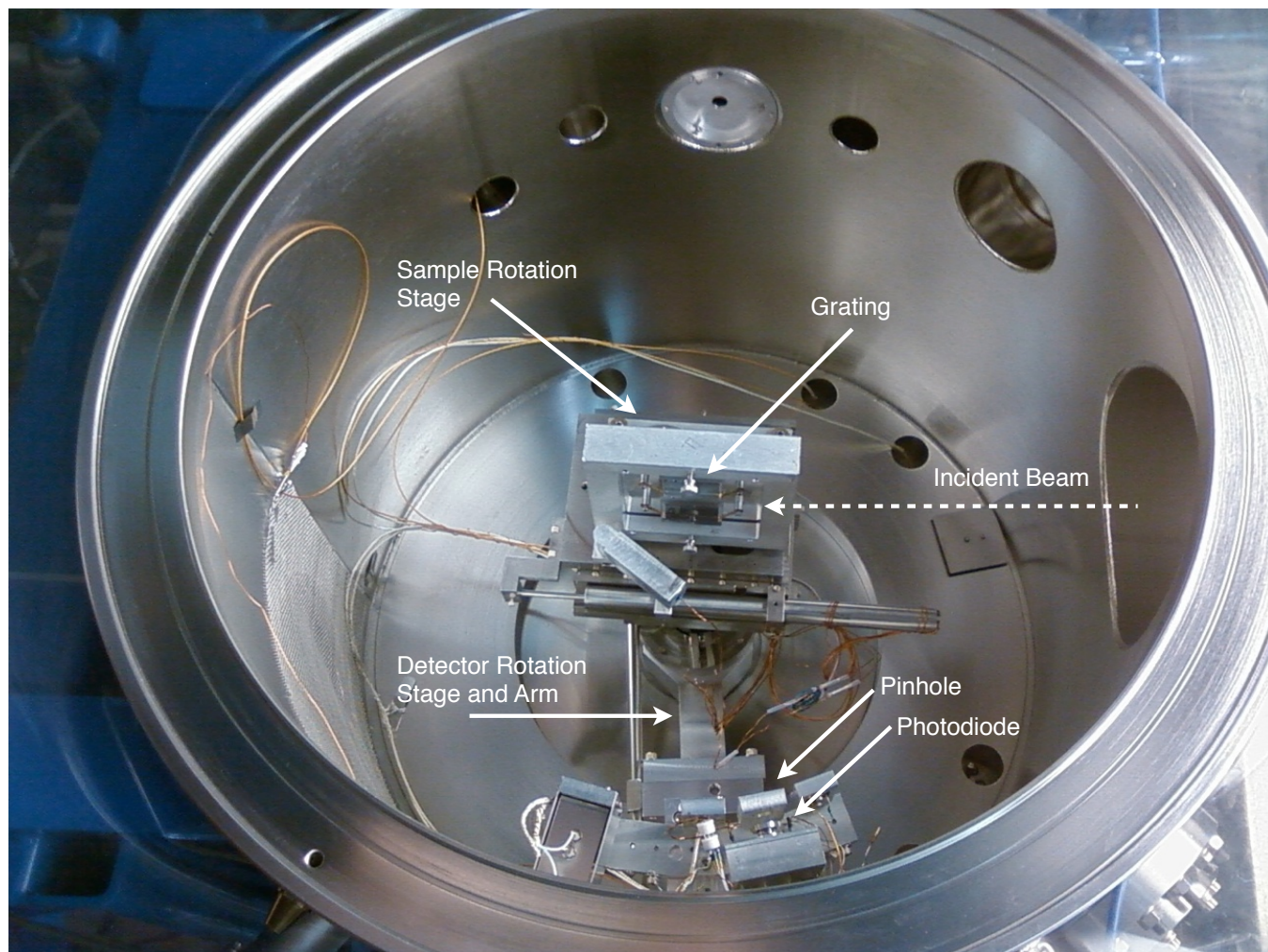


**Figure 6.2:** The diffractometer on Beamline 6.3.2 at the Advanced Light Source allows for independently setting the angle of the gratings in the beam, and setting the angle of a pinhole photodiode detector. Upstream, filters in the beamline are used to remove contamination from the higher-order light of the monochromator.



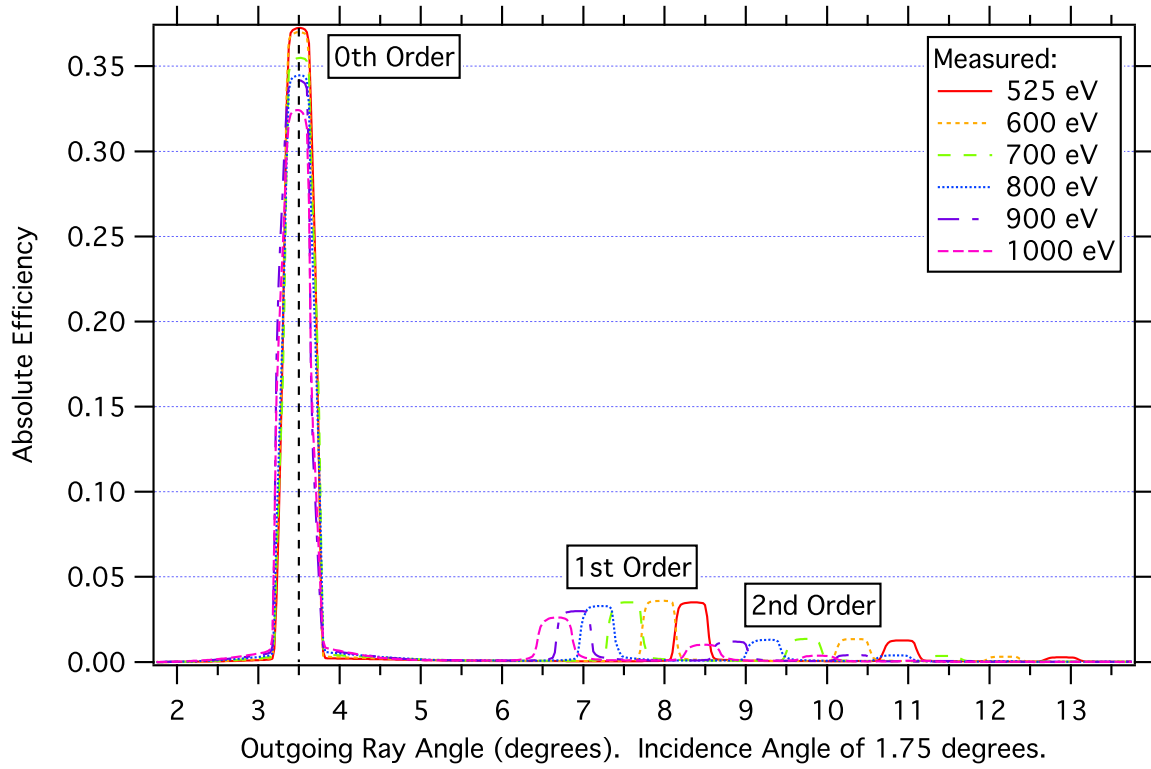


**Figure 6.3:** The simplest diffractometer experiment scans the detector angle while illuminating the grating with a constant photon energy. The diffraction orders are visible as peaks along the outgoing angle axis (here, measured up from the grating surface at  $0^\circ$ ). The 0th order (reflection) peak is easily visible at twice the incident angle. (Grating: HRHEG)

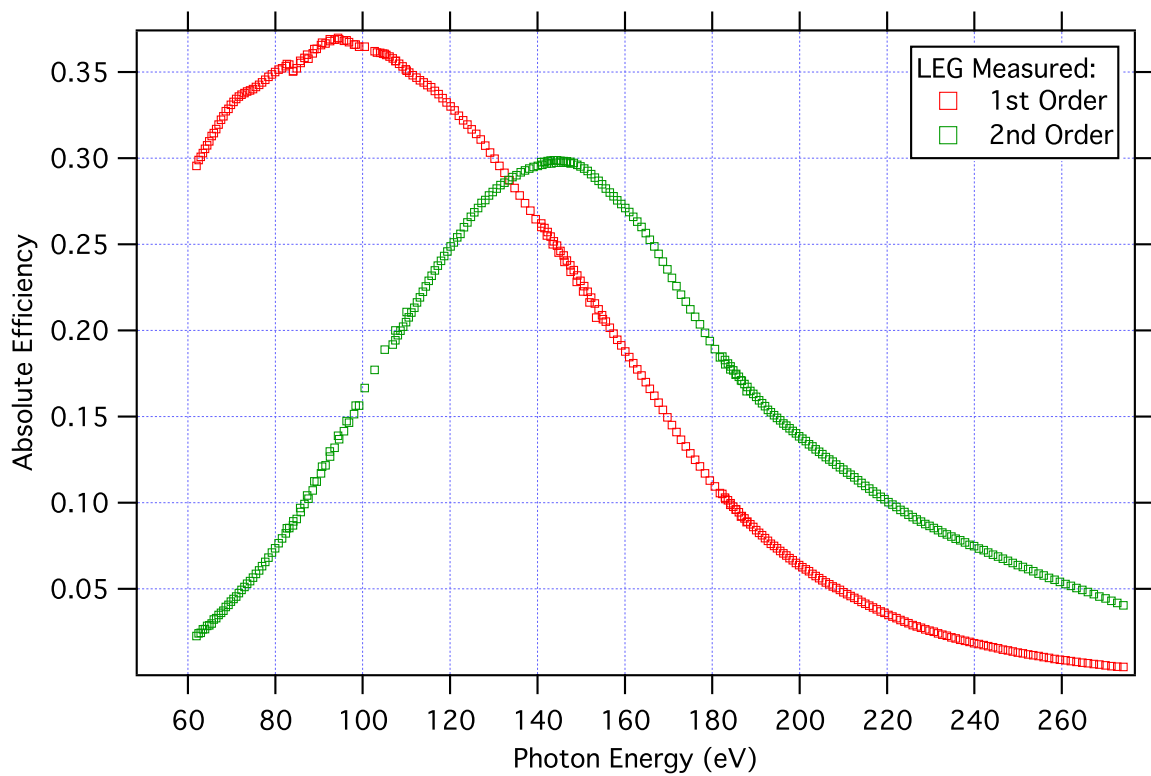


**Figure 6.4:** When the groove density of a grating is accurately known, the detector angle can be scanned in synchronization to keep it on the diffraction peak as the incident photon energy is scanned. This allows faster, continuous efficiency measurements as a function of photon energy. (Grating: LEG)

TODO: Find reference and descriptive math...

- Not modelled. Accept a uniform constant reduction (usually about 50%) lower due to scattering.

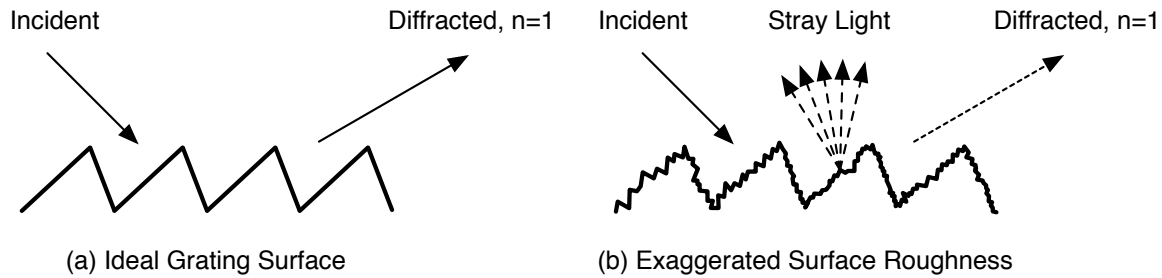


**Figure 6.5:** Roughness of the grating surface scatters stray light outside the diffraction orders

Dust, scratches, pinholes act as scattering centers

Irregularities in the groove position create ghost peaks

Irregularities along the groove direct light elsewhere

reflect off axis... reduce periodicity... disrupt the perfect grating model. May be directed or diffuse.

### 6.3.2 Blaze angle errors shift the efficiency peak

### 6.3.3 Coating oxidation changes the reflectivity spectrum

## 6.4 Grating results

: (and comparison to theoretical)

### 6.4.1 LEG

(gold): profile clean; as expected; blaze angle off. [modelled]

### 6.4.2 IMP

(nickel): Profile clean, blaze angle off [modelled]. Oxidized Modelled as NI, layer of NiO.

TEST: NiO on top of Ni? layer thickness Caveat: Henke data reflectivities are not correct at/near absorption edges... shouldn't totally match theoretical shape.

- compare AFM and fitted

### 6.4.3 MEG

(nickel): profile ok, blaze angle off [modelled]. Oxidized Modelled as combination of NiO and NiO<sub>2</sub>.

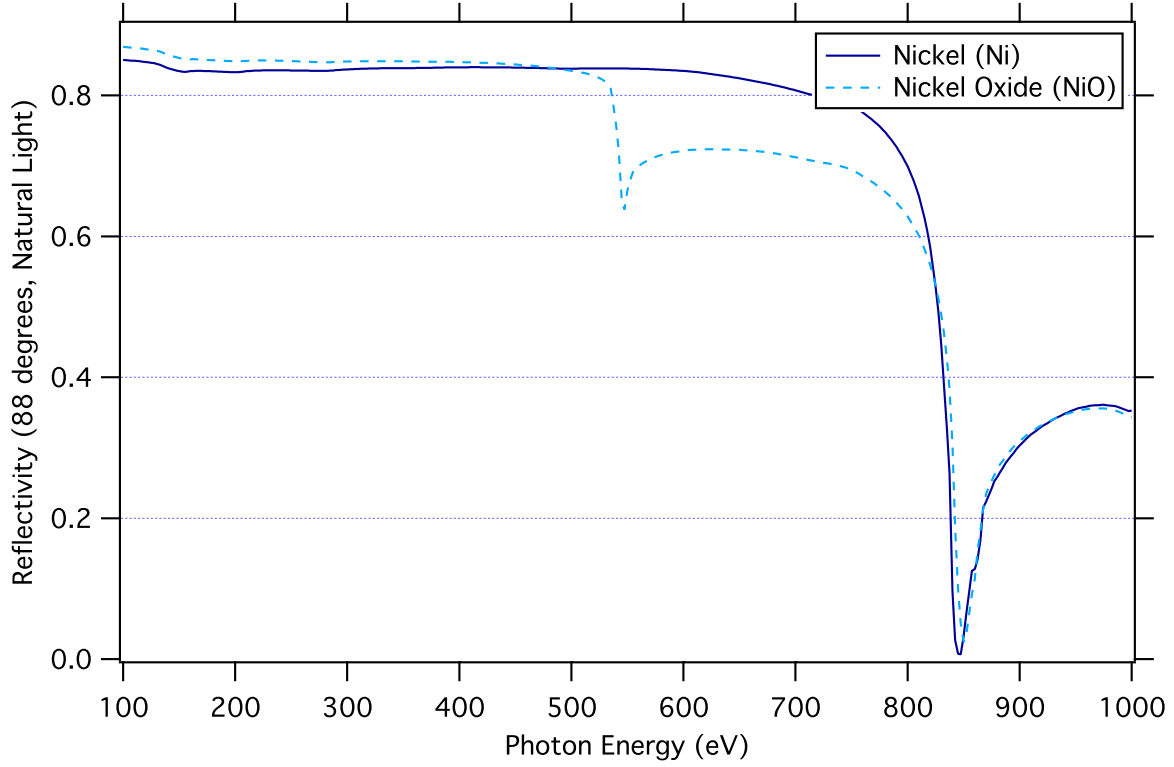


**Figure 6.6:** Unprotected Nickel quickly forms a surface oxide of NiO, which strongly reduces the reflectivity at the Oxygen edge (525eV)

#### 6.4.4 HEG

(Pt): almost no diffraction performance at all. AFM: revealed double-peak structure; not ruled correctly.  
Sent back to manuf.

#### 6.4.5 HRMEG and HRHEG

(Pt): blaze angles very off Unsuitable for actual application in 3rd order. - Temporary plan: Using HRHEG (2600l/mm) in place of HEG (2000l/mm) since blaze angle error makes it suitable for use in 1st order. -  
DATA 5q: plot expected reduction in efficiency

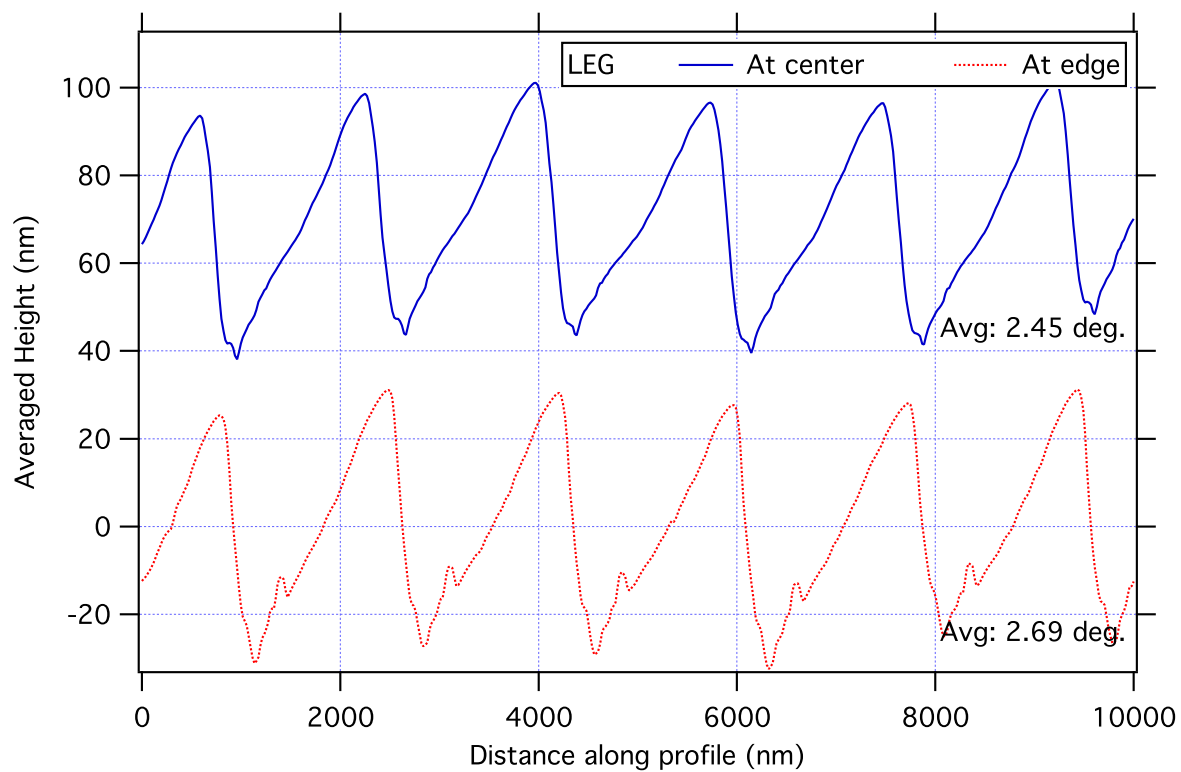


**Figure 6.7:** AFM measurements of the Low Energy Grating (LEG) profile, averaged along the grooves (TODO  $\mu\text{m}$  x TODO  $\mu\text{m}$ ). The best-fit blaze angle is at the centre of the grating.

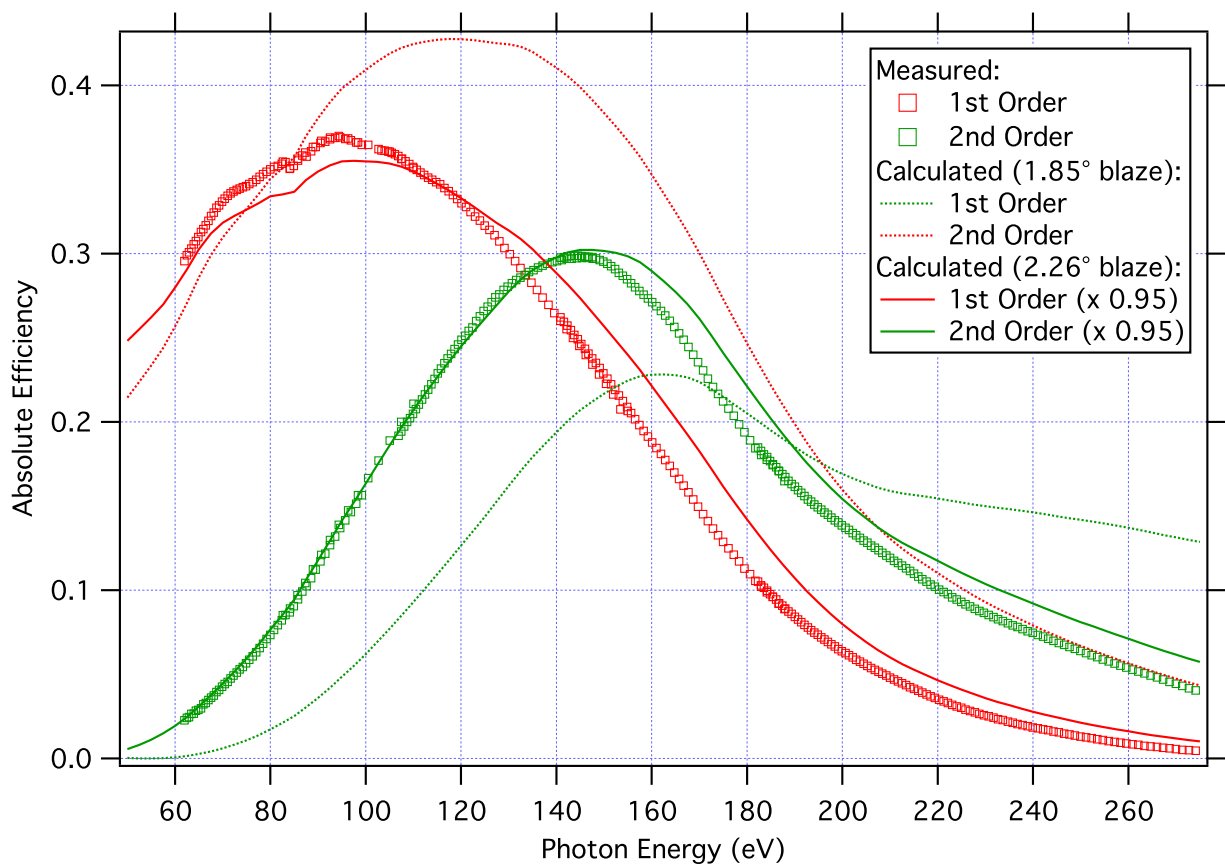


**Figure 6.8:** Theoretical and measured efficiency of the Low Energy Grating (LEG).

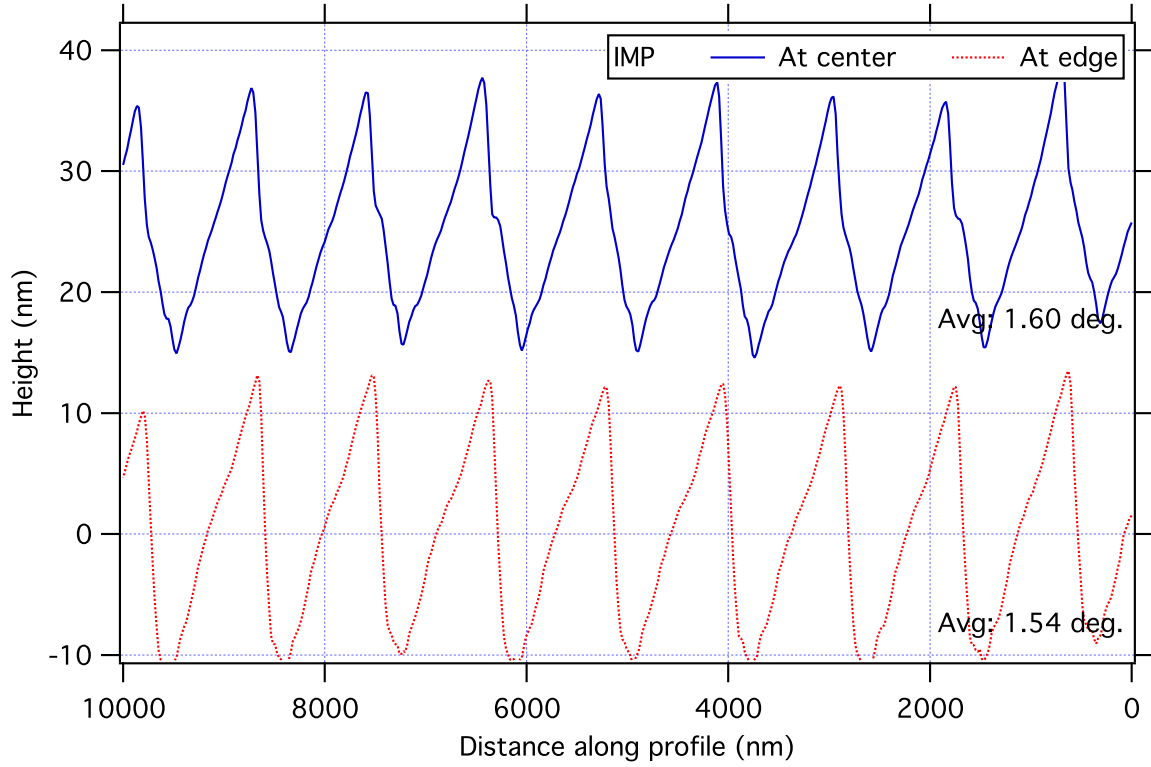


**Figure 6.9:** AFM measurements of the Impurity Grating (IMP) profile, averaged along the grooves (TODO  $\mu\text{m}$  x TODO  $\mu\text{m}$ ). The best-fit blaze angle is at the centre of the grating.

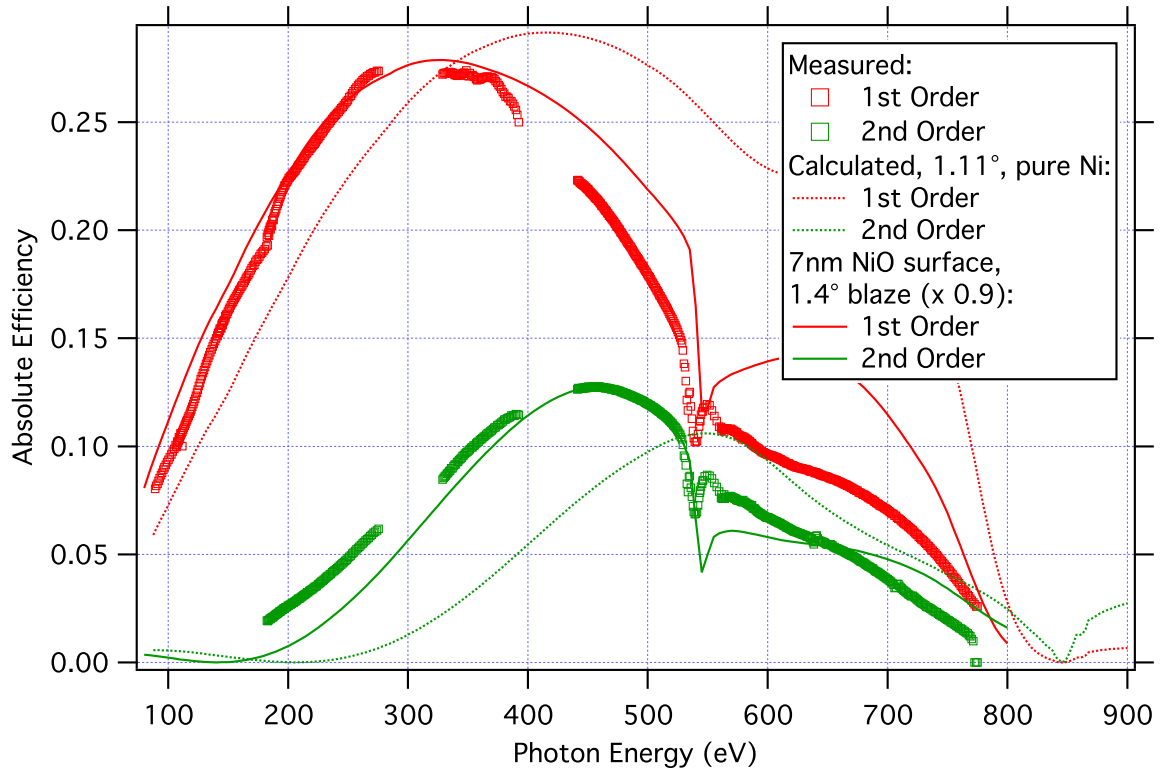


**Figure 6.10:** Theoretical and measured efficiency of the Impurity Grating (IMP).

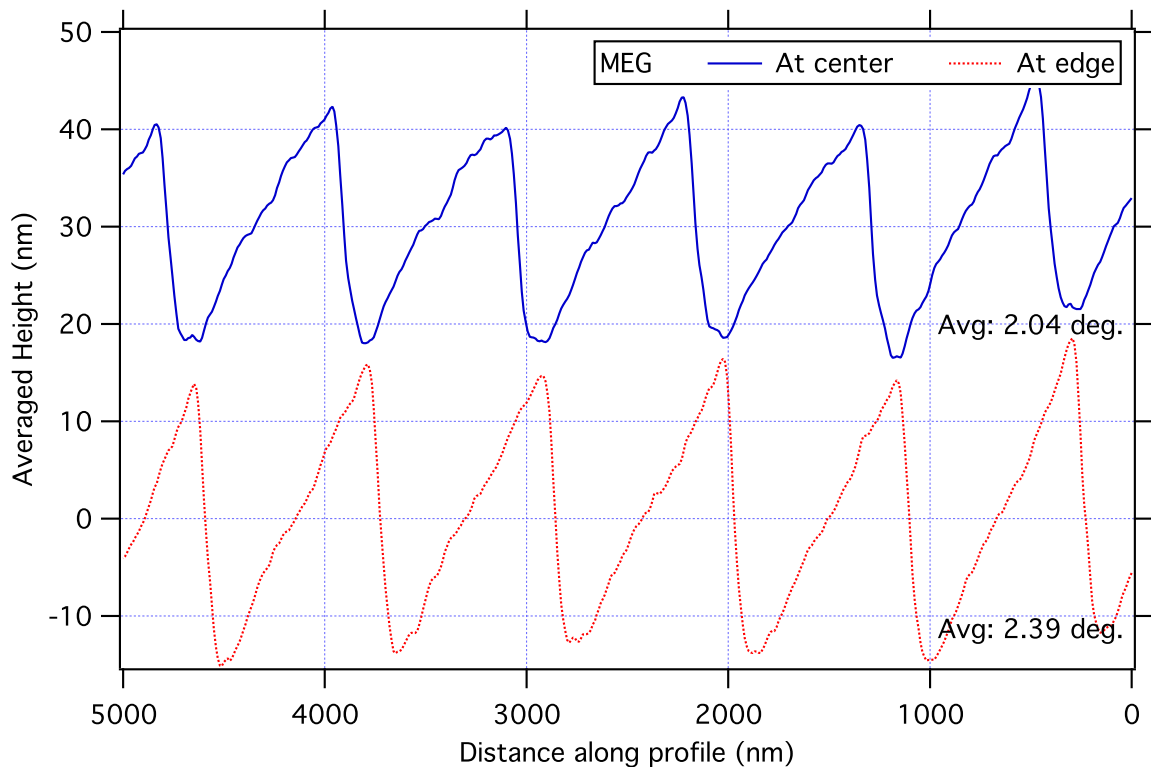


**Figure 6.11:** AFM measurements of the Medium Energy Grating (MEG) profile, averaged along the grooves (TODO  $\mu\text{m}$  x TODO  $\mu\text{m}$ ). The best-fit blaze angle is at the centre of the grating.

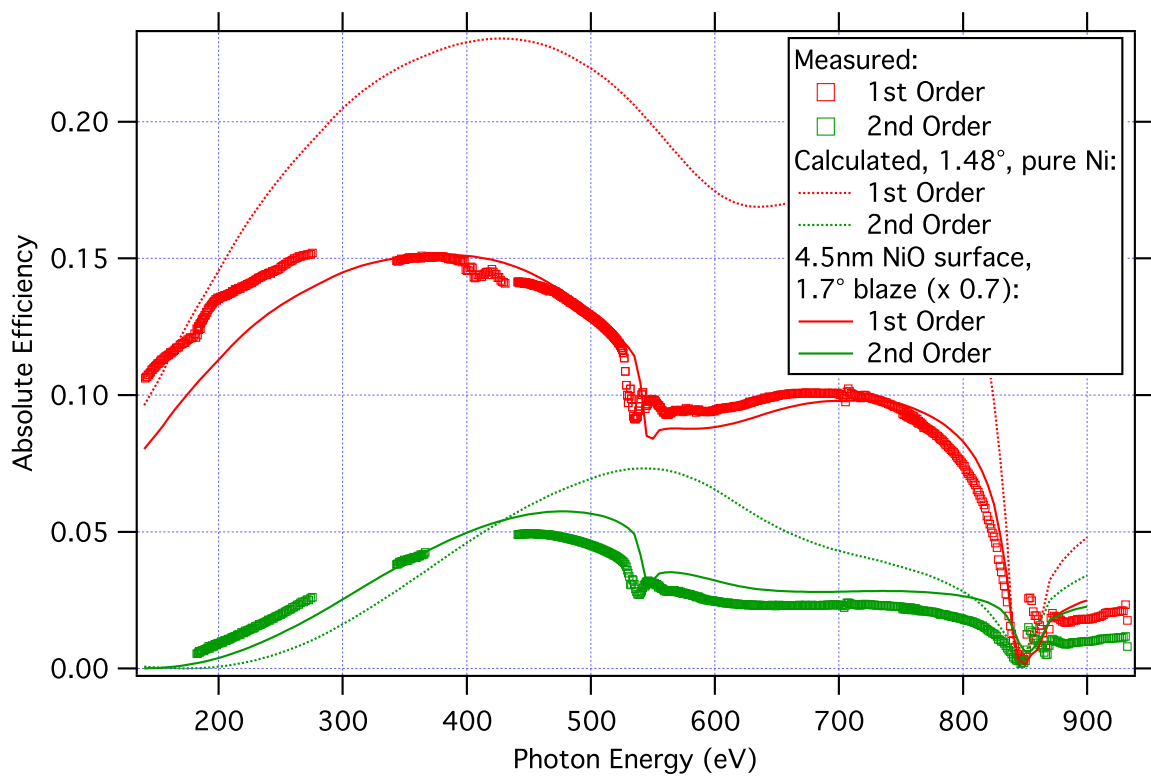


**Figure 6.12:** Theoretical and measured efficiency of the Medium Energy Grating (LEG).



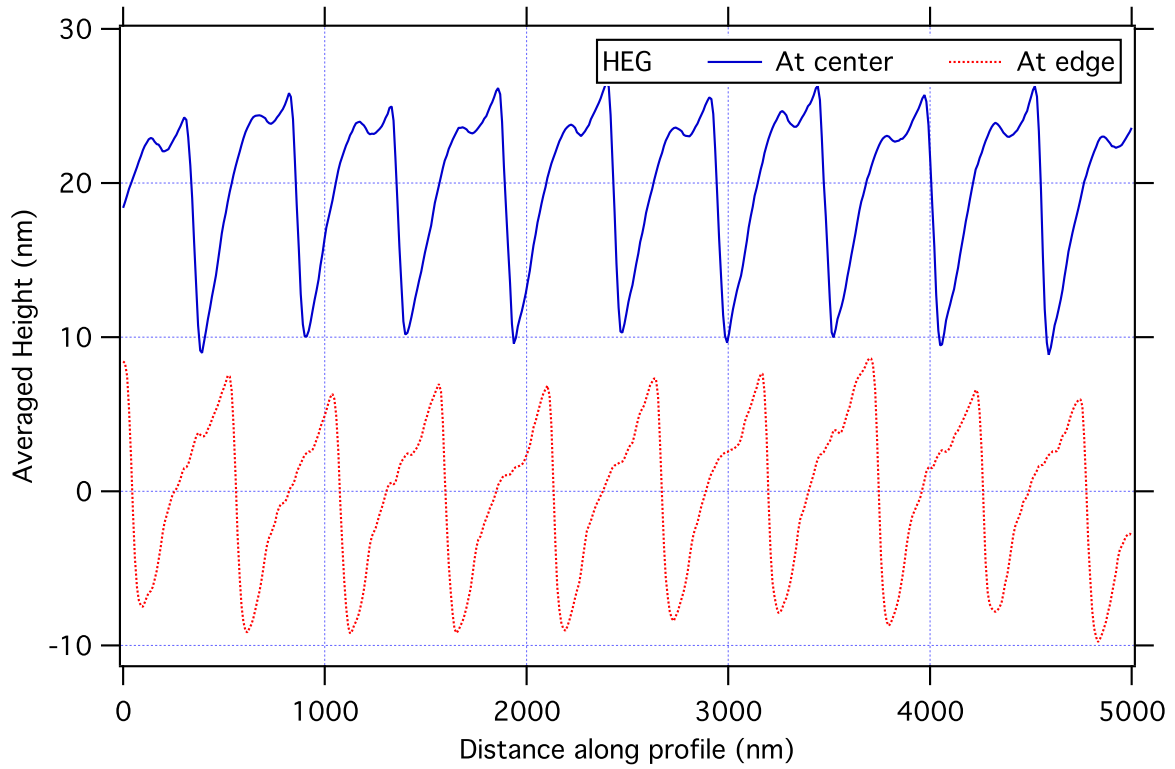


**Figure 6.13:** AFM measurements of the High Energy Grating (HEG) profile, averaged along the grooves (TODO  $\mu\text{m}$  x TODO  $\mu\text{m}$ ). Severe ruling errors were apparent. The profile wasn't sufficiently triangular to attempt to fit a blaze angle.

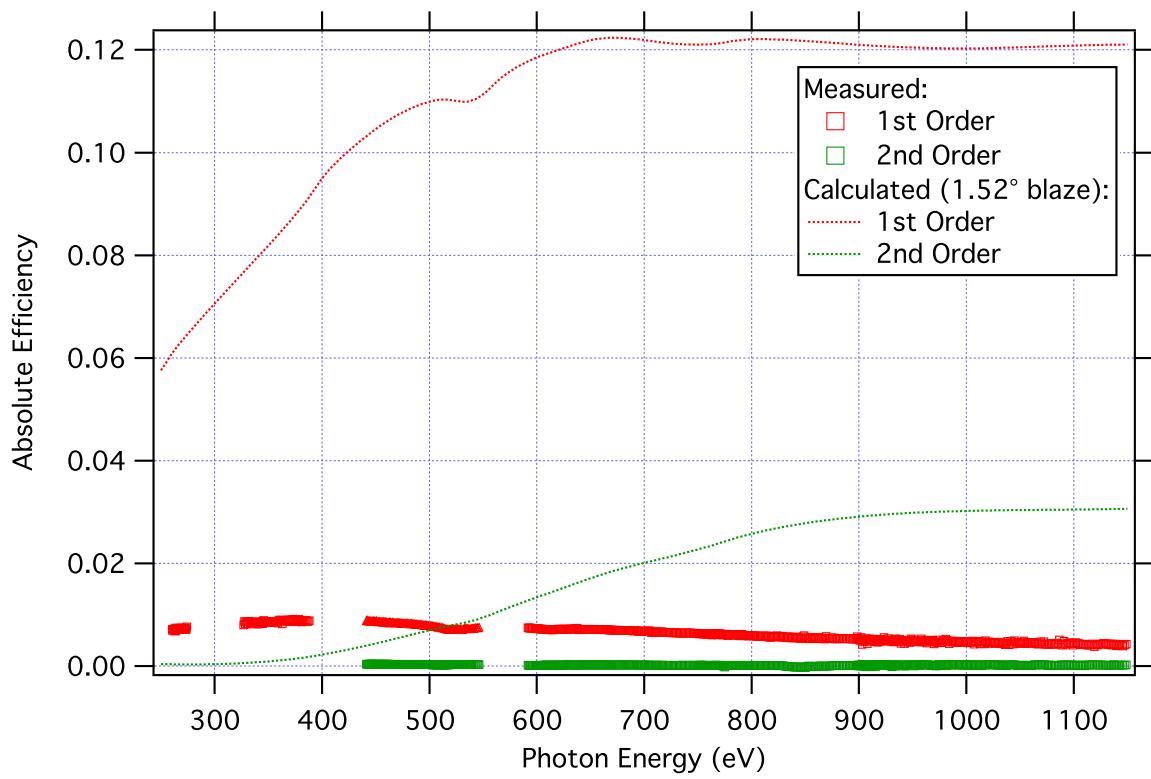


**Figure 6.14:** Theoretical and measured efficiency of the High Energy Grating (LEG).

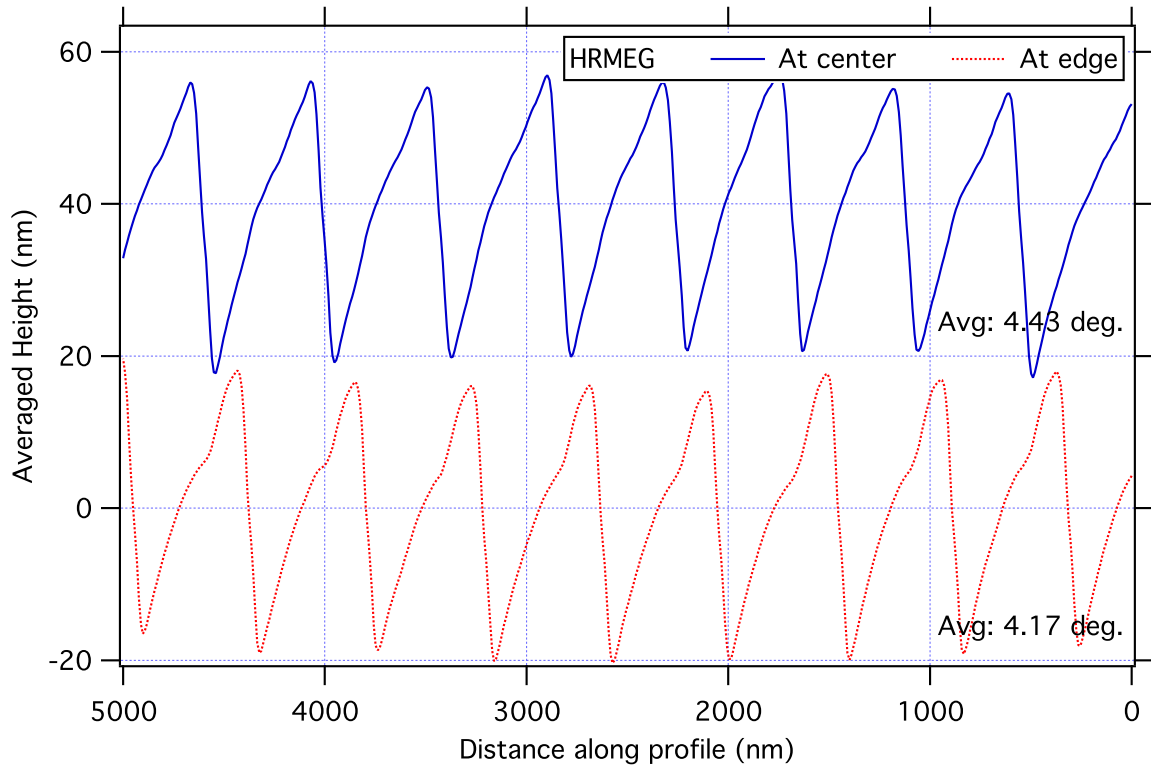


**Figure 6.15:** AFM measurements of the HighRes Medium Energy Grating (HRMEG) profile, averaged along the grooves (TODO  $\mu\text{m}$  x TODO  $\mu\text{m}$ ). The best-fit blaze angle is at the centre of the grating.

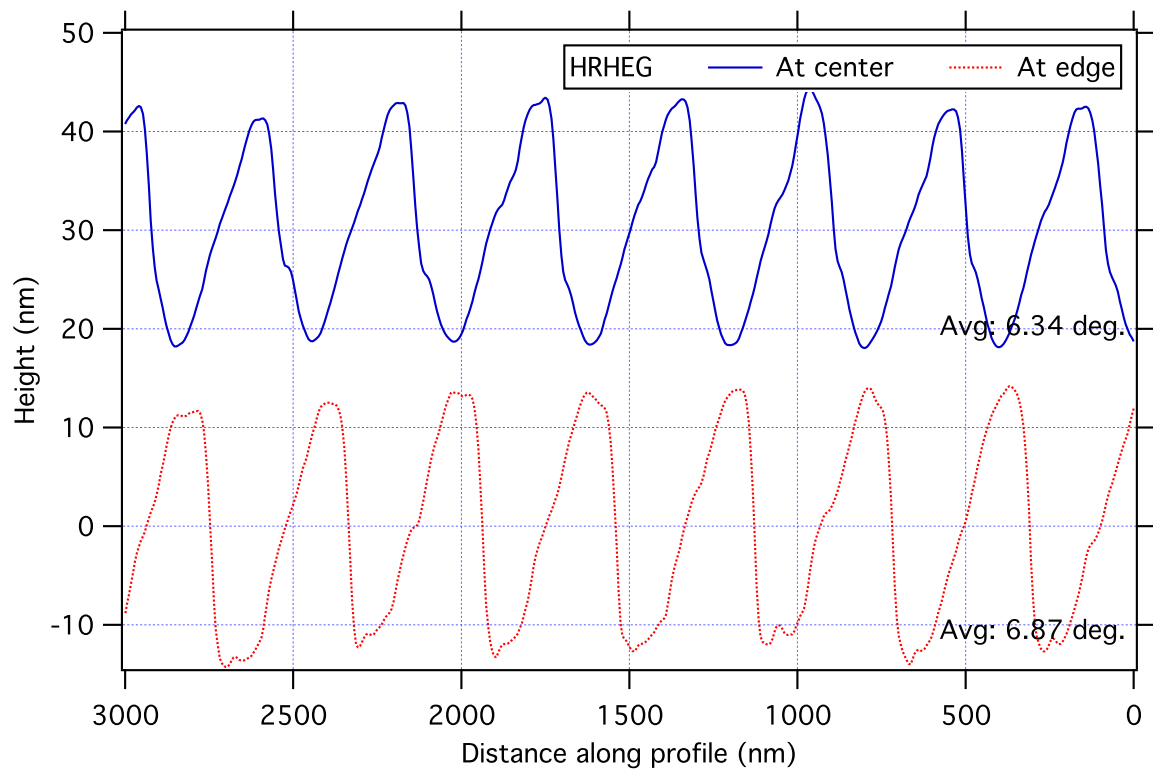


**Figure 6.16:** AFM measurements of the HighRes High Energy Grating (HRHEG) profile, averaged along the grooves (TODO  $\mu\text{m}$  x TODO  $\mu\text{m}$ ). The best-fit blaze angle is at the centre of the grating.

## CHAPTER 7

### REAL-WORLD RESULTS: WHY THERE AREN'T ANY YET

- Real-world results: - Unfortunately none yet... Problems with spectrometer: - Mechanical design flaws (crashing; hexapod range) - electrical wiring and noise problems (sensitive detector in-vacuum; can't be on long signal cables) - Grating manufacturing, as covered above.

## CHAPTER 8

### FUTURE WORK: WHAT SHOULD HAVE BEEN IN CHAPTER 6

- Grating efficiency engine: own open-source software [combine differential method and RCWA use as check on each other, or within areas of applicability] - Cloud computing: distribute over many cores, but only for a short time. Calculations can be done massively in parallel. - web service accessible to beamline designers everywhere - Make beamline work Publish actual spectrometer results

# APPENDIX A

## SAMPLE APPENDIX

Stuff for this appendix goes here.

# APPENDIX B

## ANOTHER SAMPLE APPENDIX

Stuff for this appendix goes here.